UNIVERSITY OF OKLAHOMA

GRADUATE COLLEGE

SEISMIC PERFORMANCE OF GROUPED HELICAL PILES IN FIXED AND PINNED CONNECTIONS

A THESIS

SUBMITTED TO THE GRADUATE FACULTY

in partial fulfillment of the requirements for the

Degree of

MASTER OF SCIENCE

By

SHAWN M. ALLRED
Norman, Oklahoma
2018

SEISMIC PERFORMANCE OF GROUPED HELICAL PILES IN
FIXED AND PINNED CONNECTIONS

A THESIS APPROVED FOR THE
SCHOOL OF CIVIL ENGINEERING AND ENVIRONMENTAL SCIENCE

BY

_____
Dr. Amy B. Cerato, Chair

_____
Dr. Kianoosh Hatami

_____
Dr. K.K. Muraleetharan

© Copyright by SHAWN M. ALLRED 2018
All Rights Reserved.

Acknowledgements

To begin I would like to thank all who made this research possible through funding, donating materials and/or their time throughout the testing sequence. With a special mention to DFI, NSF, Torcsill, RamJack, and Magnum Piering.

I would like to acknowledge Dr. K. K. Muraleetharan and Dr. Kianoosh Hatami for agreeing to be on my committee and providing their feedback on my research and writing, along with all the knowledge they have shared with me during this journey.

Next thanks go out to my fellow graduate students for all their feedback, cooperation and patience throughout this process. Special shout out to Tatiana Vargas and Maryam Shahbazi.

With all the gratitude in the world, I owe thanks to Dr. Amy Cerato for her guidance, ambition, dedication, and understanding. She has seen me through difficult trials and was always there to push me forward through them. It goes without saying that none of this would be possible without her.

Finally, my parents, brothers, and my girlfriend Kourtney Fox who have given unfailing support and love through this research and my life in general. For every time I have not said it but should have, thank you so much.

Shawn Allred

Table of Contents

List of Tables

List of Figures

Abstract

Helical piles have yet to be nationally considered an acceptable foundation for structures in areas of high seismic activity. This remains despite evidence of helical pile survival stories from recent earthquakes where other foundations failed, and helical pile systems sustained minimal damage. This study investigates the seismic behavior of grouped helical piles to begin the process of their acceptance as viable foundations in these seismically active environments. A full-scale shake-table test program was conducted on individual and grouped helical piles in a dense sand medium. The shake table simulated base motions recorded from past earthquakes. This paper discusses analysis and results of the grouped helical pile-soil system's performance characteristics when subjected to seismic loads. Additionally, comparisons are made between the two commonly used types of pile group connections: pinned and fixed. In summary, pinned connections revealed better performance under seismic loads when compared to fixed connections for grouped helical piles. The pinned connection demonstrated higher damping ratios, lower lateral deflections, and lower bending moments than fixed connections. Overall, the helical piles performed satisfactorily in seismic conditions and did not reveal any type of pile deformations following the five-day testing sequence.

1. Introduction

A helical pile is a deep foundation element consisting of a central shaft with one or more screw-bearing plates, or helices. They are installed by applying a compressive force and rotation by use of torque motors or rotary drill rigs, which effectively screw the piles into the soil. The helical bearing plates allow these deep foundation elements to achieve high uplift capacities (Prasad and Rao 1994; Cerato and Victor 2008, 2009), and can add to their lateral resistance if the helix resides in the active length of the pile, or length of the pile which deflects under lateral load (Prasad and Rao 1994, 1996; Perko 2009). The addition of helical bearing plates to a steel shaft, creates many advantages.

Helical piles are typically associated with low mobilization costs since the installation equipment is small and inexpensive. Unlike driven piles, installing helical piles does not produce much noise or vibrations. The installation equipment can be as small as handheld torque motors, which makes helical piles ideal foundation elements for projects with very limited space, such as retrofitting failing foundations on an existing structure or urban construction. Furthermore, the installation can be completed in any type of weather condition. While used to support compressive loadings in many situations, the helical bearing plates are also used to resist uplift forces, making them excellent foundation elements for tall slender structures such as lighthouses, wind, communication and energy towers. The design of the helical pile is based on the type and magnitude of loads, subsurface conditions and the specific application, as are all deep foundation elements. However, one of the major benefits of helical piles is that it is relatively easy to alter the helical pile design in the field if

conflicting subsurface conditions are encountered. Small shaft diameters lead to high slenderness ratios (embedment depth/shaft diameter) and small shaft surface area. Small shaft surface area can reduce the influence of expansive soil heave while high slenderness ratios are associated with high damping characteristics (Perko 2009). Testing on the helical pile can be conducted immediately after the installation is completed to ensure the bearing capacity, and in many situations, the construction can begin immediately following these tests because there is no curing period for these foundation elements. Finally, helical piles can be easily removed, recycled, and re-used for temporary structures (DFI 2013).

Rigorous bearing capacity helical pile and anchor design methods include the cylindrical shear method and individual bearing method described in Perko (2009). In addition, the industry has developed a torque correlation method that relates installation torque to capacity through an empirical factor based on parameters such as shaft size and soil type (Hoyt and Clemence 1989). However, these design methods were developed for static loading situations, and there has been no seismic design method developed for helical piles. In the United States, requirements for the design of helical piles are detailed in the International Code Council – Evaluation Service Report (ICC-ESR) on the Acceptance Criteria for Helical Pile Systems and Devices (AC358) (ICC-ES 2013). AC358 was written by an Ad Hoc committee of helical pile manufacturers and engineering consultants and presented to the ICC-ES; a private, for-profit evaluation company authorized by the International Building Code (IBC) to evaluate products (Perko 2007). This document was vetted and adopted by the

ICC-ES, who issued an official "Evaluation Service Report (ESR)" that could be used to aid a building official in assessing whether helical piles meet their building code.

It should be noted that AC358 is a product evaluation tool, not a guide. The development of this acceptance criteria was to supplement general requirements for helical piles in the International Building Code (IBC) (IBC 2015). However, the criteria were arbitrarily limited by the ICC-ES to helical pile systems and devices used to support structures only in Seismic Design Categories (SDC) A, B or C (AC 358 Section 1.2.1) to limit the ICC-ES liability and/or responsibility as an evaluating agency. In other words, the ICC-ES established the SDC limits that would apply to their evaluation. The application and use of helical piles in areas with SDC D, E, and F would require further analysis by a registered design professional. It is the responsibility of the design professional and general contractor to be sure materials used in construction meet the code for seismic applications. It is the responsibility of the building official to enforce this.

The limit on SDC D, E and F remains despite evidence of helical pile survival stories from recent earthquakes in New Zealand, Japan (Woods July, 2016), and the United States (Perko 2009) which have revealed helical piles can remain as sustainable foundations through earthquakes and aftershocks. The 2011 Christchurch earthquake caused many structures to collapse due to foundation failure. However, most of the structures on helical pile foundations sustained minimal structural damage (Woods July, 2016). This research is part of a helical pile seismic study, which seeks to affirm helical piles as sustainable deep foundation elements to be added to seismic design categories D, E, and F in AC358. The focus of this research is to quantify the

behavior of grouped helical piles in seismic design category C, while comparing two different types of connections to the superstructure: pinned and fixed connections.

1.1.Hypotheses and Objectives

1.1.1. Hypotheses

Helical piles are not yet included in the acceptance criteria as adequate deep foundations for supporting structures in IBC seismic categories D, E, and F, while according to survival stories from New Zealand, Japan and the US, many structures bearing on helical pile foundations sustained minimal structural damage through earthquakes and aftershocks. Testing full scale helical piles in seismic conditions will provide data to help engineers design foundations more effectively in seismically active areas.

A big concern when considering what foundation to use in a seismically active area is deflection and/or rotation of the pile head. The smallest deflection or rotation of the pile head can cause massive deflections at the top of tall structures and could result in overturning or collapse. Therefore, it is not only imperative to choose the correct type of deep foundation for this situation, but to also consider the type of connection between the foundation and the superstructure. Typically, structural engineers model superstructure behavior by assuming a fixed connection; obviously the connection to the ground, the foundation system and the soil type significantly affects the superstructure's behavior. By quantifying the seismic behavior of full-scale helical piles under both pinned and fixed connections the structural engineers will better understand how their super structure behaves with varying types of foundations and soil type and be able to more safely design structure.

The following hypotheses have been developed:

1) Grouped helical piles will reveal high damping ratios (i.e. greater than five percent) for both pinned and fixed connections
2) Pinned connections will perform better than fixed connections by reducing deflections

1.1.2. Primary Objectives

It is the objectives of this research to:

1) Understand the seismic behavior of grouped helical piles
2) Compare the seismic behavior of grouped helical piles in pinned vs fixed connections
3) Determine the damping characteristics of the grouped helical piles.

1.2.Scope of work

To accept helical piles as sustainable deep foundations for area of high seismic activity, extensive full-scale field testing was conducted. From this, experimental data was obtained to be analyzed and determine the effective behavior of the helical piles. The helical piles in this study were tested in a dry dense sand medium constructed in a laminar box on top of the University of California – San Diego (UC-SD) full-scale shake table. Once installed, the shake table was instructed to simulate two different earthquakes with known ground acceleration data. These earthquakes were chosen as the 1994 Northridge earthquake and the 1995 Takatori earthquake. The testing program was originally developed by Cerato (2016b,c), in which further details can be found. The research consisted of six main tasks:

Task 1: Strain gage instrumentation

Task 2: Construction and instrumentation of the dense sand medium

Task 3: Installation of helical piles

Task 4: Shake sequences

Task 5: Soil Testing

Task 6: Compilation of Results/Data Analysis

This thesis focuses specifically on Task 6 for testing days 4 and 5: grouped helical piles with fixed and pinned connections, respectively. The data analysis consisted of developing a code via the MATLAB software to estimate damping and stiffness properties of the pile-soil system, and how these properties changed throughout the five-day testing sequence. Results from the data analysis were used to make comparisons between the two types of pile group connections: fixed and pinned; along with determining how pile installation and pile grouping affected the soil system with respect to these dynamic properties. Additionally, a large liquefaction literature review was performed to further understand pile behavior when subject to dynamic loadings and to aid future research on helical piles in liquefiable soils.

2. Literature Review

2.1. Discussion of IBC

The International Building Code (IBC) does not currently provide a design methodology for helical piles for Seismic Design Categories (SDC) D, E, or F. However, the IBC does not limit the use of helical piles in these areas, whether it is left to the geotechnical engineer, building official, and/or registered design professional. Areas susceptible to liquefaction fall under SDC's D, E, or F and therefore the IBC leaves the choice of foundation type to the design professional. Although, throughout reading the sections in the IBC pertaining to foundation design in SDC's D, E, and F, it becomes clear what is recommended to use in these areas. This is due to multiple subsections and notes in the IBC that provide recommended reinforcement designs for concrete piles in these Seismic Design Categories. The IBC continuously implies to use reinforced pre-cast or cast-in-place concrete piles throughout its discussion of foundation design in these seismically active areas. The perfect example of this can be found in section 1810.2.4.1 of the IBC which states:

> *"For structures assigned to SDC D, E, or F, deep foundation elements on Site Class E or F sites, shall be designed and constructed to withstand maximum imposed curvatures from earthquake ground motions and structure response. Curvatures shall include free-field soil strains modified for soil-foundation-structure interaction coupled with foundation element deformations associated with earthquake loads imparted to the foundation by the structure.*

- *Exception: Deep foundation elements that satisfy the following additional detailing requirements shall be deemed to comply with the curvature capacity requirements of this section.*
  - *1. Precast prestressed concrete piles detailed in accordance with Section 1810.3.8.3.3.*
  - *2. Cast-in-place deep foundation elements with a minimum longitudinal reinforcement ratio of 0.005 extending the full length of the element and detailed in accordance with Sections 21.6.4.2, 21.6.4.3 and 21.6.4.4 of ACI 318 as required by Section 1810.3.9.4.2.2."*

These subsections, notes, and exceptions can be found throughout the SDC's D, E, and F foundation design sections the IBC and ASCE-7, which is referred to by the IBC for design recommendations in these sections as well. This remains despite the numerous survival stories associated with helical piles throughout past earthquakes, in New Zealand (Woods 2016, July), Japan, and the United states (Perko 2009). Woods (2016, July) described how approximately 300 structures were supported by helical piles prior to the 2011 Christchurch earthquake which caused numerous foundations to fail and structures to collapse. He stated that out of the 300 structures supported by helical piles, less than 10 suffered significant structural damage while many structures supported by driven piles and concrete piles did. Similar stories exist from the 1994 Northridge Earthquake in the United States; however, they have never been well documented. Perko (2009) describes one such story through his communication with an engineer who surveyed some structures after the 1994 Northridge Earthquake and found that helical piles performed better than other types of surrounding foundations. The story describes a few structures that had to undergo partial foundation repair prior to the earthquake. The partial repair for these structures

consisted of installing helical piles to support the parts of each structure where the previous foundation had not performed adequately. The survey concluded that these particular structures suffered significant foundation and structural damage where the previous foundation had remained in place, while the parts of each structure supported by helical piles suffered minimal structural or foundational damage.

2.2. Ultimate Capacity of Single Helical Piles After Axial Cyclic Loading

While understanding the behavior of helical piles during seismic events is beneficial, it is also imperative that these deep foundation elements sustain their ultimate design capacity following a seismic event. A seismic event can be simplified as a series of cyclic loadings on the structure. These events can cause high amounts of disturbance to the soil surrounding the foundation, which can effectively decrease the axial and lateral capacity of the pile. Research has been conducted (El Naggar and Abdelghany 2007) in order to quantify the amount that the ultimate axial capacity reduces after a seismic event. El Naggar and Abdelghany (2007) subjected three plain helical screw piles (HSP) and four grouted helical screw piles (Grout HSP) in cohesive soils to 15 load cycles, which was determined as the average number of "effective" load cycles of an earthquake. These tests were followed by static axial compressive tests to failure. The ultimate capacity was determined using torque correlations and compared with the axial compressive failure loads of the final tests. Based on the results, it was concluded that after being subjected to 15 cyclic loadings the ultimate bearing capacity reduced five to ten percent. Due to this, it was suggested that HSP axial cyclic behavior performed satisfactorily and warranted a consideration for seismic applications in cohesive soils (El Naggar and Abdelghany 2007).

Cerato and Victor (2008, 2009) conducted research on helical anchors to determine effects of long-term dynamic loading, fluctuating water table, and helical geometries. Helical anchors used as foundation systems for wind tower guy cables are subjected to constant dynamic tensile forces from wind turbine vibration and environmental loads such as ice, water, snow, and wind. As a result of being constantly subjected to these forces, helical anchors can experience creep, or anchor movement under load over time. To determine these effects, five helical anchors were dynamically loaded in axial tension for 2-4 weeks while being constantly monitored. This was followed by post-dynamic static tests. Included in the five helical anchors were three different helical geometries, which were two-helices, three helices, and four helices. A sixth anchor was only tested statically as a benchmark comparison. Dynamic loads were applied in sustained-repeated loading at 3 to 5 Hz and ensured the anchors were subjected to constant tension throughout. From these tests it was concluded that long-term creep can be minimized, and static uplift capacity of helical anchors can be increased significantly by pre-loading them with dynamic loads at high ratios of high cyclic loads to static uplift capacity (0.25-0.40). This increase was attributed to densifying the soil after installation. It was also observed that a significant rise in water table can greatly reduce the anchor uplift capacity. As a result, it was recommended to install the uppermost helical plate below the lowest known ground water table location to prevent uplift capacity reduction. Additionally, the optimum helix geometry determined for this study was three helices. The two-helix geometry performed poorly as it underwent excessive creep. Furthermore, the

addition of a fourth helix revealed similar behavior to that of three helices and did not display additional strength as expected.

El Sharnouby and El Naggar (2012) researched the axial cyclic and monotonic compression performance of steel-fiber reinforced helical pull-down micropiles (RHPM). The effect of the steel-fiber reinforced grout shaft was also investigated by testing a plain helical pile and comparing the results. The experiment was performed in two phases. Phase one consisted of statically loading one plain helical pile, and six RHPM to a minimum deflection equal to 8% of the average helical plate diameter. Phase two consisted of cyclically loading the six RHPM which was followed by axial loading until the load approached the 890 kN capacity of the load cell. The cyclic loading of phase two consisted of 15 load cycles each applied over two-minute durations. The average cyclic load magnitude was 300 kN, with a maximum of 390 kN, and minimum of 210 kN. Results displayed significant contribution of the grout shaft at working load levels, which attributed for 72-80% of the total resistance. However, this contribution decreased to a range of 36-50% of the total resistance at higher load levels. Because of this decrease in grout shaft contribution to total resistance, the load is transferred to the first helix on the lead section. The RHPM demonstrated good behavior during cyclic loading as no degradation was observed after 15 load cycles, and the resulting displacement was observed to be less than 1.77% of the shaft diameter. Additionally, the ultimate capacity of the test piles was found to increase after application of one-way cyclic loading with the average and maximum cyclic loading greater that 40% and 54% of the ultimate capacity,

respectively. From these results, it was concluded that RHPM are a viable foundation system in axial monotonic and one-way cyclic loading applications.

Abdelghany (2008) studied the effect of axial cyclic loading on the ultimate axial capacity of 23 helical piles installed in cohesive soils. This was performed by conducting initial quick compression tests before applying 15 cyclic loadings. These were followed by post cyclic quick compression tests conducted in the same manner as the initial compression tests. The quick compression tests were conducted to failure, which was the applied load at an axial deflection equal to 10% of the average helix diameter. The piles had similar geometries, and all had three helices on the lead sections, which decreased in diameter towards the pile tip to assist with the installation process. However, many types of reinforcement were applied to several of the test pile. These include: Grouted Helical Screw Piles (G-HSP), Grouted Reinforced Helical Screw Piles (RG-HSP), and Fiber Reinforced Polymer Grouted Helical Screw Piles (FRP-G-HSP). Plain Helical Screw Piles (PHSP) were also tested for a baseline comparison. The effect of cyclic loading proved to be insignificant to PHSP as their ultimate capacity slightly reduced within the range of 5-10%. RG-HSPs revealed the largest capacities of all piles tested, and on average was approximately double that of PHSP before and after cyclic loading and reached up to 187% of their predicted capacity from empirical torque correlations. In many of the tests conducted, the effects of cyclic loading benefited the capacities of the piles. In general, the RG-HSPs, G-HSPs, and FRP-G-HSPs (with no outside grout) showed increases in ultimate compressive capacities as a result of cyclic loading effects. Some were significant increases, up to approximately 50% increase for a few of the G-HSPs and

FRP-G-HSPs. This was attributed to the cyclic loading of piles stiffening the surrounding soil which had been previously disturbed from the pile installation process. Abdelghany (2008) concluded that HSPs perform satisfactorily under axial cyclic loading conditions, and therefore should be considered in seismic applications in cohesive soils.

2.3. Ultimate Capacity of Single Helical Piles After Lateral Cyclic Loading

Abdelghany (2008) conducted further research on the effect of lateral cyclic loading of helical piles in cohesive soils. The test piles were the same as used for the axial monotonic and cyclic tests and 50 lateral load tests were performed on 20 of them. Initial lateral load tests were conducted to determine the ultimate capacities of the test pile, which is considered the applied lateral load at a horizontal pile head deflection of 6.25 mm. The initial lateral load tests were conducted until pile head displacement reached 12.5-15.0 mm. The lateral resistance of the PHSP were found to be insignificant and were not considered for lateral cyclic tests. Three of the G-HSP were subjected to monotonic and cyclic lateral load tests. It was found that their lateral resistance significantly decreased from the cyclic lateral loading. This was attributed to the cracking and separation of the grout around the shaft. Abdelghany found that RG-HSP performed best before and after lateral cyclic loading revealing three to seven times higher lateral capacity than the G-HSP. Four RG-HSPs were subjected to lateral cyclic loading, three of which showed ~55% reduced lateral capacity as a result. However, the last RG-HSP tested revealed ~55% increase in

lateral capacity. In conclusion the use of RG-HSP warranted consideration in seismic applications in cohesive soils (Abdelghany 2008).

Similarly, El Sharbouny and El Naggar (2013) conducted monotonic and cyclic lateral test on steel-fiber composite grout reinforced helical pulldown micropiles. During monotonic testing the piles were subjected to displacements greater than 150% of the pile width and 50% of the steel-fiber reinforced grout column diameter and did not show any significant decrease in stiffness. The grout column surrounded the square shaft of the pile, but separation was noticed during testing. After unloading, the piles recovered ~70% of the deflection from static tests. Later cyclic testing was conducted over five different loading levels. At each load level the piles were subjected to five two-way load cycles. The results displayed degradation of the pile stiffness as a result of the gap formation between the reinforced grout column and the square shaft. Reductions in lateral capacity at typical failure pile head deflection criteria (6.25 and 12.5 mm) were comparable to that of RG-HSPs tested in Abdelghany (2008), at ~55% by the end of cyclic testing.

2.3.1. Comparison in Reduction of Uplift Capacity of Driven Pile Vs Helical Pile after Lateral Cyclic Loading

Installation torque correlations developed by Hoyt and Clemence (1989) are used to calculate the ultimate pullout (uplift) capacity of helical piles. It is usually assumed that the ultimate uplift capacity of helical piles is approximately 87% of the theoretical compressive capacity (Perko 2009). This allows the torque correlation method to be used whether the helical pile is designed to resist uplift forces or support compressive loads. Driven piles are often used in similar applications, and therefore it is beneficial

to compare these two types of foundations. Furthermore, while earthquakes cause axial cyclic loads to foundations via surface waves, they also cause lateral cyclic loads via primary and secondary waves, or shear waves. This can be simulated in the same manner as surface waves, by simplifying them as lateral cyclic loads.

Research has been conducted (Prasad and Rao 1994) to quantify the behavior of driven and helical piles under lateral cyclic loading and analyze the effect it has on the ultimate uplift capacity, while also comparing the two types of foundations. Prasad and Rao (1994) conducted a three-phase testing sequence on a total of three small-scale piles: two model piles and one helical pile. These foundations were installed in cohesive soils in a laboratory setting. Phase one consisted of static lateral tests to determine the ultimate lateral capacity. The ultimate lateral capacity was defined as the lateral load at which the load-displacement curve generated from the tests became linear. Phase two consisted of lateral cyclic loading. The lateral cyclic loading tests were conducted on small-scale driven and helical piles by subjecting them to varying numbers of cycles. The number of cycles was determined during testing and was ceased when the deflection of the pile became stabilized (did not change). It was noted that this usually occurred after a few hundred cycles, but the testing never exceeded 500 cycles (Prasad and Rao 1994). Furthermore, lateral cyclic tests were conducted at three different load levels. The load levels were calculated as percentages of the maximum lateral capacity determined from Phase one. The load levels ranged from 30% - 75% of the maximum lateral capacities. After subjecting the foundations to a maximum of 500 cycles for each load level Phase three was initiated, which consisted of pullout tests to failure in order to determine the effect of

the soil disturbance on the ultimate uplift capacity. Failure of the pullout tests was achieved when the recorded pull-out load stopped increasing and remained unchanged with additional upward movement.

The study determined that at low load levels (30%) for both types of foundations, neither experienced a decrease in the ultimate pullout capacity. When the load level increased to 50% on the driven piles the deflections of the pile head dramatically increased, which caused high soil disturbance and decreased the ultimate pullout capacity by an average of 23%, while the helical pile pullout capacity was left unchanged. At a load level of 70% the driven piles failed after 150 cycles, which is compared to the helical pile failure that occurred at 400 cycles at the corresponding load level. Furthermore, the 70% load level caused a reduction of the driven pile uplift capacity by 30%, while the helical pile only experienced a reduction in uplift capacity of only three percent. The reduction of the uplift capacity for the helical pile only occurred when its top helix was embedded deep enough for the shaft above to create adhesion with the soil. This indicated that the uplift capacity of the helical bearing plates was left unchanged, rather since the pile was embedded deeper it gained uplift capacity before the cyclic load tests from the shaft adhesion (Prasad and Rao 1994).

Typically, when helical piles are designed for uplift or compressive support, the skin friction, or shaft adhesion is neglected to be conservative, and therefore this reduction in uplift capacity would not be noticed for design purposes. The reason for the drastic decrease in the driven pile uplift capacity was because a driven pile in uplift takes all its capacity through skin friction and the high lateral deflections that formed gapping around the pile shaft reduced that skin friction. This gapping also

occurred around the helical pile. The difference was that the driven pile does not have the helix plate to help with uplift capacity when the soil gaps around the shaft; all of the support provided by the helical pile is through its helical bearing plates. In summary, the report states, that when considering the effects of lateral cyclic loadings on static uplift capacity, helical piles are recommended over driven piles (Prasad and Rao 1994).

While these studies show that single helical piles react well to seismic loading induced at the top of the pile, in many different soil types, there has not been any studies published on the helical pile behavior in groups, which is what this thesis focuses on. Most of the pile group work has been performed on drilled shafts or driven piles, and under liquefaction conditions. All of the group behavior of those piles will be discussed in the Liquefaction section to understand the breadth and depth of testing and how the pile group fared post-earthquake. This background knowledge is important in proposing any future testing.

2.4.Liquefaction

Liquefaction is a known phenomenon commonly associated with large seismic events. Loose, saturated, typically alluvially deposited sands of a young geologic age, are typical to be susceptible to liquefaction. This is because during shaking pore water pressure increases, and the loose sand attempts to densify, prohibiting drainage. Pore water pressure continues to increase, and as a result the effective stress in the soil decreases and reduces the ability of the soil to carry vertical and lateral loads. Historically, liquefaction events cause foundations to collapse, excessively settle, overturn, fail, crack, and/or permanently deform laterally. Liquefaction literature was reviewed for this study as it was found to be a major contributor to research pertaining to piles subject dynamic and cyclic loading. Furthermore, the following information will aid future research on helical piles in liquefiable soils.

When considering deep foundations in liquefiable soils, two separate loading conditions are possible. The first can be referred to as a “passive foundation” condition. In a passive foundation condition, the soil surrounding the pile becomes liquefied and spreads laterally. In this instance, the pile subject to the passive pressure of the soil (Gerber 2003; Cubrinovski et al. 2006). The second can be referred to as an “active foundation” condition. In this case, the foundation is displaced, and its movement is resisted by the soils passive pressure on the leading side and its active pressure on the trailing side of the foundation. Therefore, one may find it appropriate to overestimate the passive pressure of liquefiable soil to avoid excessive loading in a passive foundation situation but underestimating the passive and active soil resistance in an active foundation situation may also be applicable, causing engineers

designing foundations in liquefiable soils extreme complications (Gerber 2003; Cubrinovski et al. 2006). Both situations must be separately considered when designing foundations in soil susceptible to liquefaction. More complications arise when considering the location of the liquefiable soil. Specifically, if the liquefiable soil is arranged between two non-liquefiable soil strata, or if the liquefiable strata is overlain or underlain by a non-liquefiable crust or bearing layer, respectively. These can be referred to as three-layered systems or two-layered systems. Furthermore, these are the two most common layered systems studied in research. Research pertaining to two-layered soil systems include: Rollins et al. (2000), Rollins et al. (2001), Mizuno et al. (2000a), Hirade et al. (2000), Gerber (2003), Rollins et al. (2005), Weaver et al. (2005), Ashford et al. (2006), Haeri et al. (2012), and Motamed et al. (2013). Conversely, research pertaining to three-layered soil systems include: Rollins et al. (2006), Cubrinovski et al. (2006), Naeini et al. (2013), and Tang et al. (2015). Additionally, research performed by Abdoun and Dobry (2002) included tests on two- and three-layered soil systems.

2.4.1. Active Foundation

Active foundation is the term associated with a liquefaction event in which the pile behavior is dominated by inertial loadings and/or ground oscillations during excitation. In research, this is simulated by inducing liquefaction via detonated explosives (Rollins et al. 2000; Rollins et al. 2001; Gerber 2003; Rollins et al. 2005; Weaver et al. 2005; Rollins et al. 2006), or applying a base excitation to a shake table (Mizuno et al. 2000, Hirade et al 2000; Haeri et al. 2012) then applying some lateral load to the pile head, or continuing to apply base excitation to induce kinetic forces

from the ground and/or superstructure oscillations. Since the pile response is dominated by inertial loadings in this scenario, piles are subjected to larger shear and bending forces as a result of the liquefied soil losing its resistance.

The Treasure Island Liquefaction Test (TILT) projects incorporates research performed by Rollins et al. (2000), Rollins et al. (2001), Gerber (2003), Rollins et al. (2005), and Weaver et al. (2005). Some of these publications were written about the same tests and results. Therefore, discussing research by Rollins et al. (2000) and Gerber (2003) will also include the remaining publications listed above. The objective of the TILT project was to understand soil and pile behavior following a liquefaction event. This was performed by installing pile groups and single piles throughout the Treasure Island project site, testing their lateral performance in the soil both before and after inducing liquefaction by detonating explosive charges placed at various depths in the soil and various distances away from the test subjects. Comparisons were made from recorded data of the pre-blast tests and post-blast tests. The pre-blast tests were performed as static displacement-controlled tests by use of hydraulic actuators to low displacements. Similarly, post-blast tests were performed as cyclic displacement-controlled tests by use of hydraulic actuators. The tests subjects included a 2x2 pile group, a 3x3 pile group, and multiple single piles. The pile group tests were all comprised of the same deep foundation elements. These were 324 mm outside diameter steel pipe piles. Single piles tested include a 0.6m outside diameter cast-in-steel-shell (CISS) concrete reinforced drilled shaft, a similar 0.9m outside diameter CISS pile, and a 324-mm steel pipe pile. The soil stratification can be generalized into a two-layered soil system for simplification. One liquefiable sand

layer underlain by non-liquefiable materials. More foundation and soil information of these tests are provided in Table 9 found in Appendix A. The results were quantified in terms of secant stiffness related to the resulting load-lateral deflection curves. By the end of post-blast cyclic tests, it was observed that the secant stiffness of the 2x2 pile group and 3x3 pile group had reduced by 70%, and 83%, respectively. Similarly, the results revealed the secant stiffness of the 0.6m and 0.9m CISS piles had reduced by 80% and 89%, respectively. Bending moments from before and after inducing liquefaction were also analyzed and compared. It was noticed that the location of the maximum bending moment changed from before liquefaction to after. The location of the maximum bending moment for the pre-blast tests was located near the middle of the liquefiable layer as compared to the post-blast test results which displayed it near the interface of the liquefiable and non-liquefiable strata for all piles tested. The magnitude of the maximum bending moment was shown to increase at least 60% in some of the test piles. Others did respond differently.

Piles in groups are known to respond differently with respect to each other due to group effects. This was also exhibited in results from the 3x3 pile group responses. It was evident that piles carry more of the lateral load based on their location in the group prior to liquefaction. This was displayed by the center row piles in the 3x3 pile group experiencing higher bending moments during the pre-blast tests as compared to the exterior piles. This is attributed to the overlapping shear zones in the soil associated with the center row of piles. Since shear zones associated with the center piles overlap with the shear zones of exterior piles on both sides, the center piles have lower soil resistance relative to the exterior pile. However, as a result of liquefaction,

it was found that group effects essentially disappear. Therefore, while the maximum moment increased from liquefaction in the exterior piles, the elimination of group effects caused the maximum moment in the center piles to decrease after liquefaction. Gerber (2003) extended this research by additional post-blast tests following liquefaction during the dissipation process to determine the residual strength of the liquefied sand after excess pore water pressure had dissipated. He found that after an hour or so of dissipation, the liquefied soil-pile system recovered up to 48% of its initial pre-blast secant stiffness. He further developed p-y curves for the liquefied soil and observed a unique concave up behavior. This means that as the pile deflection increases, so does the soil resistance. This unique concave up shape was attributed to a phase change from contractive to dilative behavior occurring in the liquefied soil during shearing, which reduces the excess pore water pressure ratio. Gerber (2003) proposed the following empirical formula for developing p-y curves for certain liquefiable sands based on his results. Applicable use of this formula was limited to potentially liquefiable medium dense sands (relative density of about 50%) that do not extend further than 6m below the ground surface.

$$p = p_d * A(B * y)^C \quad \text{... Equation 1}$$

Where,

$A = 3.00 \times 10^{-7} * (z+1)^{6.05}$

$B = 28.01 * (z+1)^{0.11}$

$C = 2.85 * (z+1)^{-0.41}$

p = is soil pressure per length of pile or resistance (kN/m)

y is deflection (cm)

z is depth (m)

p_d = a pile size correction factor defined by the following equation

$p_d = (0.438 + 1.736*d) * (d/0.324)$

d = the diameter or width of the pile or shaft in meters

Research performed by Mizuno et al. (2000) and Hirade et al. (2000) included testing the response of a two pile groups in liquefiable sand by use of a shake table. The piles tips were fixed to the laminar box at the base and therefore, the soil stratification can be simplified to a two-layered system which extended 5.82 meters in total depth. One liquefiable layer beginning at the ground surface and extending to the pile tips underlain by a non-liquefiable material. The test piles were solid steel square sections of 40 cm length and 10 cm width. The objective of this research was to understand the soil and pile behavior during liquefaction and after liquefaction during the dissipation process. Liquefaction was induced in the sand by applying a base excitation to the deposit via a shake table. After liquefaction, oscillator tests were performed during the dissipation process. Similar to Rollins et al. (2000) and Gerber (2003), Mizuno et al. (2000a) found that the depth of the maximum moment increases as a result of liquefaction. This was explained by the deeper soils losing resistance before shallow soils. Furthermore, Hirade et al. 2000 made similar observations to Gerber (2003) as he witnessed a regain in soil stiffness as excess pore water pressure dissipated. This caused the maximum moment to redistribute towards the head of the pile.

Rollins et al. (2006) tested a large diameter (2.59 m outside diameter) shaft in liquefied sand. The test subject was a CISS pile, just as in the TILT project. The soil stratification can be generalized into a three-layered soil system for simplification. A non-liquefiable crust, underlain by a liquefiable layer, which is underlain by non-liquefiable materials. Following the TILT project, Rollins et al. (2006) induced liquefaction by use of explosive charges. Pre-blast static lateral load-controlled tests were conducted prior to inducing liquefaction and post-blast lateral cyclic load-controlled tests were performed following the liquefaction event. Results of the pre- and post-blast tests were compared to determine the effect of liquefaction on soil and pile response. It was observed from the post-blast test results that the maximum bending moment increased up to 100% as compared to that determined from the pre-blast test, which indicated a significant loss in soil resistance. Additionally, similar to Rollins et al. (2000), Gerber (2003), and Mizuno et al. (2000) and Hirade et al. (2000), the location of the maximum moment increased in depth following liquefaction as compared to the pre-blast location. Rollins et al. (2006) further derived p-y curves for the liquefied sand based on the results. These p-y curves were found to be comparable to p-y curves developed in Gerber (2003). Rollins et al. (2006) generated estimated p-y curves based on the empirical formula proposed by Gerber (2003) for the 2.59 m CISS pile. Based on the results, it was determined that the estimated p-y curves developed from the empirical formula proposed by Gerber (2003) agreed well with the p-y curves generated from the test results.

2.4.2. Passive Foundation

Passive foundation is the term associated with a liquefaction event in which the pile behavior is dominated by monotonic pressure applied by a displacing, or laterally spreading soil. In research, this is simulated in multiple ways. Abdoun and Dobry (2002) conducted small-scale centrifuge tests on a single pile and 2x2 pile group in two-layered system. The soil was deposited into a flexible laminar box which was placed on a shake table at a slight incline in the direction of shaking to induce lateral spreading. Cubrinovski et al. (2006) used a laminar box on a large-scale shake table to test a steel pile and a concrete pile simultaneously. After shaking to induce liquefaction of the three-layered system, a loading arm was mounted on the outer side of the box along its height to forcibly displace the surface of the liquefiable layer. Ashford et al. (2006) conducted blast-induced liquefaction tests on a nine-pile group, four pile group, and single piles. The test piles were installed in a generalized two-layered soil system on a mild slope behind a quay wall. Blast-induced liquefaction caused lateral spreading of the surrounding soils towards the quay wall. Haeri et al. (2012) tested aluminum alloy pipe piles using a large-scale shake table and a rigid container. Liquefaction induced lateral spreading was caused by base excitation from inclining the two layers of the soil deposit a few degrees in the direction of shaking, leaving free water downslope of the piles. Motamed et al. (2013) performed large-scale shake table testing on a 2x3 pile group behind both sheet pile and gravity-type quay walls. The two-layered soil system was deposited into a rigid container. The pile group was installed behind a quay wall retaining a free body of water. Liquefaction was induced by base excitation and caused lateral spreading of the surrounding soils

towards the quay wall. Similarly, Tang et al. (2015) used a large-scale shake table and a laminar container to test a single reinforced concrete pile. The pile was installed in a three-layered system behind a quay wall.

Abdoun and Dobry (2002) performed centrifuge tests on piles installed in two- and three-layered systems to compare the effects of each scenario on pile response. The aluminum pipe pile had an outside prototype diameter of 0.6 m. Four of these piles were also grouped together to analyze a 2x2 pile group response of the two-layered system. Frame effects were observed as moments in the grouped piles were decreased when compared to the single pile. The results of the two-layered and three-layered systems were compared for the single pile tests. In both tests, the maximum moment occurred at the interface between the liquefied and non-liquefied strata. Specifically, the three-layered system revealed two maximum moments of relatively similar magnitude, which occurred at both interfaces between the liquefied and non-liquefied manner. However, the magnitudes of these maximum moments were nearly double that of the two-layered system. The maximum moment in each test occurred shortly after liquefaction, during the beginning of lateral spreading. After which, the moment time histories revealed a steadily decreasing moment, which indicated the soil had reached some ultimate soil pressure and then lost resistance. It was visually evident to the authors as they witnessed the soil flowing around the pile in the two-layered system, and the surface crust failed in the three-layered system. When the surface crust failed, the pile cap and head also snapped, which indicated that the pile was pushing into the soil at shallow depths

Haeri et al. (2012) also performed tests on aluminum pipe piles in a two-layered system, but in a large-scale shake table. Seven total piles were installed. One was placed against the wall for visual inspection, and measurements of this pile were not taken. The second pile was installed as a single pile, and far enough away to avoid cross-interaction effects with the other test subjects. Two piles were installed in a line parallel with the direction of shaking. These were considered a two-pile group and the results were compared with the single pile to determine leading and trailing effects. The remaining three piles were considered a pile group and installed in a line perpendicular to the direction of shaking to measure neighboring effects of grouped piles in liquefied soils. The results were comparable to that of Abdoun and Dobry (2002). Specifically, maximum moments in the piles occurred shortly after liquefaction, during the beginning of lateral spreading and were located at the interface between the liquefied and non-liquefied strata. After which, the moment time histories revealed a steady decrease in moment with continued shaking. Which also indicated the soil had reached some maximum ultimate soil pressure applied to the pile, then failed and continued to flow around the piles.

The two single piles tested in Cubrinovski et al. (2006) were a solid steel pipe pile and a pre-stressed high strength concrete (PHC) pile of similar diameter, 31.8 cm and 30 cm, respectively. The results were compared to determine the difference in performance of each. The PHC pile revealed low lateral resistance and displaced with the ground surface throughout the duration of lateral spreading. The high displacement quickly caused the PHC pile to reach its ultimate moment and a plastic hinge was generated at the base of the liquefied layer. The passive pressure of the

surface crust was never able to develop on the PHC pile as there was very low relative displacement between the two. In contrast, the steel pile displayed high lateral resistance and did not follow the ground surface displacement causing high relative displacement between the two. In the initial stages of lateral spreading the steel pile reached a maximum deflection of 5 cm, then resisted further movement as soil continued to flow around it. This behavior is comparable to results found in Abdoun and Dobry (2002). The surface soil reached a maximum passive pressure to the steel pile causing high bending moments at both interfaces of liquefiable and non-liquefiable strata. However, unlike the PHC pile, maximum moments only reached approximately 60% of the steel piles yield moment, which maintained throughout the duration of lateral spreading similar to its deflection. Stiffness degradation factors can be used with the subgrade reaction modulus (k) of a potentially liquefiable soil to estimate p-y curves associated with its liquefied state. Cubrinovski et al. (2006) derived p-y curves of the liquefied soil throughout the test. These were compared with estimated p-y curves derived from a pseudo-static analysis, assuming a constant value of k equal to 15 MN/m^3 throughout the liquefied layer. Stiffness degradation factors were iterated in the pseudo-static analysis until the developed p-y curves agreed well (within 10%) with the curves derived from the measured data. The best-fit stiffness degradation factors were found in the range of 1/30 – 1/80. The lower range values were found to be associated with higher ground displacements (> 40cm). However, at low ground displacements (< 20cm) the influence of the stiffness degradation factor decreases, and the acceptable range was very wide (0.002-0.05).

Lateral spreading has been observed to cause substantial damage to structures near free water. This poses concerns for foundations supporting off-shore structures and quay walls. Research has been conducted to determine the behavior of piles and pile groups located behind quay walls retaining bodies of water subjected to liquefaction induced lateral spreading (Ashford et al. 2006; Motamed et al. 2013; Tang et al. 2015).

Piles used in Ashford et al. (2006) were steel pipe piles with 318 mm outside diameters, 10.5 mm wall thicknesses, and 400 MPa yield strength. As previously mentioned the test piles were installed as single piles, a four-pile group (2x2), and a nine-pile group (3x3). The soil stratification is slightly more complicated than other research presented since this was performed in the field. Generally, the site consisted of a 4m thick loose sand layer beginning at the ground surface, underlain by 3.5m of soft fat clay, followed by a 1m thick layer of loose sand. These materials all rested on dense gravel bedrock. The water table was located at a depth of 1m and therefore, the top 1m of loose sand was not considered liquefiable, but loose sand under the water table (at depth ranges: 1m – 4m, and 7.5m – 8.5m) were liquefiable. Lateral spreading of the loose sand layers caused the clay layer to mobilize with them and subject the piles to its maximum passive pressure. Therefore, this can be generalized as a two-layered system for the purposes of this review. The LPILE software was used to generate curves for comparison with measured data of the single and grouped piles. Grouped piles were simulated in the software as an equivalent single pile with four and nine times the flexural stiffness of a single pile for the 4-pile group and 9-pile group, respectively. P-multipliers were also used in the software analysis to account

for group effects. Additionally, a rotational spring was applied at the equivalent pile head to account for frame effects. For the analysis, the measured free-field soil displacement was imposed on Winkler springs. This was termed a "push-over analysis." Standard p-y curves were developed for all non-liquefiable strata, while the relative density of the liquefiable strata was not high enough to consider any soil resistance. Results computed from this analysis were found to compare well with the measured results. The free-field soil was found to displace more than the piles, which indicated that the loading was being controlled by the passive pressure of the mobile clay layer applied to the piles during lateral spreading. Free-field soil measurements indicated a pattern of increasing ground displacement as the distance from the quay wall decreased. While the mobile clay layer exerted the driving force on the piles, the dense gravel bedrock was applying the resisting force. Maximum bending moments occurred at shallow depths in the dense gravel layer for all tests. Maximum moments experienced by grouped piles were about 50% of that experienced by the single pile for both the 4-pile group and 9 pile group as were pile head displacements. The grouped pile all experienced similar moments with respect to other piles in their group. There was a slight increase in moment magnitude in piles closer to the quay wall as opposed to piles in the same group further from the quay wall observed in the 4-pile group. Two piles in the 9-pile group were of shorter length than the other seven. Therefore, the two shorter piles were not installed as deep into the dense gravel bedrock as their companions. This resulted in a significant decrease in maximum moment experienced by the two short piles as compared to the other seven. Which

indicated that the more fixed the pile tip is installed, the greater moments the pile will experience from a lateral spreading event.

Motamed et al. (2013) evaluated the response of a 2x3 pile group behind quay walls retaining a free body of water using a large-scale shake table shown in Figure 1 below. The test subjects were six steel pipe piles with outside diameters of 152.4 mm and wall thicknesses of 2.0 mm. The piles were grouped by a pile cap and supported 4 steel columns above the ground surface which were loaded with a "superstructure." The setup was shaken with an input base ground motion recorded from the 1995 Kobe earthquake and scaled to 8% of its acceleration amplitude. Ground displacement measurements showed similar behavior to that displayed in Ashford et al. (2006), such that a pattern was observed where ground displacements increased as distance from the quay wall decreased. By the end of shaking, all piles had failed evident by formation of plastic hinges shown below in Figure 3. Additionally, the pile cap tilted seaward, causing the supported columns and superstructure to end in the free body of water shown in Figure 2 below. Pile heads displaced laterally 1.0 – 1.4 m and the top of the quay wall displaced laterally 2.2 m. All piles experienced large bending moments at their connections to the pile cap. Maximum bending moments occurred at the interface between the liquefied and non-liquefied strata for the row of piles on the landward side, while the maximum bending moments in the row of piles on the seaward side occurred at a depth of 2.0 m. This was the same depth to which the quay wall extended. It was concluded that the row of piles on the seaward side were subjected to larger lateral soil pressures, which caused them to experience larger

lateral deflections and bending moments as compared to the row of piles on the landward side.

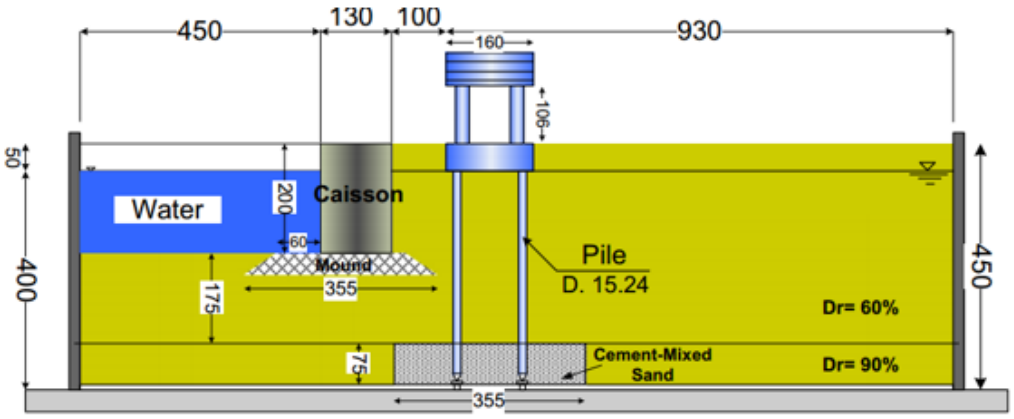

Figure 1: Cross section view of test set-up (all units are in centimeters)

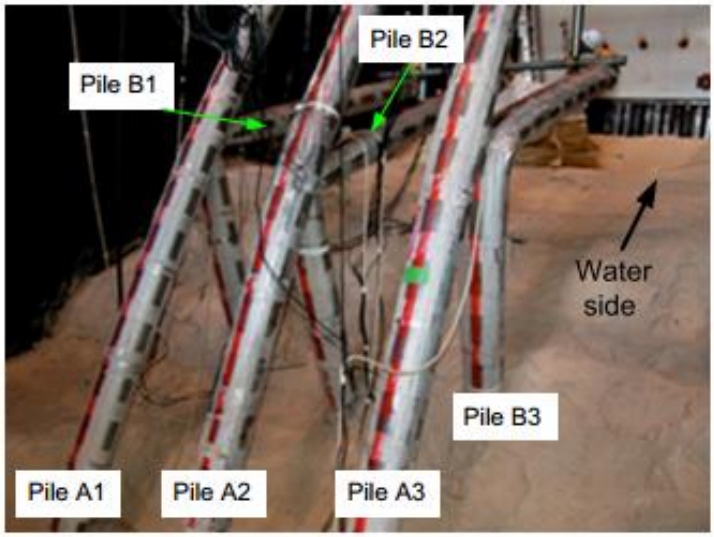

Figure 2: Exhumed Piles After Completion of Test (Motamed et al. 2013)

Figure 3: Plastic Hinge Formation in Test Piles (Motamed et al. 2013)

Tang et al. (2015) conducted a similar shake table study to investigate liquefaction spreading effects on a reinforced concrete (RC) pile. The RC pile had a diameter of 0.1 m and was installed behind a sheet pile quay wall retaining a free body of water. The pile was fixed at the base of the box, and the soil deposit consited of a non-liquefiable clay layer underlain by a layer of medium dense liquefiable sand. This can be considered as a generalized three-layer system for simplification. The model was subjected to a base sine wave excitation with a peak acceleration of 0.2g. Additionally a 60kg weight was mounted to the pile head to simulate a supported "superstructure" for inertial effects. The superstructure was observed to reach a peak acceleration nearly three times that (0.58g) of the input base motion which occurred prior to liquefaction of the soil. After liquefaction, the accelerations of the pile and superstructure reduced significantly. The bending moment increased with depth in the pile. The maximum bending moment occurred after liquefaction, during the initial stage of lateral spreading, at the base of the pile. After which, the monotonic moment

began to decrease as the soil continued to flow around the RC pile, and the pile reponse was controlled by inertial loading. This is comparable to results from Ashford et al. (2006), and the landside row of piles in Motamed et al. (2013).

2.4.3. Mitigation Measures

Some of the presesnted studies on liquefaction have additionally researched methods to lessen the potential and effects of liquefaction. Rollins et al. (2000) conducted pre- and post-blast displacement controlled cyclic lateral tests before and after the installation of stone columns arrayed around the test site. This possible mitigation measure can imporve the performance of the liquefiable deposit in four ways: densification of the soil by virabtion and replacement, increasing lateral stress of the surrounding soil, providing reinforcement as the stone columns are stiffer than the soil, and providing drainage paths to prevent the build up of excess water pressure (Rollins et al. 2000). The twenty-four stone columns were each 0.9 m in diameter and installed in a 4 x 6 grid around the test piles. Additionally, they were spaced 2.4 m center-to-center as shown in Figure 4 below, and installed to the bottom of the liquefiable stratum at a depth of ~6 m. The results revealed significant improvement in secant stiffness of the soil pile systems. The installation of the stone columns increased the pre-blast secant stiffness of the 4 pile group and single pile to 9.3 kN/mm and 10.8 kN/mm, respectively. These are opposed to the pre-treatment, pre-blast stiffnesses of 7.5 kN/mm for both the pile group and single pile. After inducing liquefaction, the treated systems both retained secant stiffnesses of 7 kN/mm, which is 75% and 65% of their respective pre-blast values. This is compared with the resulting stiffness of the two systems before stone column treatment which was 1.8

kN/mm for the pile group, and 1.5 kN/mm for the single pile. The pre-treatment post-blast stiffness only retained 24% and 20% of their respective pre-blast values.

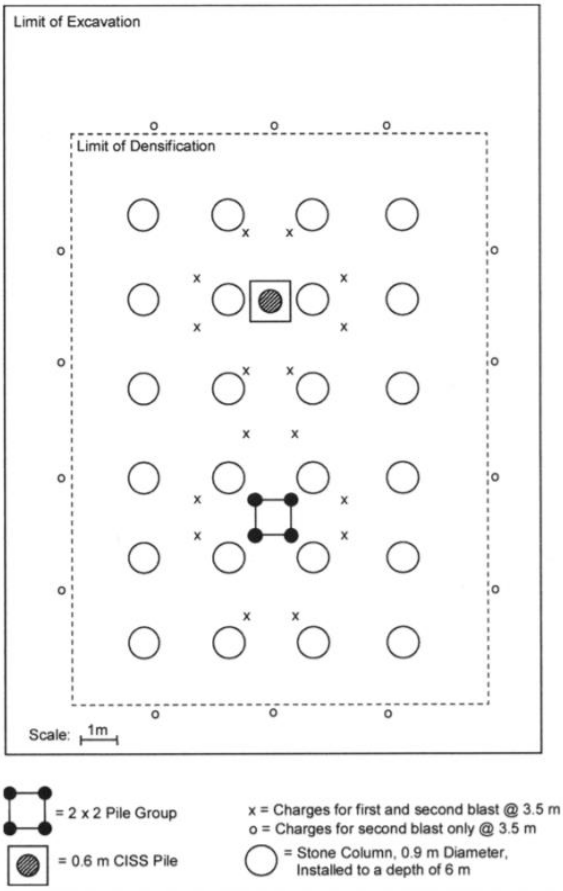

Figure 4:Plan View of Stone Column Placement and Test Set-Up (Rollins et al. 2000)

Mizuno et al. (2000) and Hirade (2000) studied the effect of installing vertical wick drains near the test piles on the liquefaction process and the dissipation of excess pore water pressure process. They found that the vertical wick drains did not prevent liquefaction, the build up of excess pore water pressure, nor did they alter the soil-pile behavior during the liquefaction process. However, the excess pore water pressure did dissipate up to four times faster with the wick drains as opposed to without, which allowed the soil to regain its maximum residual strength much faster.

Abdoun and Dobry (2002) attempted to mitigate the effets of liquefaction of the three layered soil system. The technique studied was to replace the non-liquefiable surface soil surrounding the test piles with frangible material that would yield under constant lateral forces. Soft clay was used to replace the non-liquefiable surface sand which surrounded the piles. This was found to significantly reduce the pile bending moment in the surface layer (from 300 kN-m to 10 kN-m) and reduce the pile head deflection by a factor of two.

Another mitigation method investigated by Mashiri et al. (2015) was mixing the liquefiable soil with recylced tyre chips (TCh) to develop an improved sand-tyre chip (STCh) composite. Strain controlled undrained cyclic triaxial tests were conducted on cylindrical specimens of poorly graded sand 100 mm in diameter and 200 mm in height. This was performed on multiple specimens containing TCh gravemetric content ranging from 0 – 40%. It was found that as the TCh content increased, the damping ratio increased up to a TCh content of approximately 33%, at which the damping ration began to decline. Furthermore, they determined that the liquefaction potential begins to decrease at TCh contents greater that 20% and decreased more as the TCh content increased up to approximately 33%.

2.4.4. Current Design Method in Liquefiable soils (New Zealand)

The following is a concise summary of the following: Ministry of Business (2012a, 2012b, 2013, and 2015) and Boulanger and Idriss (2008). The following summarizes key points in the Canterbury Supplemental Guidelines. This entails some repair, and rebuilding recommendations along with a simple design method and a liquefaction triggering method developed by Boulanger and Idriss (2008) for

cohesionless soils. The New Zealand Method is presented as helical piles are an accepted and commonly used foundation in liquefiable zones.

The Supplemental Guidelines (Ministry of Business 2012a, 2012b, 2013, and 2015) state that for design and repair of foundations in liquefiable soils, Lightweight materials are preferred, particularly for roof and wall cladding which reduces the load on foundations and therefore, reduces settlement from future seismic events expected to cause liquefaction of subsurface materials. Foundations are required to be stiffened and tied together to resist ground deformations and lateral stretch of the underlying soil. Foundation slabs are also recommended to reduce lateral spreading at the ground surface. Shallow foundations are used to minimize penetration of the ground between the surface and the liquefiable strata to prevent liquefaction ejections, a primary mechanism of ground deformation and soil loss. They are also supplied with an underlying slip layer to resist ground deformations at the surface. However, it is not recommended to mix foundation systems within the same structure. Recent research has also demonstrated that decreasing horizontal inertial loads decreases the propensity for vertical settlements during liquefaction events from soil-structure interaction "ratcheting" (Ministry of Business 2013). The first step is then to determine the triggering potential of the liquefiable soil. Boulanger and Idriss (2008) developed a simple method of determining the triggering potential of the liquefiable soil and it is summarized below.

The liquefaction triggering factor is defined as the ratio between the cyclic resistance ratio (or liquefaction resistance ratio) to the cyclic stress ratio. It is defined by the following equation (Boulanger and Idriss 2008).

$$F_L = \frac{CRR}{CSR} \text{ …. Equation 2}$$

Where,

F_L = Liquefaction triggering factor

CRR = Cyclic resistance ratio (liquefaction resistance ratio)

CSR = Cyclic stress ratio

Liquefaction will be triggered if $F_L \leq 1.0$. The triggering factor is determined for the liquefiable soils throughout the depth of the deposit. CSR and CRR are determined from data collected by SPT, CPT, and/or shear wave velocity measurements.

$$CSR = \frac{\tau_{cyc}}{\sigma'_{vo}} \text{ …. Equation 3}$$

Where,

τ_{cyc} = cyclic shear stress

σ'_{vo} = effective overburden pressure at depth Z

$$CSR = 0.65 \frac{a_{max}}{g} \frac{\sigma_{vo}}{\sigma'_{vo}} r_d \text{ … Equation 4}$$

Where,

a_{max} = Estimated PGA (peak ground acceleration)

g = acceleration of gravity

σ_{vo} = total vertical stress

r_d = stress reduction factor accounting for soil flexibility determined by:

$r_d = 1.0 - 0.00765\ z$	for $z \leq 9.15$ m
$r_d = 1.174 - 0.0267\ z$	for $9.15\ m < z \leq 23$ m
$r_d = 0.744 - 0.008\ z$	for $23 < z \leq 30$ m
$r_d = 0.50$	For $z > 30$ m

Or

$$r_d = \frac{(1.000 - 0.4113z^{0.5} + 0.04052z + 0.001753z^{1.5})}{(1.000 - 0.4177z^{0.5} + 0.05729z - 0.006205z^{1.5} + 0.001210z^{2})} \text{ ... ...}$$

Equation 5

CRR is has been empirically correlated to the aforementioned in-situ tests for a magnitude M = 7.5 earthquake and defines the stress ratio that induces liquefaction in 15 cycles. Magnitude scaling factors, or MSF, are then used to estimate CRR for events of different magnitudes and/or different number of cycles. In-situ measurements of shear wave velocity are typically used for gravelly soils while data collected from SPT and CPT can be used to estimate CRR in liquefiable sands, non-plastic silts, or fine-grained soils with PI ≤ 12. Figure 5 below is CRR correlated to SPT data. Measured blow counts must be corrected to the normalized blow count depending on factors such as soil type, plasticity, hammer type, rod length, hammer energy, etc. as follows. The correction factors can be determined from Table 1 below (Boulanger and Idriss 2008).

$$(N_1)_{60} = N_m C_N C_E C_B C_R C_S \text{ ... ...}$$ Equation 6

Where,

N_M = Measured blow count

C_N = Correction for overburden pressure

C_E = Correction for energy ratio

C_B = Correction for borehole diameter

C_R = Correction for rod length

C_S = Correction for sampling method

Table 1:Corrections to SPT (Modified from Skempton, 1986) as Listed by Robertson and Wride (1997)

Factor	Equipment Variable	Term	Correction
Overburden Pressure		C_N	$(P_a/\sigma'_{vo})^{0.5}$ $C_N \leq 2$
Energy ratio	Donut Hammer Safety Hammer Automatic-Trip Donut-Type Hammer	C_E	0.5 to 1.0 0.7 to 1.2 0.8 to 1.3
Borehole diameter	65 mm to 115 mm 150 mm 200 mm	C_B	1.0 1.05 1.15
Rod length	3 m to 4 m 4 m to 6 m 6m to 10 m 10 to 30 m >30 m	C_R	0.75 0.85 0.95 1.0 <1.0
Sampling method	Standard sampler Sampler without liners	C_S	1.0 1.1 to 1.3

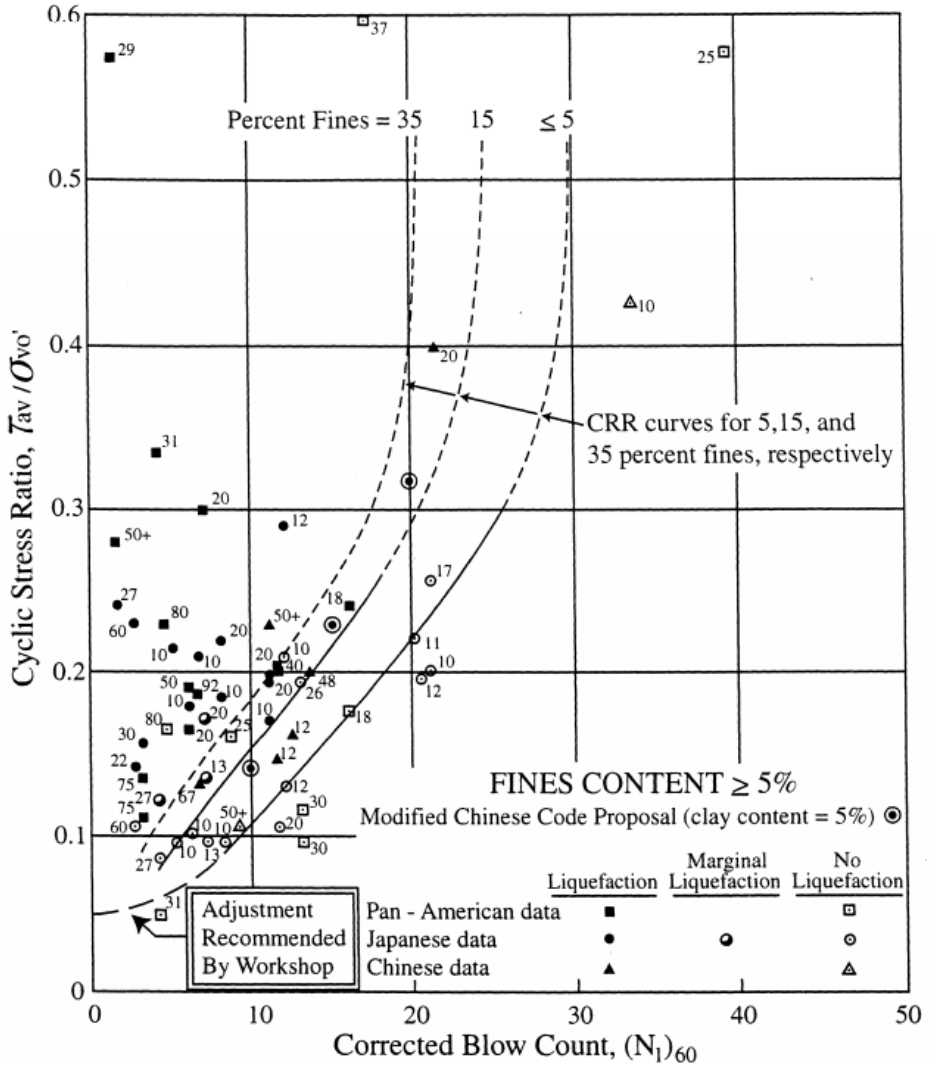

Figure 5:Simplified Base Curve Recommended for Calculation of CRR from SPT data along with Empirical Liquefaction Data (modified from Seed et al., 1985)

(Youd et al., 1997)

After this step is foundation considerations and the design method for deep foundations for potential liquefaction. The following key points are outlined in Ministry of Business (2012a, 2012b, 2013, and 2015):

- Subsurface of the site must contain a clearly identifiable bearing stratum to provide adequate support for the pile type being used

- The bearing stratum must be sufficiently thick to reduce the effects of underlying liquefiable layers and provide enough bearing capacity for piles (3 to 4 meters)
- The bearing stratum must extend far enough along the site to provide uniform support to the entire footprint of the proposed construction
- The piles must adequately transfer the superstructure load to the bearing stratum reliably while also complying with settlement requirements. This must hold true under circumstances such as a liquefiable layer overlying the bearing stratum
- The chosen pile foundations must be designed to withstand potential moderate lateral movement of at least 300 mm at the ground surface relative to the bearing stratum without undergoing brittle shear failure. This must hold true for sites with and/or without surface evidence of lateral movement
- Pile foundations should not be considered suitable for locations where severe global lateral movement, greater than 300 mm, has occurred without special engineering

Similar to any design one must consider the benefits of each foundation option available to them. Ministry of Business (2013) provides advantages and disadvantages of multiple foundation types. They state that helical piles are beneficial as foundations in liquefiable soils. This is due to their unique helical bearing plates which provide the support for most of the structural load. Measurements taken during the torque installation process provide confidence that the helix gets embedded into the target bearing stratum, ensuring that it is supporting the structural load. Since helical piles transfer the structural load to the end bearing via the helical plates, there is minimal skin friction along the shaft of the pile; therefore, preventing excess down-

drag forces along the shaft during a liquefaction event of the overburden materials. However, piles with more than one helical bearing plate cannot contain helixes embedded in the liquefiable strata, or in any deposits which have underlain liquefiable strata. Once installed, the hollow shaft can be filled with concrete, increasing the shaft ductility and allowing the capacity to sustain global lateral movement and limit settlement of the superstructure (Ministry of Business 2013).

A pseudo-static approach is used in the pile design for liquefiable soil, which is comprised of the following six steps (Ministry of Business 2012a, 2012b, 2013, and 2015):

Steps: 1) Formulate ground model

2) Estimate free-field ground deformation

3) Estimate soil-spring parameters

4) Estimate pile moment-curvature relationship

5) Numerical analysis

6) Assess results of analysis

Step 1: Formulate a ground model

The clearly identifiable bearing stratum, which provides adequate support for the structure, must be thick enough to prevent effects from underlying liquefiable soil (3-4 meters). Determine from a deep investigation. Identify the thickness of both surface crust and liquefiable layer.

Step 2: Estimate Free-Field Ground Deformation

The key assumption in this simplified procedure is that the maximum displacement relative to the bearing stratum at the base is 300 mm for residential

projects. If greater lateral movement is expected, then deep pile foundations may not be appropriate. Included in this assumption is the surface crust will displace as a rigid body and the bearing stratum will not displace at all. It is appropriate to assume a linear distribution of lateral movement through each of the liquefiable layers as a simplification. Figure 6 below demonstrates the ground and pile deformation following this procedure.

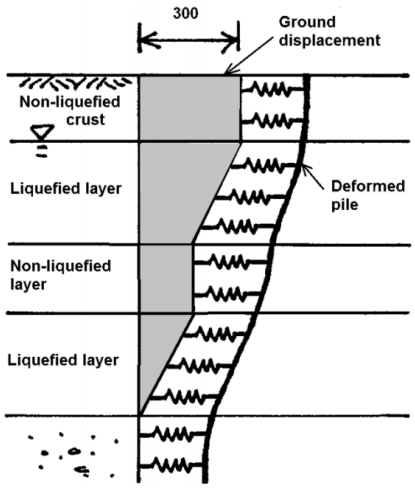

Figure 6: Example of free-field ground displacement for two liquefied layers separated by a non-liquefied layer (Ministry of Business 2013)

Step 3: Estimate Soil Spring Parameters

The simplified procedure estimates soil parameters using Winkler soil-springs. These parameters are estimated following the procedures listed below.

Non-liquefied soils:

P-y curves for non-liquefied soil layers are estimated using empirical methods developed for static lateral pile loading. The soil spring stiffness is given by the equation below.

$$k_i = k_o s D_o \quad \text{... Equation 7}$$

Where,

k_i = spring constant

k_o = coefficient of subgrade reaction

s = spring spacing

D_o = Pile diameter (width)

An empirical relationship has been developed for estimating the soil coefficient of subgrade reaction for laterally loaded piles, k_o, where standard penetration data has been obtained. This can be determined based on the following equation.

$$k_o = 56N(100D_o)^{-0.75} \text{ ... ...} \text{ Equation 8}$$

Where,

N = representative SPT blow count for the soil layer

The representative SPT blow count for the base layer should be taken as the average value over the depth of embedment of the pile into the layer.

Where cone penetrometer tests (CPT) have been conducted instead of SPT then the following equation can be used to estimate the equivalent SPT blow count, N from the CPT data.

$$N \approx 2.5q_c \text{ ... ...} \text{ Equation 9}$$

Where,

q_c = CPT tip resistance (applies to sandy soils)

The yield strength of the soil spring is given by one of the following equations:

$p_{i\text{-}max} = 4.5P_psD_o$ (for non-cohesive soils, surface crust)

$p_{i\text{-}max} = 3P_psD_o$ (for non-cohesive soils, deeper layers)

$p_{i\text{-}max} = 9S_usD_o$ (for cohesive soils)

Where,

$p_{i\text{-}max}$ = yield strength of soil spring

P_p = Rankine passive pressure

S_u = undrained shear strength

s = spring spacing

D_o = Pile diameter (width)

This method provides a linear relationship of soil resistance to a maximum soil resistance as shown in Figure 7 below.

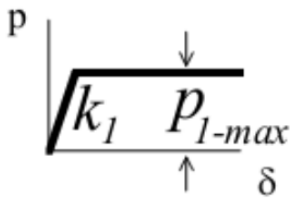

Figure 7:Typical p-y curve for non-liquefiable soils (Ministry of Business 2013)

Liquefiable Soils:

This estimation uses the same method as above, but with some reduction modifications. The soil spring stiffness is reduced by a stiffness degradation factor β_2 after liquefaction has occurred, which can be assumed to equal 0.01. The soil yield resistance is then given by the following equation.

$p_{i\text{-}max} = S_r s D_o$ (for liquefied soils)

Where,

S_r = Residual strength of the liquefied layer

There are methods of measuring the residual strength of liquefiable soils discussed later. However, for this simplified procedure the residual strength can be assumed to be 5 kPa, with a likely range between 5 kPa and 15 kPa. This method should provide a typical p-y curve for liquefiable soils as shown in Figure 8 below.

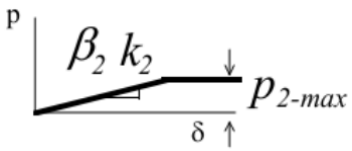

Figure 8: Typical p-y curve for liquefiable soils (Ministry of Business 2013)

Step 4: Estimate pile moment-curvature relationship

This step is extremely important as lateral spreading can induce significant curvatures and plastic hinge formations on deep pile elements near the interfaces of the liquefiable and non-liquefiable soil layers. The plastic hinge formations and yielding are acceptable up to certain strain limits, which are established to ensure the axial capacity of the piles will not be compromised. The moment-curvature relationship must be analyzed well passed the elastic range if it is to provide useful predictions of pile strains. It is noted that simple assumptions of elastic response and first yield moment limits will result in very conservative pile designs. Since the moment-curvature relationship depend significantly on the simultaneous axial loading in the pile, these relationships need to be developed to encompass the range of maximum to minimum axial loading expected during the earthquake. The limiting values of pile curvature should be established in each case based on the recommended extreme fiber strain limits provided in Table 2 below.

Table 2: In-ground plastic hinge strain limits for residential piles (Ministry of Business 2013)

Pile Type	Strain Limits
Pre-stressed solid concrete piles	$\varepsilon_c \leq 0.008$ ($\varepsilon_c \leq 0.005$)* $\varepsilon_p \leq 0.015$
Steel pipe piles	$\varepsilon_s \leq 0.010$
Steel pipe piles (concrete filled)	$\varepsilon_s \leq 0.010$
Timber piles (normal and high density)	$\varepsilon_t \leq 0.0034$

Where,

ϵ_c = extreme fiber concrete compressive strain

ϵ_p = pre-stressing strand tensile strain

ϵ_s = steel shell extreme fiber stain

ϵ_t = timber extreme fiber strain

Step 5: Numerical analysis

The Winkler spring method should be analyzed using suitable software with the following features:

- Spring spacing should be 0.1 m and not larger than 0.2 m
- Elastic-plastic soil spring model
- Bi-linear pile model (tri-linear preferred for reinforced concrete piles)
- Estimated free-field ground displacement as input
- Output including pile curvature versus depth (or bending moment versus depth in format able to be converted to curvature versus depth)

The most commonly used software with the aforementioned capabilities include: LPILE published by Ensoft Incorporated, and Seismostruct published by Seismosoft Ltd.

The end of pile conditions should be set realistically: For most residential dwellings the pile head is unlikely to achieve a structurally fixed condition. For the standard sliding head detail, the pile head should be considered as pinned. The pile head may achieve an effective fixed condition in the surface crust but should be determined by the Winkler spring analysis.

Step 6: Assess results of analysis:

The key output from the Winkler spring analysis should be a plot of pile curvature versus depth along the full length of the pile. A plot of pile displacement versus depth should also be obtained as a useful reality check of the analysis. The peak values of pile curvature should be located near the critical interfaces in the ground model, such as the interfaces between the liquefiable and non-liquefiable layers. If the maximum pile curvature is found to exceed the design limit for the pile than the pile should be considered unsuitable and a different pile section should be selected for another analysis. In general, more flexible and ductile piles will work better than stiffer or more brittle piles.

For rare cases where the water table is at the ground surface and liquefaction may extend to the ground surface without any significant crust to resist lateral instability, then the effect of P-Δ moment should be evaluated and should not exceed 50% of the design limit moment capacity of the piles.

Furthermore, Boulanger and Idriss (2008) suggest a correlation method between the clean sand corrected SPT blow count, or $(N_1)_{60cs\text{-}Sr}$, and the residual shear strength ratio of non-plastic liquefied soils, noted as S_r/σ'_{vo}. After analyzing 17 case studies, which were chosen based on ample in-situ data collected from SPT and CPT testing of the pre-earthquake liquefiable soils, and the reasonably accurate post-earthquake geometries of the failure planes, it was concluded that there should be two different correlations between the clean sand corrected SPT blow count and the residual shear strength of liquefied soil ratios. One correlation for when the void redistribution of the liquefied soil is expected to be significant, while the other is derived for when the

void redistribution can be assumed to be negligible with certainty. Boulanger and Idriss (2007) explain how the former circumstance will occur if the liquefiable layer is confined by strata with extremely low permeability, and there is no escape for the excess pore water pressure induced by ground motion. While the latter of the two circumstances would likely be the case when the excess pore water pressure is able to dissipate quickly, resulting in a reconsolidated layer of denser soil. In order to correlate these values, $(N_1)_{60cs\text{-}Sr}$ must be determined. $(N_1)_{60}$ is first calculated by including multiple correction factors to the measured blow count, including: hammer efficiency, borehole diameter, rod length, etc. Another correction factor must then be included to consider the fines content, or FC. This is shown in the equation below.

$$(N_1)_{60cs-S_r} = K_s(N_1)_{60} \text{ ... ... Equation 10}$$

Where,

K_S = Correction factor for fines content defined by,

$$K_s = 1 + \left[\left(\frac{0.75}{30}\right)(FC - 5)\right] \text{ ... ... Equation 11}$$

If the void redistribution is expected to be significant, then the residual shear strength ratio is defined by the following equation,

$$\frac{S_r}{\sigma'_{vo}} = exp\left(\frac{(N_1)_{60cs-S_r}}{16} + \left(\frac{(N_1)_{60cs-S_r}-16}{21.2}\right)^3 - 3.0\right) \leq tan\varphi' \text{ ... ... Equation 12}$$

And if the void redistribution can be assumed as negligible,

$$\frac{S_r}{\sigma'_{vo}} = exp\left(\frac{(N_1)_{60cs-S_r}}{16} + \left(\frac{(N_1)_{60cs-S_r}-16}{21.2}\right)^3 - 3.0\right)\left(1 + exp\left(\frac{(N_1)_{60cs-S_r}}{2.4} - 6.6\right)\right) \leq tan\varphi' \text{ ... ... Equation 13}$$

2.5. Damping

There are many benefits of placing piles in groups; one of which includes the soil-pile damping capabilities. Damping can be defined as the dissipation of energy in a system subjected to vibrations or cyclic loading. In soil systems, damping is commonly divided into two categories: radiation damping, and hysteretic or material damping. Radiation damping is associated with the absorption of energy through the soil system as waves radiate out from the point of loading and travel through the volume of the soil. As vibrations cause soil to be loaded and unloaded, visco-plastic deformations occur, and the energy loss associated is defined as hysteretic damping. In research, the radiation and hysteretic damping has been determined in soil systems by analyzing hysteretic load-deflection curves or stress-strain curves (Lundgreen 2010). Past studies commonly relate soil damping with shear modulus and have used different means to analyze these properties in different types of soil. Hardin and Drnevich (1972) outlined parameters which greatly influence shear modulus and damping, specifically in sands, to be shear strain amplitude, effective stress level, void ratio, and number of load cycles. Past researchers focused on evaluating soil damping as a function of these parameters. Many studies derived hysteretic stress-strain or load-deflection loops and analyzed damping and shear modulus by use of cyclic triaxial or resonant column testing (Idriss et al. 1978; Kokusho 1980; Kokusho et al.1982; Seed et al. 1986; Wilson 1988; Vucetic and Dobry 1991; Rollins et al. 1998), centrifuge testing (Ellis et al 1998; Zeghal et al. 1999; Teymur and Madabhushi 2002; Pitilakis et al. 2004; Brennan et al. 2005), or analysis of earthquake records (Chang et al 1989; Zeghal and Elgamal 1994; Zeghal et al. 1995). This thesis specifically

calculates damping for the two pile groups in both pinned and fixed conditions using a center-of-mass accelerometer, which will be discussed in more detail in the Methods and Materials section.

3. Methods and Materials

The purpose of this study was to understand the seismic behavior of helical piles in a group configuration under actual seismic loads. In order to get to the point of analyzing the data to start to understand this group behavior, many steps had to be completed over a short timeframe and this chapter discusses those steps.

3.1. Task 1: Strain Gage Instrumentation

Strain gage instrumentation was the most important task because the gages are extremely sensitive. The accuracy of their measurements is a function of tedious pile preparation and gage attachment. Torcsill Foundations LLC and Ram Jack donated newly manufactured helical piles with properties shown below in Table 3. All piles were prepared for instrumentation by sanding down the strain gage locations shown below in Figure 9 through Figure 11. Strain gages must be attached to clean steel for them to stick effectively and record accurate data throughout installation and testing, so sanding off rust and galvanized coatings was essential. As recommended by the strain gage supplier, the strain gage locations were sanded with sand papers of 60 grit, then 120 grit, and finished 220 grit was the final step of sanding. Once sanded, holes were drilled to feed the strain gage wiring through the inside of the piles. After this, the strain gage locations were cleaned with acetone and lacquer thinner to ensure there was no residue or moisture. Strain gages were glued to the steel surfaces and a coat of epoxy was applied to ensure the gages remained locked in place. All strain gages were then tested to ensure they were all in working order before proceeding.

Screwing the piles into dense sand creates high frictional resistance along the pile surface. Therefore, the gages were also covered in fiber glass fabric and resin in

an attempt to keep them protected during installation. Once complete, strain gages were tested again to ensure they were working properly before transportation.

Table 3: Properties of Test Piles and Applied Weights for Phase 3

PILE	TYPE	Outside Diameter (in)	Inner Diameter (in)	Cross Sectional Area (in^2)	Moment of Inertia (I) in^4	Yield Strength, Fy (ksi)	Length of Pile (ft)	Embedment Depth (ft)	No. of Weights	Total Weight on Pile (lb)
P1	3.5" SINGLE HELIX THREADED COUPLE	3.47	2.97	2.16	2.88	65	13	12	2	1693
P2	3.5" SINGLE H. DOUBLE TRHU-COUPLE	3.47	2.97	2.16	2.88	65	12	11	2	1652
P3	3.5" SINGLE H. DOUBLE TRHU-COUPLE	3.47	2.97	2.16	2.88	65	12	11	2	1714
P4	3.5" DOUBLE HELIX	3.47	2.97	2.16	2.88	65	12	11	2	1648
P5	PUSH PILE	3.47	2.97	2.16	2.88	65	12	11	1	818
P6	SQUARE			2.44	3.02	60	12	11	1	955
P7	5.5" SINGLE HELIX THRU-BOLT	5.5	4.65	6.6	21.6	80	14	11.17	3	2724
P8	5.5" SINGLE HELIX THRU-BOLT	5.5	4.65	6.6	21.6	80	14	11.17	2	1731
P9	5.5" SINGLE HELIX THRU-BOLT	5.5	4.65	6.6	21.6	80	14	11.17	2	1545
P10	5.5" SINGLE HELIX THRU-BOLT	5.5	4.65	6.6	21.6	80	14	11.17	3	2742

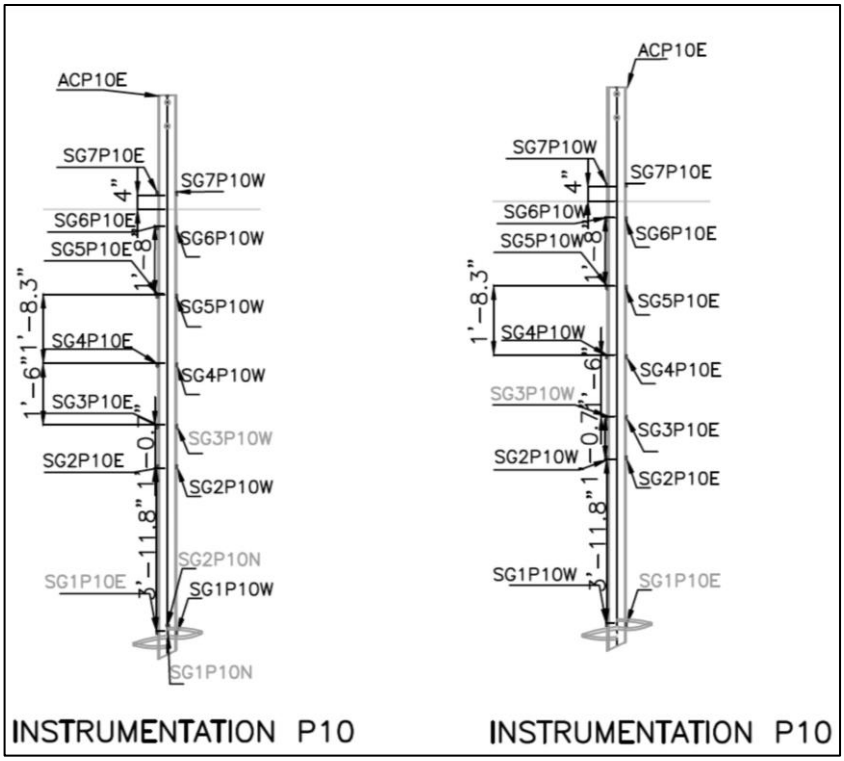

Figure 9: Instrumentation for all 5.5" O.D. Piles (North and South Views)

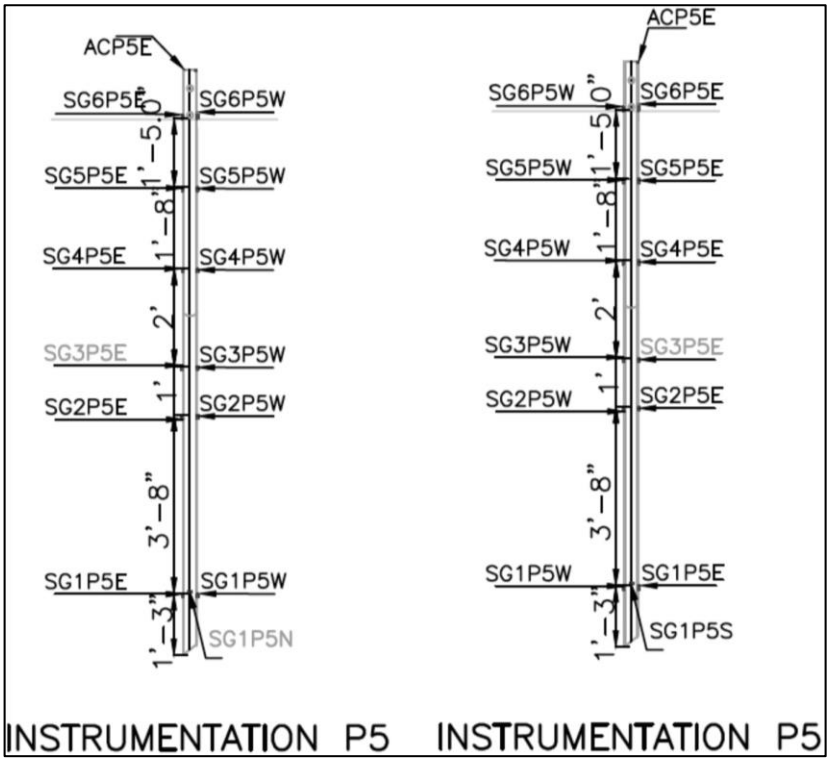

Figure 10: Instrumentation of all 3.5" O.D. Piles (North and South Views)

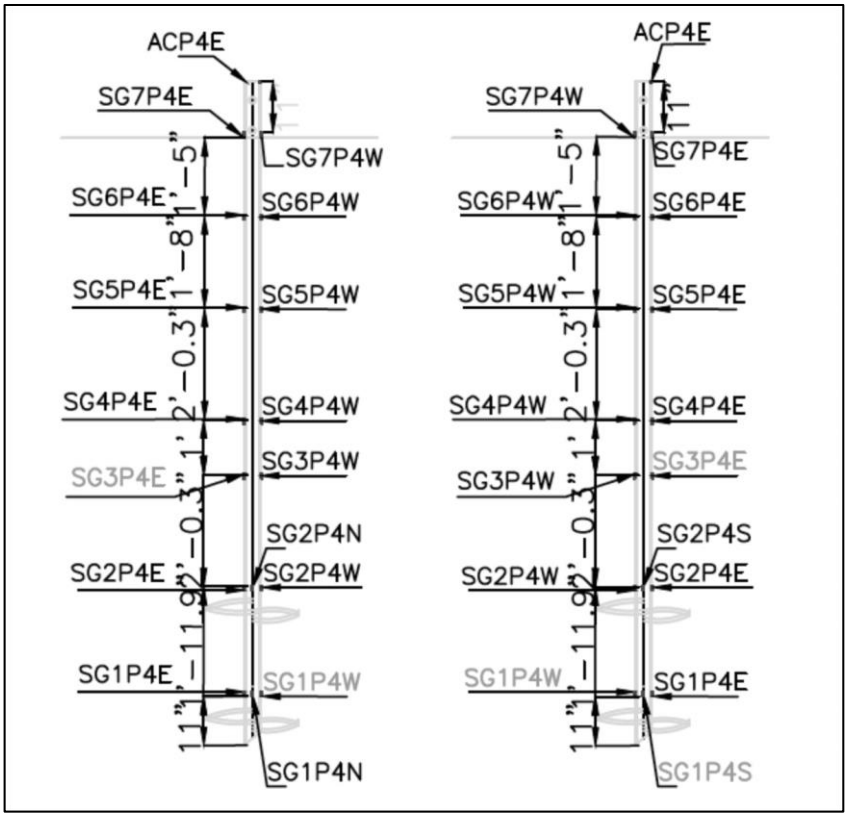

Figure 11: Instrumentation of Double-Helix Pile (North and South Views)

3.2. Task 2: Construction and Instrumentation of the Dense Sand Medium

Collaboration with the University of California – San Diego faculty ensured the laminar box was setup prior to arrival, with 6 feet of instrumented well graded sand already compacted. Therefore, the first task upon arriving at the test site was to compact the dry sand into the laminar box. This was done in 1-foot layers to achieve 100% compaction of the sand. In addition, accelerometers were placed at various locations throughout the sand bed and at the top of each pile to measure the acceleration being applied to the supported weights as shown below in Figure 12. This will help analysis by estimating maximum expected deflections and bending moments the piles experience. Furthermore, string potentiometers were placed at various

locations along the height of the laminar box to measure relative deflections of the soil.

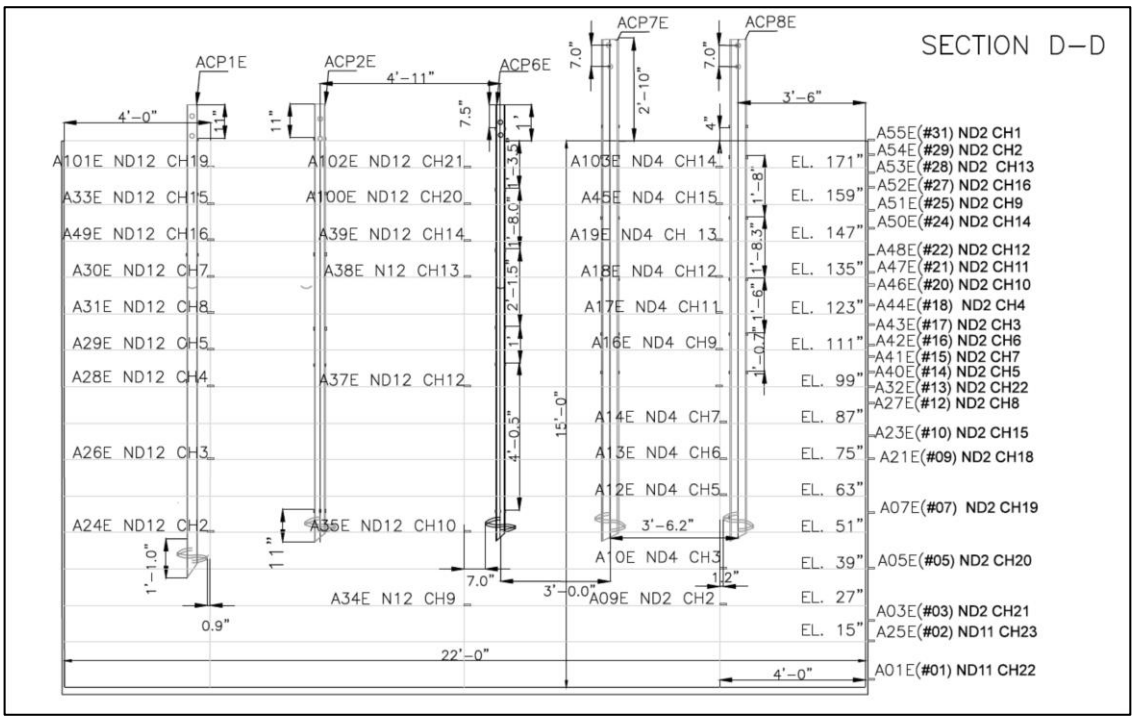

Figure 12: Profile view of Accelerometer Placement

3.3.Task 3: Installation of the Helical Piles

After the sand was compacted into the laminar box, the first shake sequence began. The first shake sequence was to shake the sand bed at 0.1 g peak acceleration pulses and white noise. Analysis of this shake sequence will estimate the shear wave velocity of the sand medium. Afterwards, the helical piles were installed by use of a torque motor, and installation torque was constantly measured so that correlations can be made to estimate the ultimate bearing capacity of each individual helical pile. The test piles were installed into the sand deposit as shown below in Figure 13 and Figure 14. Once installation was complete, a dynamic cone penetrometer test was conducted in the center of the box to determine the relative stiffness of the sand and correlations

will be made to estimate Standard Penetration Test (SPT) N-values, which are commonly used in geotechnical engineering practice.

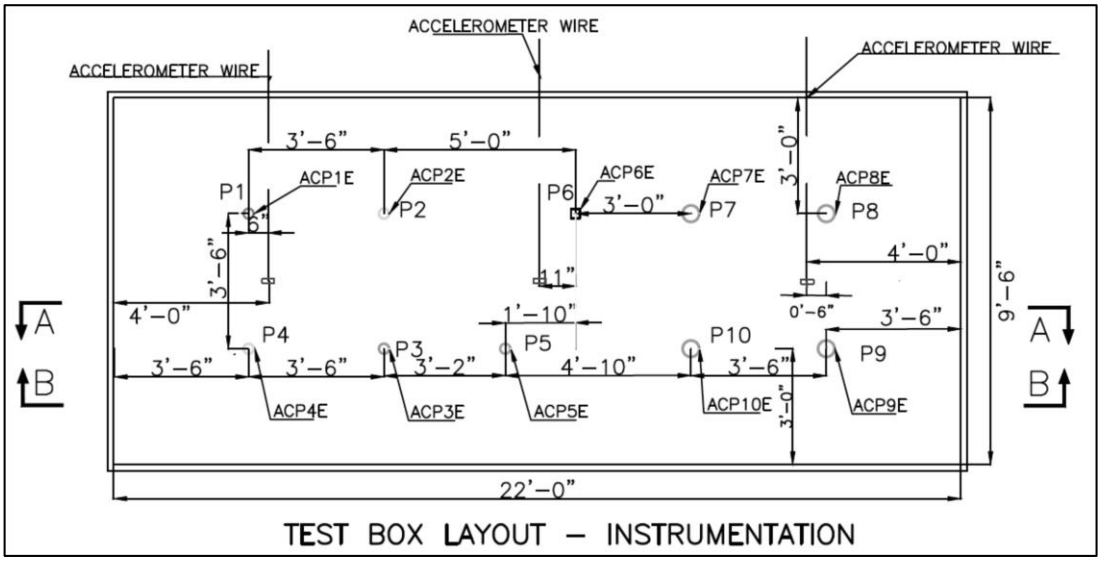

Figure 13: Plan View of Test Set-Up

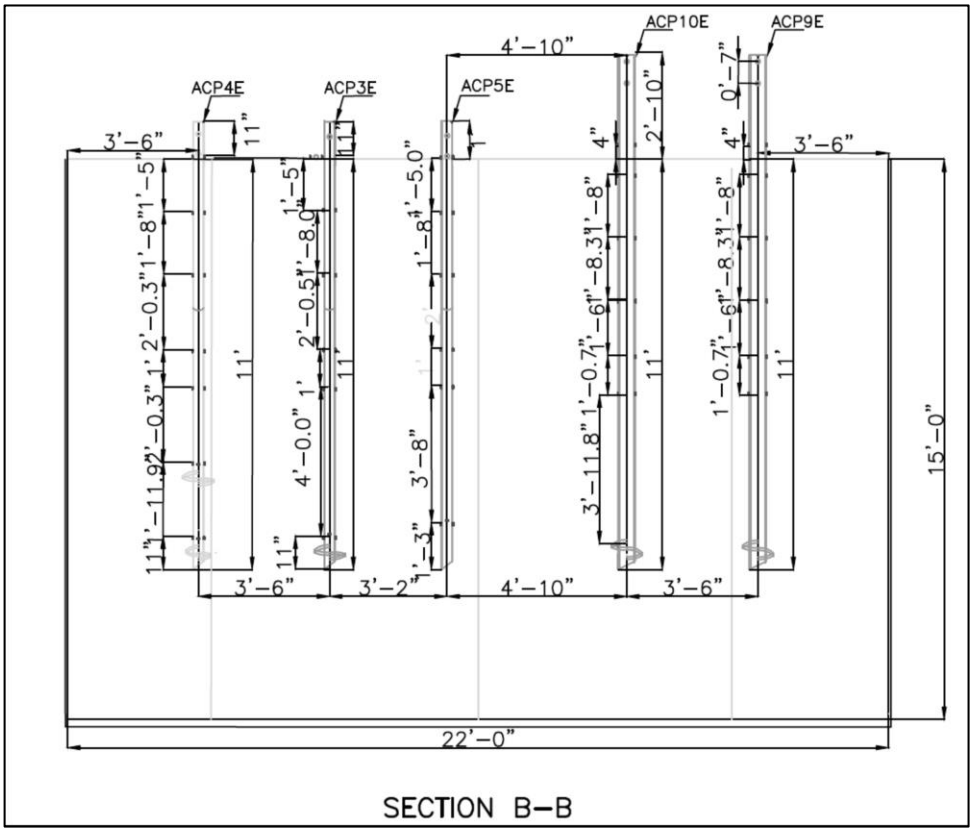

Figure 14: Profile View of Test Set-Up

3.4. Task 4: Shake Sequences

There were four more phases to the shake sequence, making five in total. The first, as mentioned above, was shaking the sand before installation to determine the shear wave velocity of the soil. The second phase subjected the piles to the simulated earthquake ground motion with no weights attached. This data was used to determine the kinematic behavior of the piles themselves. In the third phase, piles were loaded with inertial weights as individual piles as shown in Figure 15. The fourth phase, the piles were loaded with a seismic skid as grouped foundation, in a fixed connection. The fifth and final phase, the piles were also loaded with the seismic skid as grouped foundation, but in a pinned connection. Phases four and five are illustrated in Figure 16 through Figure 21 below. The skids were 7 feet wide by 7 feet deep and 5 feet in height. The skid which connected the 5.5" test piles in a group was filled with approximately 4 feet of loose sand while the skid which connected the 3.5" test piles in a group was filled with approximately 2 feet of loose sand. The measured total weight of the skids and loose sand were approximately 14 kips and 22 kips for the 3.5" and 5.5" pile groups respectively. These weights were measured by the crane used to install them on the test piles. After the desired amounts of sand were placed in each seismic skid, the crane approximately measured the applied weights by lifting each individual skid. The pile caps were constructed to fit the pile heads tightly as shown in Figure 18 and Figure 19 below. Bolts were inserted through the pile caps and pile heads to achieve the desired connection type. Figure 20 illustrates a double bolt connection which simulated a fixed connection by not allowing rotation of the pile caps with respect to the pile heads. Alternatively, Figure 21 demonstrates the

single bolt connection used to simulate a pinned connection by allowing rotation of the pile caps with respect to the pile heads. The bolt connections were chosen as time constraints eliminated concrete pads as an option for fixed connection types.

As mentioned before, the shake table was instructed to simulate two different earthquakes with known ground acceleration data: the 1994 Northridge earthquake and the 1995 Takatori earthquake. The shaking sequence for each phase of testing is listed below and consisted of multiple shakes for each earthquake. The simulations began at 50% amplitude of both earthquakes, then increased to 75% amplitude of both, before finally achieving 100% amplitude of the earthquakes. Furthermore, a simulation of the 1994 Northridge earthquake was conducted on a compressed timescale to model prototypes for future research. In between each shake, the shake table was subjected to an impulse with a peak ground acceleration of 0.1g. This was done to estimate how the shear velocity of the sand is changing from each shake.

Figure 15: Profile View of Phase 3 Test Set-Up

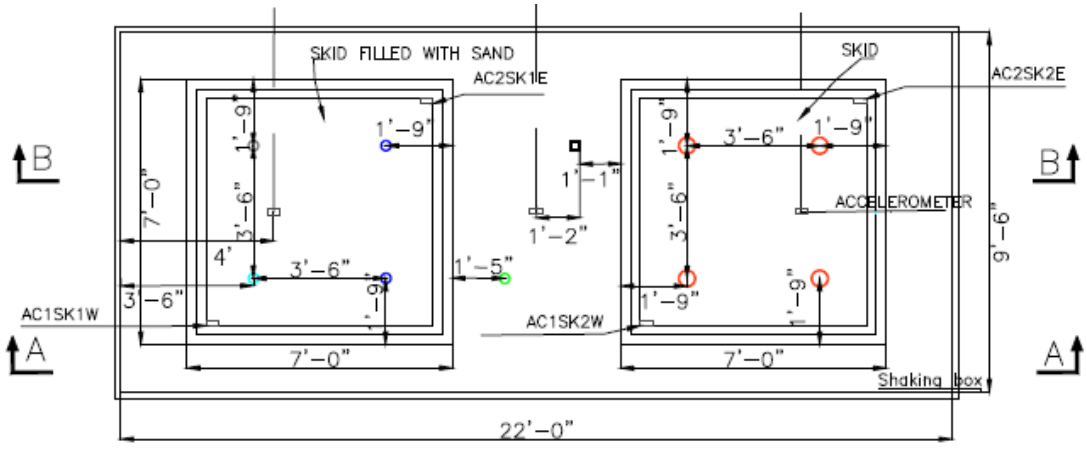

Figure 16: Plan View of Test Set-Up for Phases 4 and 5 with Seismic Skid Dimensions

Figure 17: Profile View of Test Set-Up for Phases 4 and 5

Figure 18: Construction of Grouped Pile Caps

Figure 19: Installation of Grouped Pile Caps

Figure 20: Illustration of Fixed Connection (Double Bolt)

Figure 21: Illustration of Pinned Connection (Single Bolt)

The list below defines the shake sequencing plan and is followed by Figure 22 and Figure 23 which show the input ground motions at 100% amplitude of the Northridge and Takatori earthquakes:

- Stage 1 – Just sand
    - Small pulse before shake to see the state of soil before (0.1g)
    - White noise – 7% g RMS (root mean square)
    - Small pulse
- Stage 2 – 10 piles, with accelerometers at pile heads, no weights (kinematic)
    - White noise – 7% g RMS (root mean square)
    - Pulse (0.1g)
    - Northridge full time-scale (T0) – small amplitude (50%)
    - Pulse
    - Northridge full time-scale (T0) – intermediate amplitude (75%)

    - Pulse
    - Northridge full time-scale (T0) – full (100%) amplitude
    - Pulse
    - Northridge compressed (2 times) time-scale (T1) – full (100%) amplitude (prototype)
    - Pulse
    - Japan (Takatori) full time-scale (T0) – small amplitude (50%)
    - Pulse
    - Japan (Takatori) full time-scale (T0) – intermediate amplitude (75%)
    - Pulse
    - Japan (Takatori) full time-scale (T0) – full (100%) amplitude
    - Pulse
- Stage 3 – 10 piles, with accelerometers at mass heads, concreate weights (inertial)
    - White noise – 7% g RMS (root mean square)
    - Pulse
    - Northridge full time-scale (T0) – small amplitude (50%)
    - Pulse
    - Northridge full time-scale (T0) – intermediate amplitude (75%)
    - Pulse
    - Northridge full time-scale (T0)– full (or more) amplitude
    - Pulse
    - Northridge compressed (2.5 times) time-scale (T1) (prototype)
    - Pulse

    - Japan full time-scale (T0) – small amplitude (50%)
    - Pulse
    - Japan full time-scale (T0) – intermediate amplitude (75%)
    - Pulse
    - Japan full time-scale (T0) – full (100%)
    - Pulse
- Stage 4 – 2 Skids loaded with 30-40kips sand, accelerometers at mass heads (grouped fixed)
    - White noise – 7% g RMS (root mean square)
    - Pulse (0.1g)
    - Northridge full time-scale (T0) – small amplitude (50%)
    - Pulse
    - Northridge full time-scale (T0) – intermediate amplitude (75%)
    - Pulse
    - Northridge full time-scale (T0) – full (100%) amplitude
    - Pulse
    - Northridge compressed (2.5 times) time-scale (T1) (prototype)
    - Pulse
    - Japan full time-scale (T0) – small amplitude (50%)
    - Pulse
    - Japan full time-scale (T0) – intermediate amplitude (75%)
    - Pulse
    - Japan full time-scale (T0) – full amplitude – 100% or more

    - Pulse
- Stage 5 – 2 Skids loaded with 30-40kips sand, accelerometers at mass heads (grouped pinned)
    - White noise – 7% g RMS (root mean square)
    - Pulse (0.1g)
    - Northridge full time-scale (T0) – small amplitude (50%)
    - Pulse
    - Northridge full time-scale (T0) – intermediate amplitude (75%)
    - Pulse
    - Northridge full time-scale (T0) – full (100%) amplitude
    - Pulse
    - Northridge compressed (2.5 times) time-scale (T1) (prototype)
    - Pulse
    - Japan full time-scale (T0) – small amplitude (50%)
    - Pulse
    - Japan full time-scale (T0) – intermediate amplitude (75%)
    - Pulse
    - Japan full time-scale (T0) – full amplitude – 100%
    - Pulse

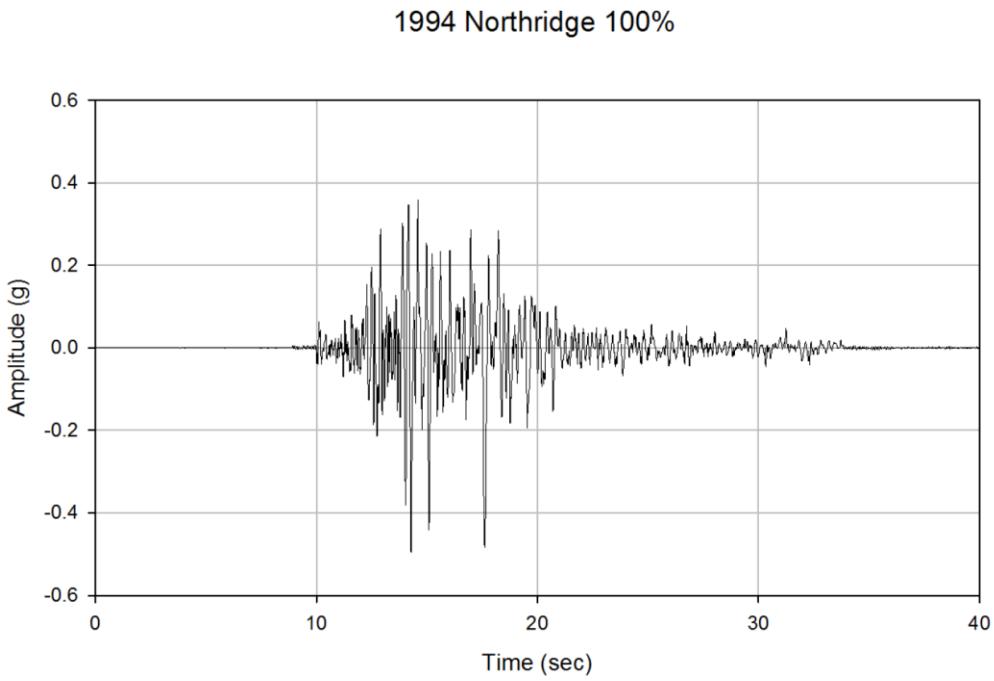

Figure 22: 1994 Northridge 100% Amplitude Input Base Excitation

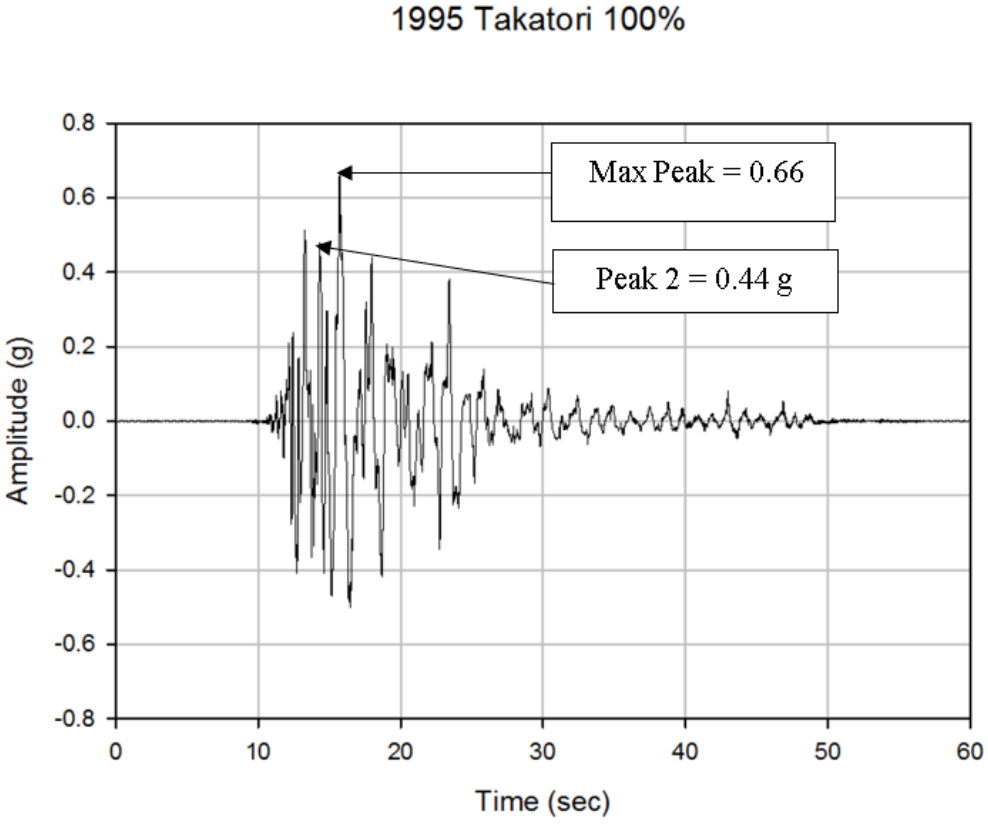

Figure 23: 1995 Takatori 100% Amplitude Input Base Excitation

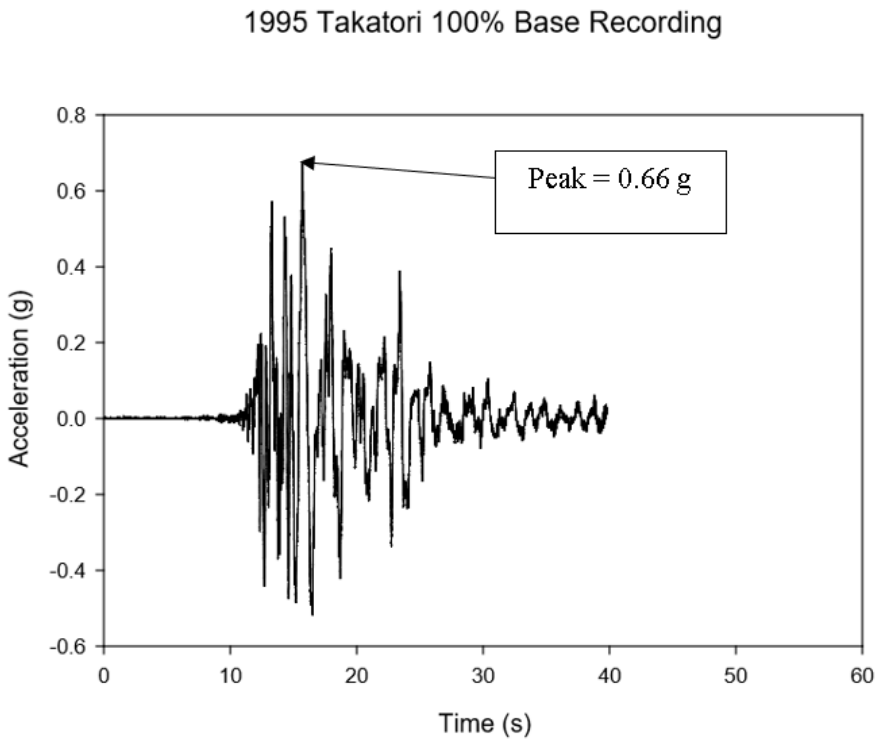

Figure 24: 1995 Takatori 100% Base Recording – Day 2

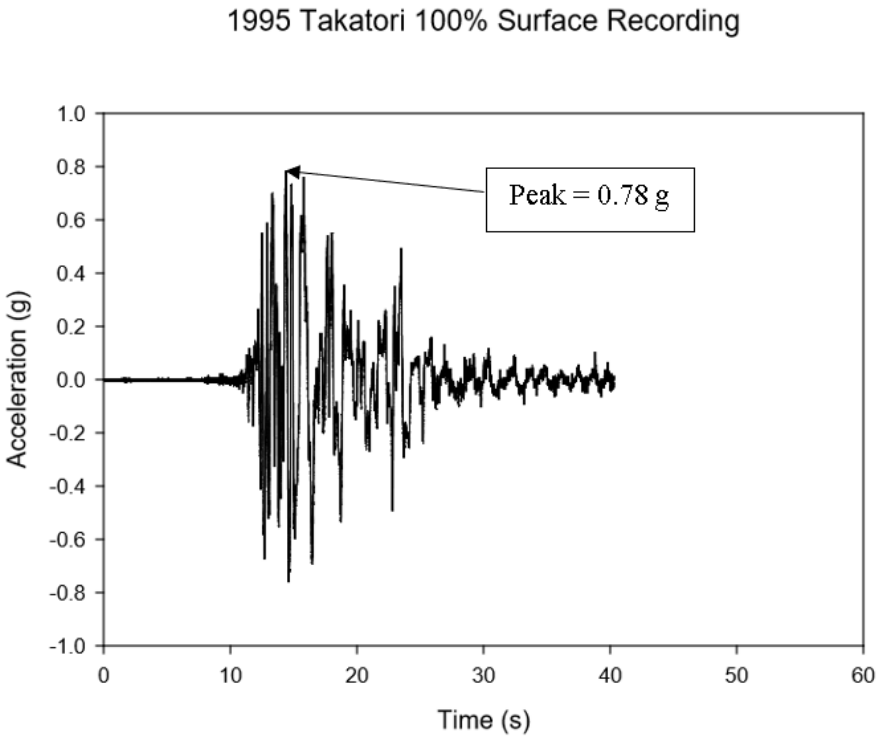

Figure 25: 1995 Takatori 100% Surface Recording – Day 2

Figure 24 and Figure 25 above show the Takatori 100% amplitude motion recorded at the base and surface of the sand bed, respectively. It should be noted that there is some soil amplification observed as the motion progressed through the soil. The input motion and the base recording are very similar, both with maximum peak accelerations of 0.66 g. However, the surface recording reveals a higher acceleration of 0.78 g, and not from the primary peak of 0.66 g shown in the input motion and base recording. Considering just the maximum peaks the system recorded, the soil amplification factor was determined as 1.18. More acceleration recordings for the soil bed and both skids during the Takatori 100% shake can be found in Appendix C.

3.5. Task 5: Soil Testing

Samples of the sand were taken and transported back to the laboratory for soil tests following procedures outlined by the American Society of Testing and Materials International (ASTM) including: moisture content tests (ASTM D4643-08 2008), maximum and minimum index density tests (ASTM D4253-16 and D4254-16 2016), direct shear tests (ASTM D3080/3080M-11 2011), and sieve analysis (ASTM D6913-04 2004).

Table 5 and Figure 27 below summarize the results of tests already conducted on samples of the dense sand deposit. Additionally, triaxial tests were conducted in a companion paper of this research project (ElSawy 2017). Shear wave velocities were estimated by analysis of impulse motions input into the soil system shown in Figure 26. The computation is the difference in depths of accelerometers being used for analysis, divided by the difference in time of wave peaks for each recording. In this example the result is approximately 315 fps. Several analyses were completed

throughout the test sequence, which averaged at 350 fps. According to this result and the site classification shown in Table 4 (ASCE/SEI 7-16) provided by the American Society of Engineers, the system would classify as Site Class E. However, the soil is not a soft clay, and an argument could be made that the depth of the soil profile tested is simply not deep enough to determine an accurate shear wave velocity in this manner. Since the soil used in this study is known to be a dense sand, due to its high relative density and friction angle, it would most likely be classified into Site Class C with a possibility of Site Class D.

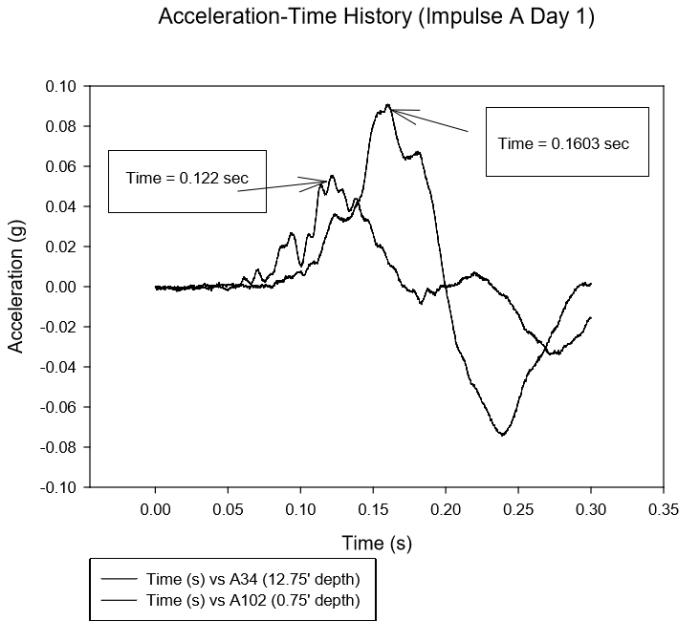

Figure 26: Shear Wave Velocity Analysis

Table 4: Site Classification (ASCE/SEI 7-16)

Table 20.3-1 Site Classification			
Site Class	$\bar{v}_s$	$\bar{N}$ or $\bar{N}_{ch}$	$\bar{s}_u$
A. Hard rock	>5,000 ft/s	NA	NA
B. Rock	2,500 to 5,000 ft/s	NA	NA
C. Very dense soil and soft rock	1,200 to 2,500 ft/s	>50	>2,000 psf
D. Stiff soil	600 to 1,200 ft/s	15 to 50	1,000 to 2,000 psf
E. Soft clay soil	<600 ft/s	<15	<1,000 psf
	Any profile with more than 10 ft of soil having the following characteristics: —Plasticity index PI > 20, —Moisture content $w \geq$ 40%, —Undrained shear strength s_u < 500 psf		
F. Soils requiring site response analysis in accordance with Section 21.1	See Section 20.3.1		
For SI: 1 ft/s = 0.3048 m/s; 1 lb/ft^2 = 0.0479 kN/m^2.			

Table 5: Determined Properties of Well Graded Sand Deposit:

Property	Variable	Measured Value	Units
Avg. Natural Water Content	ω_n	5.5	%
Avg. Maximum Index Density	γ_{dmax}	115.2	pcf
Avg. Minimum Index Density	γ_{dmin}	97.6	pcf
Relative Density	D_r	100	%
Calculated In-Situ Unit Weight	γ	121.5	pcf
Friction Angle (DST)	ϕ_{DST}	47.56	degrees
Peak Friction Angle (CIDC Triaxial)	ϕ_p	53.2	degrees
Constant Volume Friction Angle (CIDC Triaxial)	ϕ_{cv}	51.9	degrees

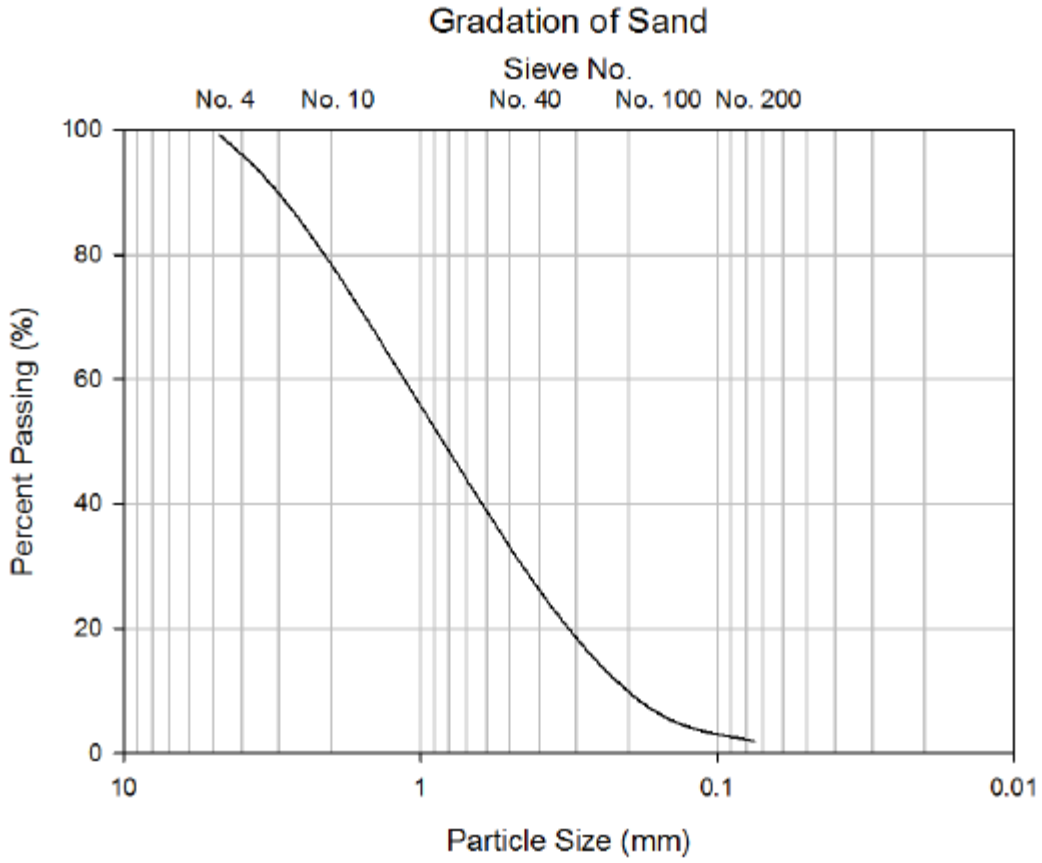

Figure 27: Sieve Analysis of Dense Sand

3.6. Task 6: Compilation of Results/Data Analysis

The strain gage data was filtered and fitted and then read into a MATLAB code to determine values such as bending moment, deflection, shear and soil-reaction curves (p-y curves). The developed soil reaction curves were used to recalculate deflection, rotation, and internal bending moments of each pile to confirm the results. Comparisons were made between the pinned connections and fixed connections of the grouped foundations.

Data collected from the strain gages was used to determine the bending moment at each strain gage for each time step of every shake using the following equation from elastic beam theory:

$$M(lb*ft) = \frac{\varepsilon_{avg}*E(psi)*S(in^3)}{12\frac{in}{ft}} \text{ ... ...} \text{ Equation 14}$$

Where,

$\varepsilon_{avg} = \frac{\varepsilon_1 - \varepsilon_2}{2}$ = Average Bending Strain

$E(psi)$ = Young's Elastic Modulus of the pile

$S(in^3) = \frac{I(in^4)}{y_c(in)}$ = Section Modulus of the pile

$I(in^4)$ = Moment of Inertia of the pile

$y_c(in) = \frac{O.D.(in)}{2}$ = Distance from the outer most fiber to the neutral axis of bending

$O.D.(in)$ = Outer Diameter of the pile

To maintain consistency throughout all calculations, prior to calculating bending moments the raw strain time history data at each gage location was filtered using a Butterworth bandpass filter with cutoff frequencies determined by Fourier Transform Analysis of the respective shake.

These calculations allowed the determination of bending moment diagrams at each time step of every shake and absolute maximum bending moment diagrams of every pile for comparisons which are discussed later in the results section. Furthermore, the bending moment diagrams were used to generate dynamic p-y curves discussed in companion papers of this research project (ElSawy 2017; ElSawy et al. 2017, 2018a, 2018b; Vargas 2017;).

3.7. Damping Calculations

Accelerometer data readings were used to estimate the damping ratios of the system throughout the testing sequence. The effects on the system damping can be determined through comparison of damping estimations calculated by sand bed accelerometer data from prior to pile installation (Day 1), after pile installation (Day 2), and after the addition of inertial weights (Day 3). Furthermore, the effects of the type of pile group connection; fixed (Day 4) or pinned (Day 5); on the system damping ratio, can be determined through damping estimations provided from accelerometers which were attached to the center of the inertial mass supported by the pile groups. Due to the accelerometer locations, separate analysis methods were used to provide more accurate estimations of the entire system damping.

3.8. Damping Estimations by Sand Accelerometer Data (Days 1 & 2)

Dynamic research methods for determining damping and shear modulus typically include analysis of accelerometer data in which multiple accelerometers are arrayed vertically through some soil depth and acceleration time histories are recorded during some applied motion or cyclic loading. From shear beam theory, shear stress at any depth z may be determined through the integration of density times acceleration $\ddot{u}$ through higher levels as shown in the equation below (Brennan et al. 2005).

$$\tau(z) = \int_0^z \rho \ddot{u} dz \quad \text{..... Equation 15}$$

Displacement time histories must be determined through the double integration of acceleration time history data. This is then used to determine shear strain γ time history at the same depth z. If two accelerometers are present a simple first order

approximation may be applied to determine shear strain at the midpoint depth *z*, as shown in the equation below (Brennan 2005).

$$\gamma(z) = \frac{u_2 - u_1}{z_2 - z_1} \text{ ... ...} \quad \text{Equation 16}$$

Once complete, shear stress time history and shear strain time history are plotted together to analyze each shear-strain hysteretic loop. A generalized isolated loop is shown in Figure 28 below.

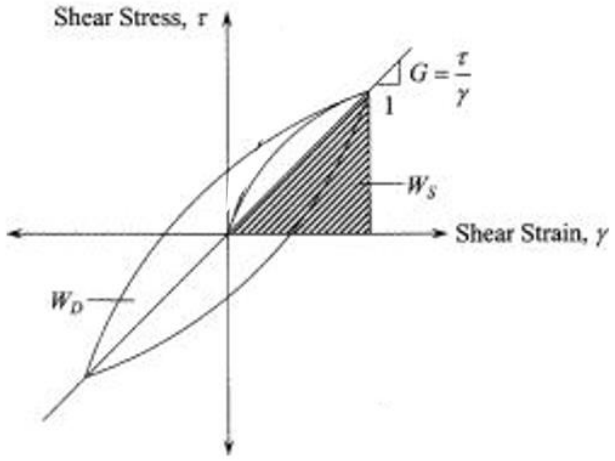

Figure 28: Generalized Stress-Strain Hysteretic Loop

The equivalent damping ratio is then determined by the net work done divided by the maximum elastic potential work times 2π as demonstrated by the equation below. The net work done, and maximum elastic potential work are shown in Figure 28 by W_D and W_S, respectively.

$$D = \frac{W_D}{2\pi * W_S} = \frac{\oint \tau d\gamma}{2\pi * 0.25 * \Delta\tau * \Delta\gamma} \text{ ... ...} \quad \text{Equation 17}$$

Additionally, the shear modulus is found by the ratio of the difference between the maximum and minimum shear over the difference between the maximum and minimum strain as shown in the equation below (Brennan et al. 2005).

$$G_{max} = \frac{\tau_{max} - \tau_{min}}{\gamma_{max} - \gamma_{min}} = \frac{\Delta\tau}{\Delta\gamma} \text{ ... ...} \quad \text{Equation 18}$$

3.9. Damping Estimations by Mass Accelerometer Data (Days 4 & 5)

Similar to the stress-strain method previously described, one can estimate the damping of a pile-soil system by analyzing hysteretic load-deflection curves caused by dynamic or cyclic loading. Rollins et al. (2009) and Lundgreen (2010) express the damping coefficient in terms of the system stiffness as opposed to the soil shear modulus from the following equation.

$$D = \frac{A_{loop}}{2\pi k u^2} \text{ ... ...} \quad \text{Equation 19}$$

Where,

A_{loop} = the area of the hysteresis loop due to one cycle of vibration

$k = \frac{\Delta F}{\Delta u}$ = the stiffness of the pile-soil system

ΔF = the overall change in load of the cycle

Δu = the overall change in displacement

u = the single amplitude displacement

Additionally, Lundgreen (2010) presents an ideal hysteretic load-displacement due to cyclic loading and unloading shown in Figure 29 below.

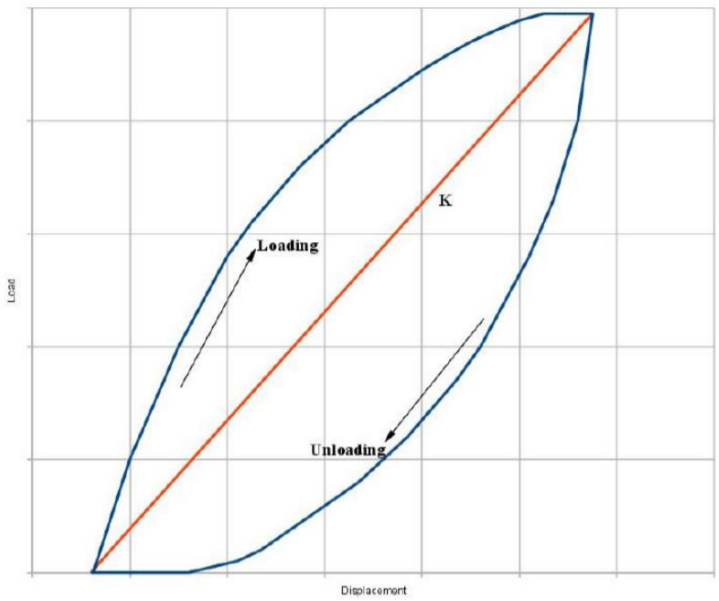

Figure 29: Generalized load-deflection loop (Lundgreen 2010)

This method allows one to estimate the damping by analyzing measurements taken from the top of the system. This is imperative to the accuracy of the damping estimation as it allows the inclusion of the combined contributions made by the soil, piles, and supported mass or structure and will be illustrated in later results.

4. Results

4.1. Bending Moments of Grouped Helical Piles

The following summarizes the results obtained from the relevant data collected during the shakes which simulated the Takatori base motion at 100% amplitude during Days 3, 4, and 5 of the testing sequence. This allows direct comparisons of the effect of grouping piles together as opposed to their behavior from loading them separately as single piles (Day 3) under seismic conditions. Additionally, effects of the group connection types; fixed (Day 4) and pinned (Day 5), are evaluated.

Table 6 below summarizes the axial and lateral loads which each pile was subjected during Days 4 and 5 of this simulation. Skid 1 refers to the 2x2 group of 3.5" outer diameter helical piles while Skid 2 refers to the 2x2 group of 5.5" outer diameter helical piles. The axial loads of both skids were measured using a scale attached to the installation crane. Skids 1 and 2 were measured as 14,000 and 22,000 pounds, respectively. The total axial loads were assumed to distribute equally among each of the four piles included in each respective group. The lateral loads were determined by multiplying the measured axial loads by the maximum horizontal acceleration recorded by accelerometers attached to the center of each skid.

Table 6: Summary of MAX Loads Per Pile from Takatori 100% Shake

	Day 4 – FIXED	Day 5 - PINNED
	SKID 1 - **PER PILE**	
Axial Load (lbs)	3,500	3,500
Lateral Load (lbs)	4,750	4,000
	SKID 2 - **PER PILE**	
Axial Load (lbs)	5,500	5,500
Lateral Load (lbs)	11,750	10,825

Figure 30 and Figure 31 demonstrate immense bending moment reductions due to grouping piles together for both the 3.5” and 5.5” diameter helical piles. The bending moment reduction is apparent in both cases despite each pile being subjected to nearly double the axial load during Days 4 and 5 as opposed to Day 3. These results demonstrate how helical piles exhibit 4 to 7 times the bending moment capacity when grouped in a 2x2 configuration as opposed to being subjected to seismic conditions as individuals.

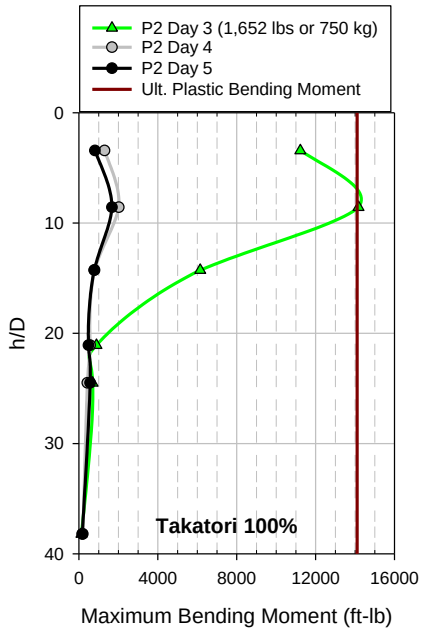

Figure 30: Absolute Max Bending Moment Diagram of 3.5” Helical Pile

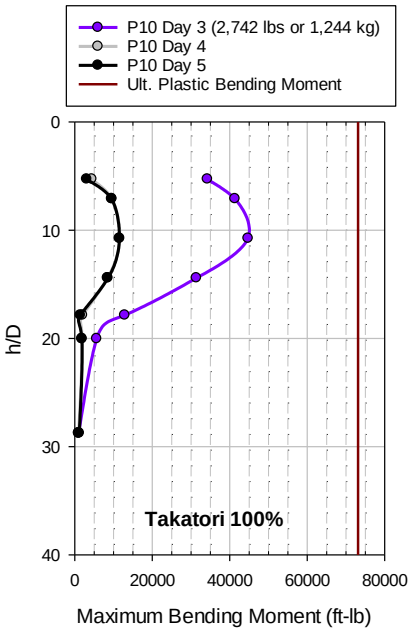

Figure 31: Absolute Max Bending Moment Diagram of 5.5” Helical Pile

Day 4 and 5 results are summarized in Table 7. The total horizontal loads applied to each group of piles was determined by multiplying the total weight of each skid by the maximum acceleration recorded by accelerometers attached to the center of each mass. Furthermore, the maximum horizontal displacements of both skids were determined through a filtering and integration method of the accelerometer records further detailed in the next section. The results indicate smaller lateral loads, displacements, and maximum accelerations for Day 5 when compared to Day 4 though the same base motion

(Appendix C) were applied in both cases. Further inspection of Figure 30 and Figure 31 above validate these trends as Day 5 resulted in slightly smaller bending moment values for both groups. These inclinations are attributed to the effect of the connection type. Steel helical piles are typically associated as ductile elements with small diameter shafts and high slenderness ratios, which therefore give rise to high damping characteristics (Perko 2009). However, the rigidity of the fixed connection appeared to combat this nature, while the pinned connection caused less transmission of the superstructure load and allowed for higher damping ratios. It can easily be seen that a rigid fixed connection to the structure will subject it to higher accelerations, lateral loads, and horizontal displacements. This sequentially causes the piles to endure larger horizontal displacements, shear forces, and bending moments. The connection effects are further explored in the following damping section. Excessive deflections are observed in Table 7 and should be noted these are absolute deflections of the Skids and are not relative to the ground surface. Relative displacements could have been determined if additional accelerometers were correctly placed on the piles just above the ground surface. Additionally, the high deflection results are a side effect of the test set up previously shown. The pile heads extended well above the ground surface and therefore, acted as free-floating beams with no lateral resistance along this length.

Table 7: Summary of Max Group Loads and Deflections from Takatori 100%

	Day 4 (Fixed)	Day 5 (Pinned)
	SKID 1	
Axial Load (lbs)	14,000	14,000
Acceleration (g)	1.34	1.18
Lateral Load (lbs)	19,000	16,000
Displacement (in)	6.8	6.6
	SKID 2	
Axial Load (lbs)	22,000	22,000
Acceleration (g)	2.11	1.94
Lateral Load (lbs)	47,000	43,300
Displacement (in)	7.5	7

4.2. Damping

4.2.1. Days 1, 2, &3

The shake sequence outlined previously in Section 3.4, lists a random content White Noise excitation at the beginning of each test day. These shakes were determined as small strain vibrations to analyze the damping of the system from day to day changes. The following outlines the step by step procedure used to estimate the damping of system during Days 1, 2, and 3.

Random white noise excitation was applied to the soil system prior to pile installation during Day 1, after installation during Day 2, and after addition of inertial weights on Day 3. Figure 32 shows the raw measured acceleration time history of the top accelerometer in the center of the sand deposit at a depth of 0.5 feet. Prior to beginning the analysis method out lined previously, this raw data must be filtered to eliminate any high frequency background noise and low frequency drift errors generated by the accelerometer. This was accomplished by using a Butterworth Bandpass Filter.

The design of the filter is a very important step, and cutoff frequencies should be thoroughly investigated. Brennan (2005) details errors associated with both over filtering and under filtering the raw data. Essentially, the filter should be designed such that data recorded prior to the start of shaking and after completion of shaking should approximately equal zero, as this high frequency noise will alter your integration results. This background noise is easily seen in Figure 32 prior to 10 seconds and post 110 seconds. However, Brennan (2005) also states that high harmonics of the main shaking frequency can exist and should not be filtered out as they contribute to your integration results. High frequency noise is a bigger problem when attempting to derive recorded data as the process of integrating numerical data naturally eliminates most high frequency noise due to unknown constants, usually termed *C*, associated with integration. On the other hand, low frequency drift is typically the biggest problem when integrating numerical data. Therefore, a Fast Fourier Transform (FFT) of the raw data was completed and is shown below in Figure 33. The FFT reveals the frequency content of the recorded motion. The main peaks observed in the frequency content are approximately 5.12 and 23.84 Hz. Further inspection revealed harmonic peaks of up to 80 Hz. Therefore, the lowpass cutoff frequency was chosen as 82 Hz. Choosing a high pass cutoff frequency was an iterative process which began at 0.3 Hz and was incrementally increased until the integrated deflection results were approximately zero displacement from 0-10 seconds and after 110 seconds. The final cutoff frequency was chosen as 3.5 Hz. The filtered acceleration time history is shown in Figure 34. The filtering process consisted of filtering the acceleration prior to integrating to determine the velocity. The velocity was again filtered before integrating to determine the displacement. The displacement was filtered

one last time, to eliminate the need for an initial position measurement, prior to being used for further calculations or results as suggested by Slifka (2004).

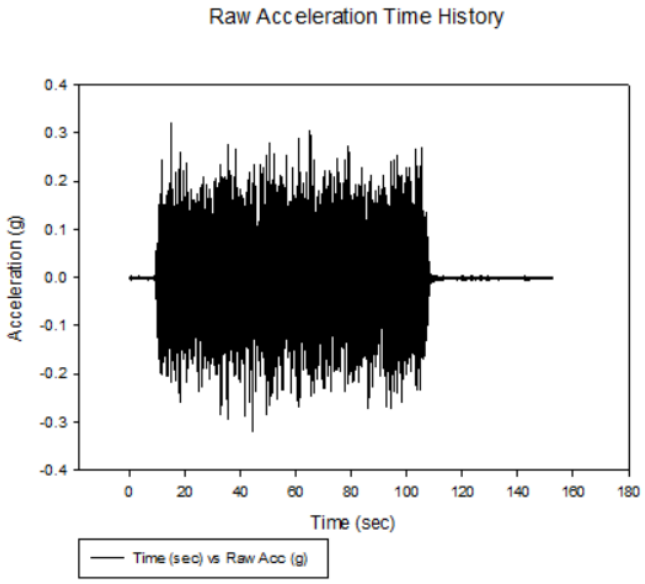

Figure 32: Raw Acceleration Time History of Sand Bed, Day 2 White Noise

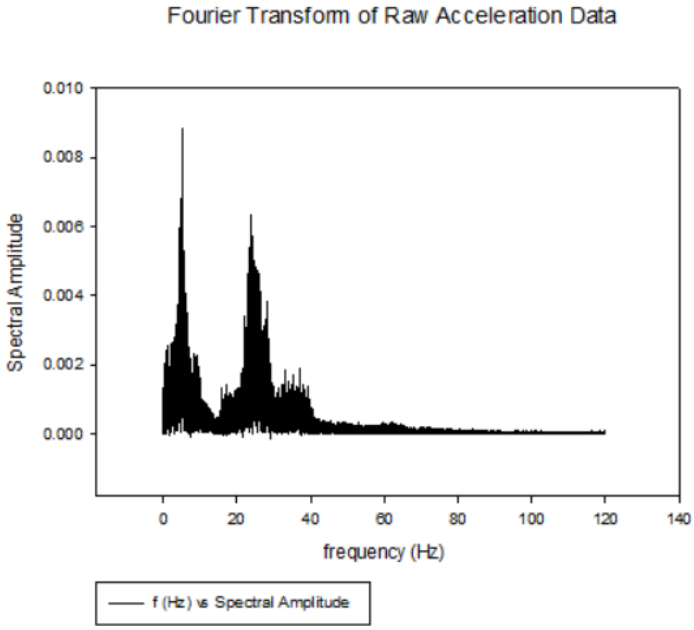

Figure 33: FFT of Top Accelerometer Data, Day 2 White Noise

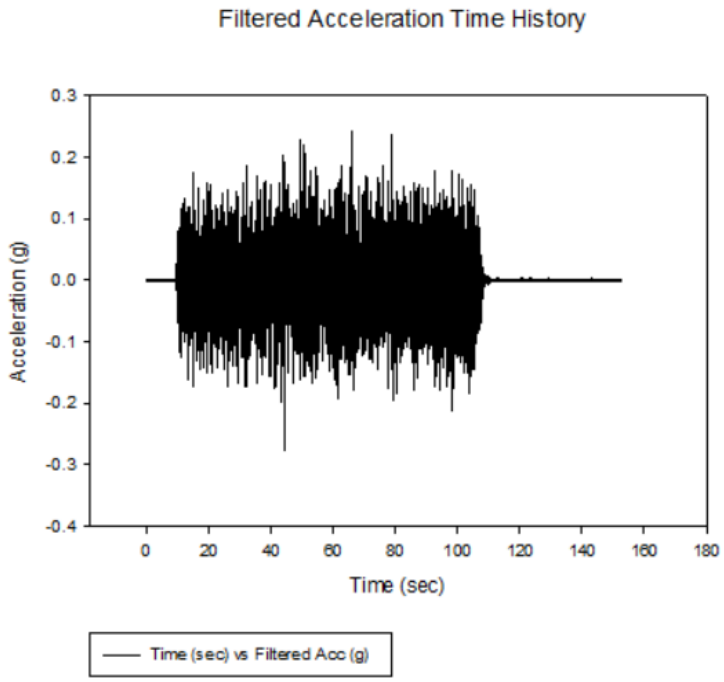

Figure 34: Filtered Acceleration Time History of Sand Bed, Day 2 White Noise

Figure 35 shows the interpolated acceleration time history at a depth of 1.75 feet. This data was obtained by interpolating the filtered acceleration time histories from accelerometers located in the center of the sand bed at depths of 0.75 and 2.75 feet. These same accelerometers were used to obtain an extrapolated acceleration time history of the ground surface. This allowed the use of the expression derived from Zeghal and Elgamal (1995) shown below to determine the shear stress time history at depth 1.75 feet, which is shown in Figure 37. Figure 36 shows the strain time history derived from the first order approximation explained in section 3.8.

$$\tau(z) = \frac{1}{2}\rho z\left(\ddot{u}(0) + \ddot{u}(z)\right) \text{ ... ...} \quad \text{Equation 20}$$

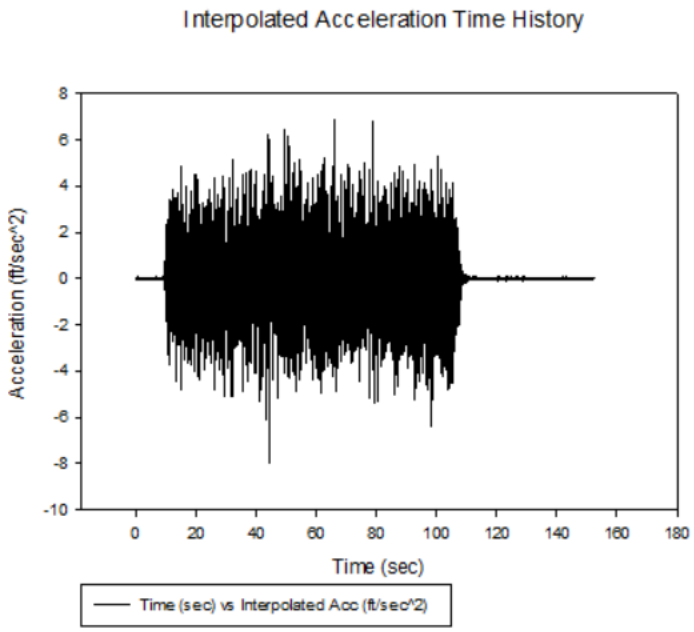

Figure 35: Interpolated Acceleration Time History of Sand Bed at 1.75' Depth, Day 2 White Noise

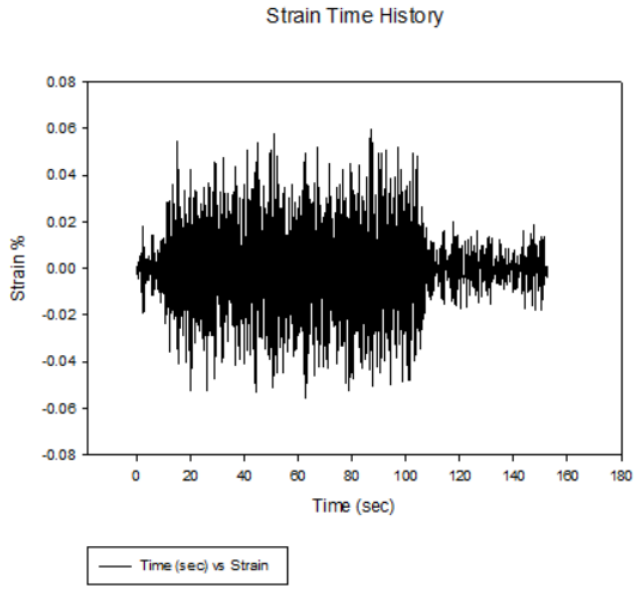

Figure 36: Extrapolated Strain Time History at 1.75' Depth, Day 2 White Noise

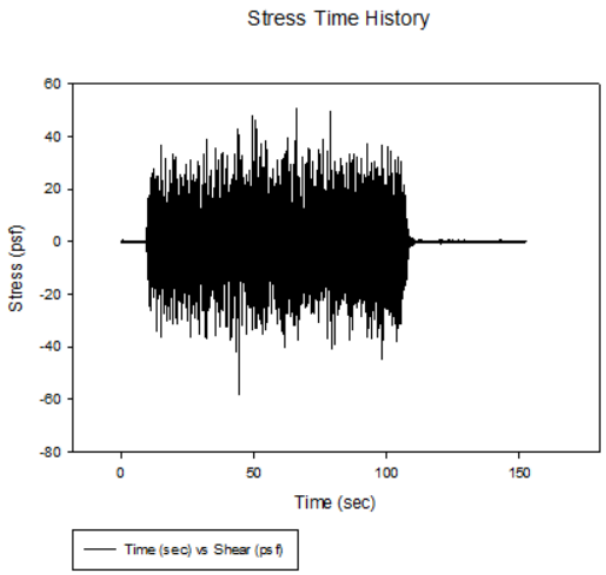

Figure 37: Extrapolated Shear Stress Time History at 1.75' Depth, Day 2 White Noise

The shear stress time history was visually inspected to find shear waves which were approximately symmetrical about the horizontal axis as demonstrated in Figure 38 and Figure 39. These waves typically provided a corresponding strain wave which was also approximately symmetrical about the horizontal axis as shown in Figure 40. The chosen stress and strain waves were then plotted against each other to obtain a complete stress-strain hysteretic loop illustrated in Figure 41 and Figure 42. Figure 42 provides the visual aid of the analysis method discussed in section 3.8 to estimate the damping of the system. This analysis was conducted on measured data collected during Days 1, 2, and 3.

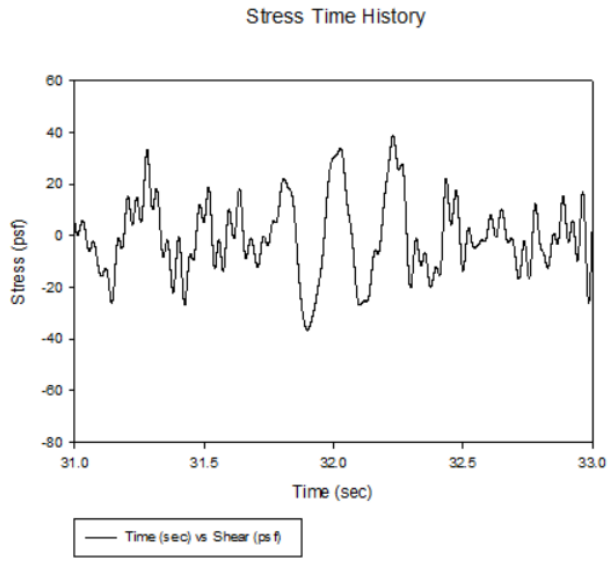

Figure 38: Visual Inspection of Shear Stress Time History at 1.75' Depth, Day 2 White Noise

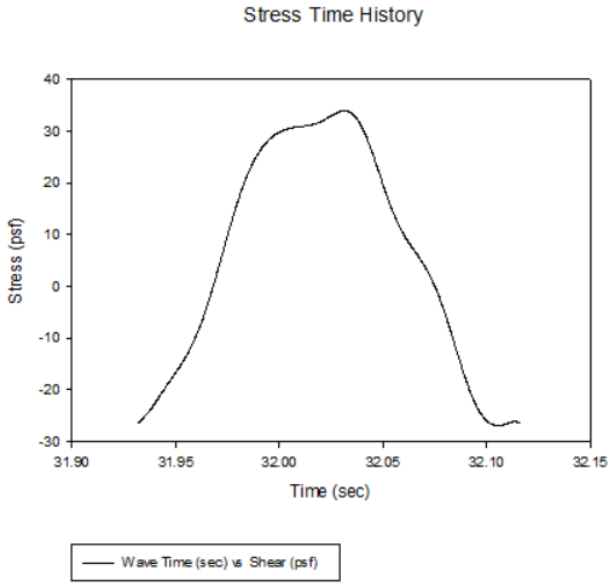

Figure 39: Isolated Cosine Shear Wave at 1.75' Depth, Day 2 White Noise, Wave Time = 31.93 to 32.12 seconds

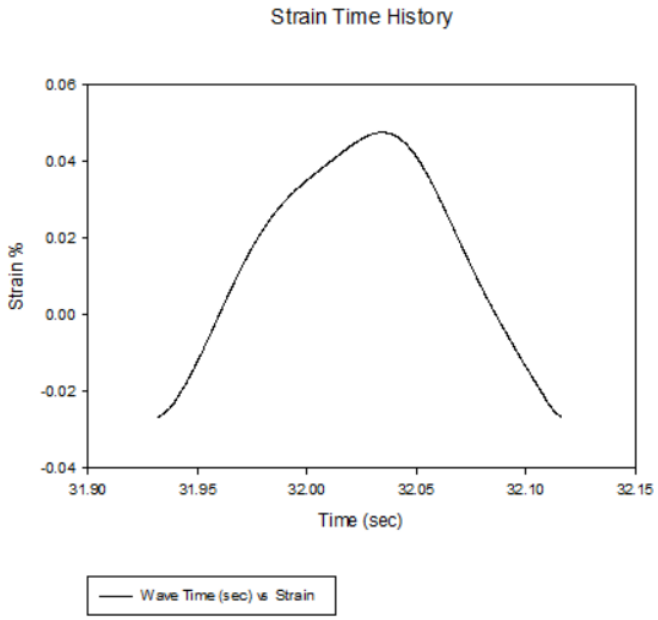

Figure 40: Isolated Cosine Strain Wave at 1.75' Depth, Day 2 White Noise, Wave Time = 31.93 to 32.12 seconds

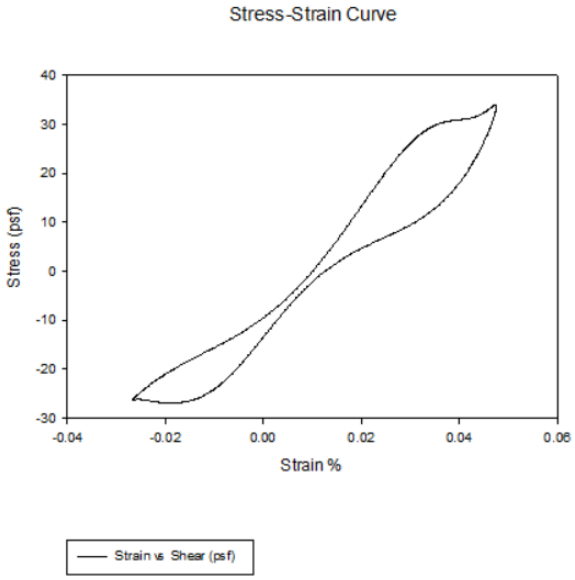

Figure 41: Derived Stress-Strain Curve at 1.75' Depth, Day 2 White Noise, Wave Time = 31.93 to 32.12 seconds

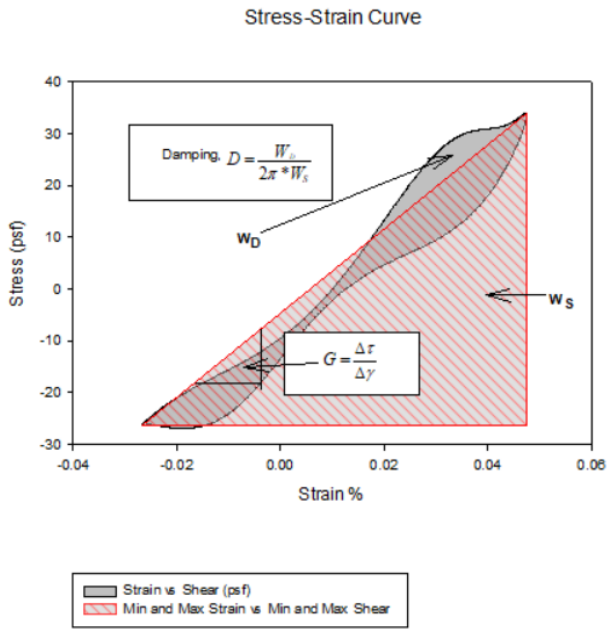

Figure 42: Derived Stress-Strain Curve at 1.75' Depth, Day 2 White Noise, Wave Time = 31.93 to 32.12 seconds

Table 8 shows the summary of the damping analysis results. The soil system from Day 1 resulted in an initial damping ratio of 6.9% with an initial shear modulus of approximately 130,000 psf. After pile installation on Day 2, the damping ratio increased to 8.1% and the shear modulus decreased to 80,000 psf. The addition of helical piles to the soil deposit had a positive impact on the damping of the system, an increase of 1.2% is approximately a 17.4% increase from that of the soil deposit alone. The 38.5% reduction in shear modulus seems large but was expected due to disturbance of the soil compaction from pile installation. Additionally, the white noise excitation on Day 1 was the first applied motion to the system after the soil deposit had been installed into the laminar box at 100% compaction. Therefore, it can be concluded that the 130,000 psf shear modulus is the initial maximum shear modulus of the system, termed G_{max}. Furthermore, it has been shown from past research that the shear modulus will decrease with increasing applied cycles and increasing shear strains (Hardin and Drnevich 1972;

Idriss et al. 1978; Seed et al. 1986; Brennan 2005; Lundgreen 2010). Accelerometers were attached to the pile caps after the addition of the inertial weights on Day 3 to conduct a load-deflection analysis, however the pile caps were oversized and did not rigidly attach to the pile heads. This caused excess vibration readings in all the accelerometers attached in this manner. Filtering procedures were performed but were unable to correct the erroneous recordings. Therefore, the sand bed accelerometers were again analyzed to compute the damping and shear modulus of the system during Day 3. The results were similar to Day 2 at 8.1% damping ratio with a shear modulus of 90,000 psf. It's obvious the Day 3 analysis contains analytical error, as the addition of inertial weights appeared to have no real impact on the system other than slightly increasing the stiffness, which disagrees with typical trends of the shear modulus decreasing with increasing shear strain amplitude, number of cycles, and soil densification due to shaking. Additionally, the damping ratio remained the exact same despite these two factors. These errors are associated with conducting the analysis in the sand bed as opposed to the center of the inertial masses. The location of the analysis caused the contribution to the damping of the loaded helical piles to be completely unnoticed. More stress-strain curves from Days 1-3 can be found in Appendix B.

4.2.2. Days 4 & 5

The following details the results from the hysteretic load-deflection damping analysis for the grouped helical pile-soil system during Days 4 and 5 of the test sequence. The filtering process was performed in the same manner as previously described, however the different frequency content found through the FFT, shown in Figure 44, resulted in different cutoff frequencies. Close inspection revealed harmonic peaks reaching up to 98

Hz, and therefore the low pass cutoff frequency was set to 104 Hz. The high pass cutoff frequency was again determined through the iterative process of starting at 0.3 Hz and incrementally increasing it until the integrated displacements were approximately zero prior to 10 seconds and after 95 seconds, when no motion was being applied to the system. The difference in the raw and filtered acceleration time histories over these time frames can easily be seen in Figure 43 and Figure 45. Accelerometers were placed on the North and South sides of both skids to perform an analysis of higher accuracy. The acceleration time histories were averaged together after filtering, prior to integration.

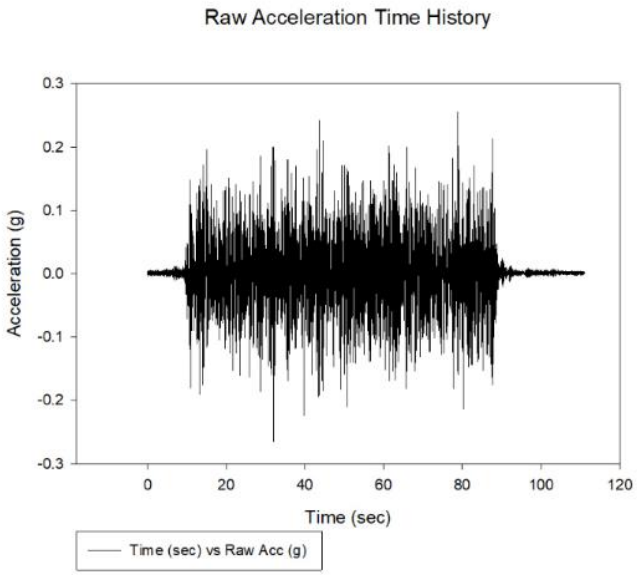

Figure 43: Raw Acceleration TIme History of Skid 2, Day 4 White Noise

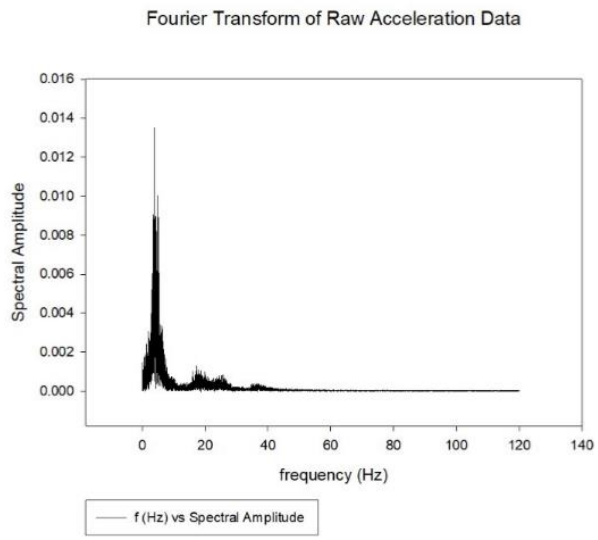

Figure 44: Fourier Transform of Raw Acceleration Time History of Skid 2, Day 4 White Noise

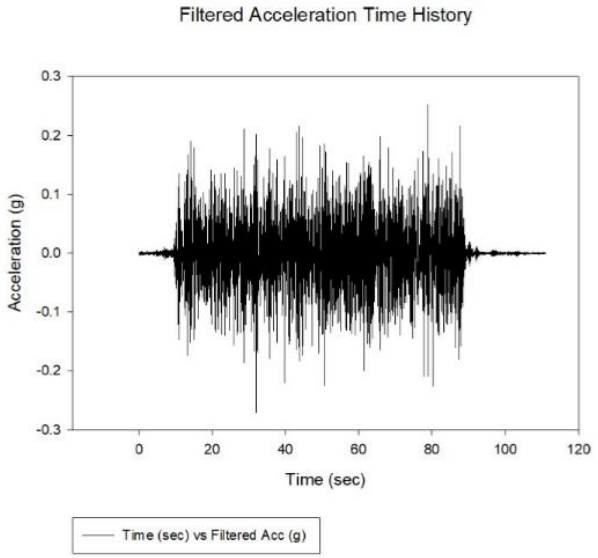

Figure 45: Filtered Acceleration Time History of Skid 2, Day 4 White Noise

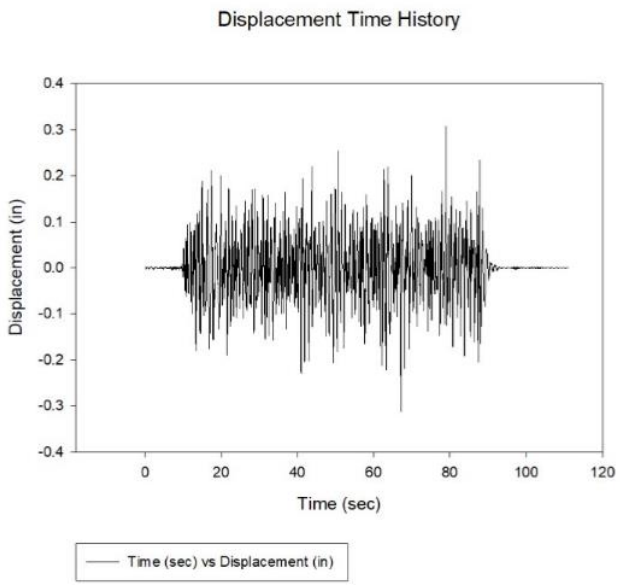

Figure 46: Displacement Time History of Skid 2, Day 4 White Noise

Figure 47 shows the load time history of Skid 2 during the White Noise excitation on Day 4, which was calculated by multiplying the total vertical load by the filtered acceleration time history. To validate the displacement time history shown in Figure 46, a static LPILE analysis was performed on a single pile equivalent. The single pile equivalent was determined by combining the moment of inertia of the four piles included in the 2x2 pile group which supported Skid 2. Since the piles were identical, the single pile equivalent analysis was conducted with a moment of inertia four times that of one of the 5.5" diameter piles. The wall thickness was left constant which resulted in a diameter 1.27 times that of the 5.5" diameter pile for the LPILE analysis. The 22,000-pound vertical axial load was applied to the single pile equivalent along with the maximum horizontal load determined through observation of the load time history provided in Figure 47. Displacement results of the LPILE single pile equivalent static analysis are provided in Figure 48 below, and revealed a maximum pile head displacement of

approximately 0.29 inches, which closely resembles the maximum skid displacement shown in Figure 46 of 0.3 inches validating the analysis method used herein.

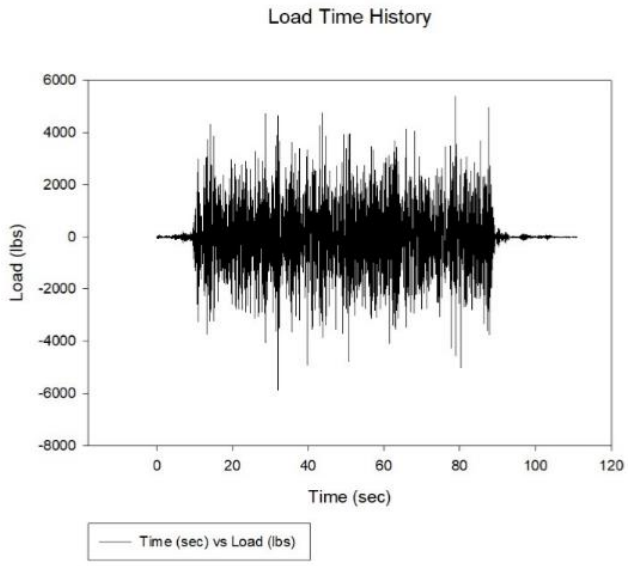

Figure 47: Load Time History of Skid 2, Day 4 White Noise

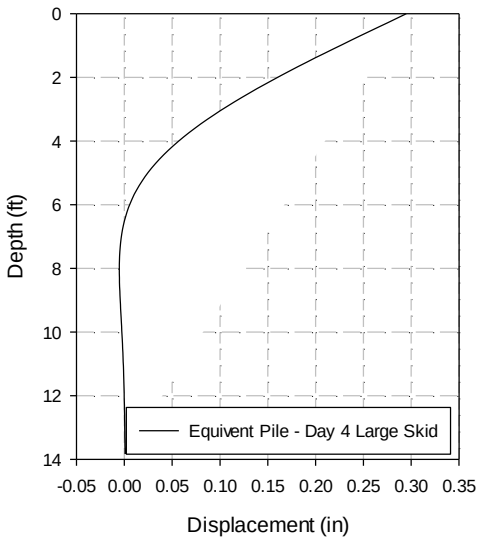

Figure 48: LPILE Static Analysis of Single Pile Equivalent

The load time history was closely inspected to find shear waves which were symmetrical about the horizontal axis as shown in Figure 49 and Figure 50. These waves typically provided displacement waves which were also symmetrical about the horizontal

axis as illustrated in Figure 51. The chosen sine waves were plotted against each other to develop the load displacement curve shown in Figure 52. This same method was also performed on Skid 1 for White Noise excitation on Day 4, and both Skids on Day 5. Figure 53 is a visual aid demonstrating the calculation conducted to determine the damping ratio and pile-soil system stiffness. These results are summarized below in Table 8 for both skids on Days 4 and 5. More load-displacement curves for Days 4 and 5 can be found in Appendix B.

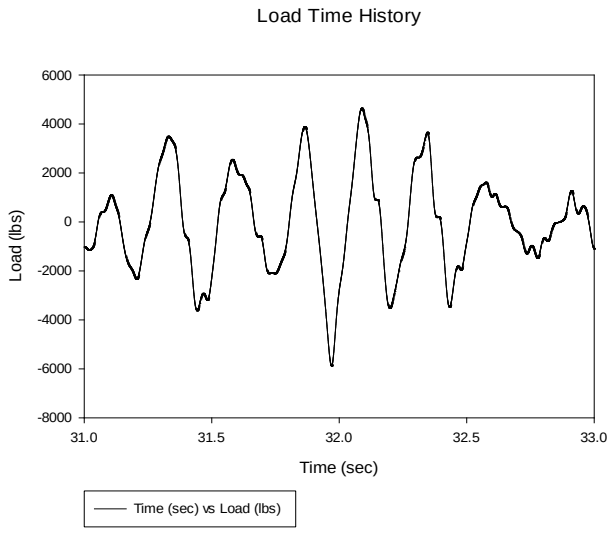

Figure 49: Visual Analysis of Load Time History of Skid 2, Day 4 White Noise

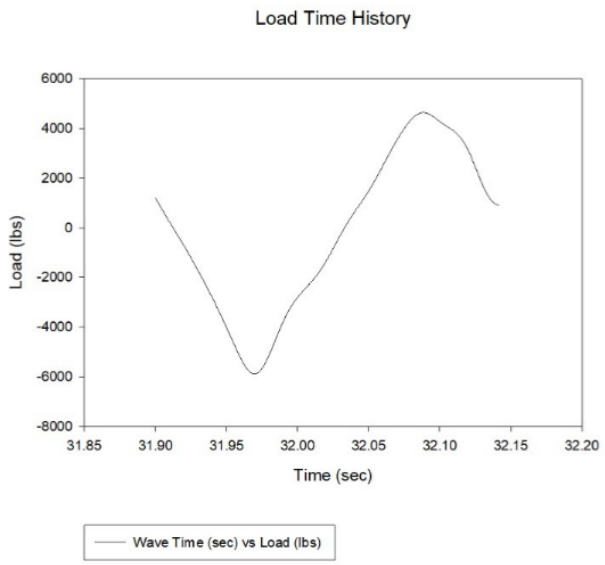

Figure 50: Isolated Load Sine Wave of Skid 2, Day 4 White Noise, Wave Time = 31.9 to 32.14 seconds

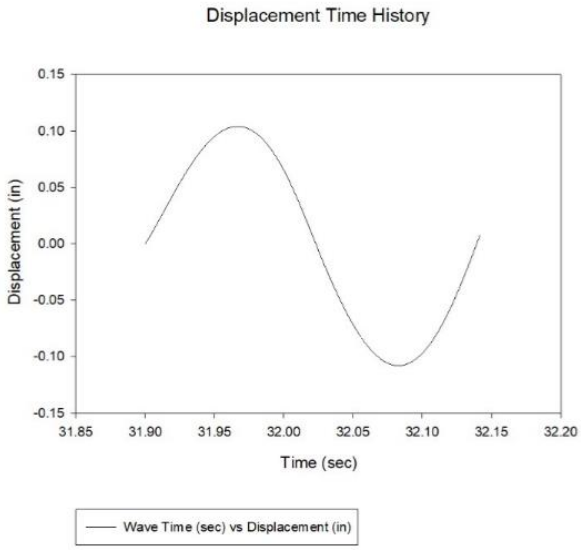

Figure 51: Isolated Displacement Wave of Skid 2, Day 4 White Noise, Wave Time = 31.9 to 32.14 seconds

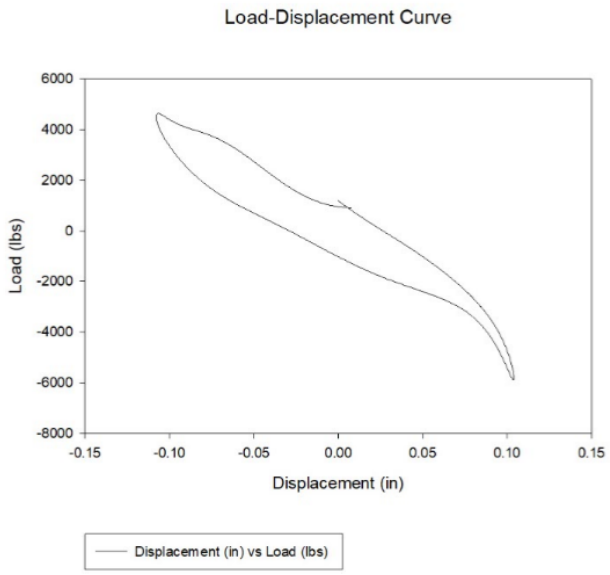

Figure 52: Load Displacement Curve of Skid 2, Day 4 White Noise, Wave Time = 31.9 to 32.14 seconds

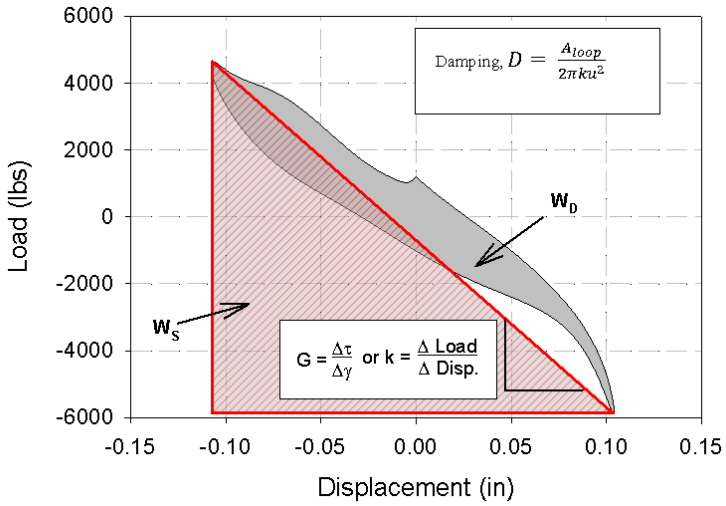

Figure 53: Load Displacement Curve of Skid 2, Day 4 White Noise, Wave Time = 31.9 to 32.14 seconds

The damping analysis of Day 4 revealed similar damping ratios from both sets of pile group. The values determined for fixed connections were 9.3% and 9.4% for Skids 1 and 2, respectively. An increase in damping ratios for both Skids was determined for Day 5. Skids 1 and 2 resulted in damping ratios of 10.6% and 10.9%, respectively. Additionally, the pile-soil system stiffness was calculated for both Skids on both Days of

the test sequence. The small pile group showed stiffness values of 38.4 and 32.6 kips/in for Days 4 and 5, respectively. The stiffness parameters of the large pile group were determined as 49.6 and 49.1 kips/in for Days 4 and 5, respectively. When comparing the Skid box analysis to the soil bed analysis for small displacements and strains, it is observed that the effective damping ratio of the grouped pile-soil system is increased by as little as 1.2% and as much as 2.8% when compared to results obtained from the soil and soil-pile systems of Days 2 and 3, respectively. Additionally, the damping ratio of the system increased by 2.4% to 4% when comparing the soil system from Day 1 to the grouped pile-soil system from Days 4 and 5. Moreover, these results agree with and further validate the observations made in section 4.1. The effect of the pinned connection is clearly visible in comparing the damping results with the values determined from the fixed connection. Grouped piles in pinned connection resulted in an average of 1.4% increased damping ratio over the two different sets of pile groups when compared to that of the fixed connection. Yet, the fixed connection, once again, showed increased stiffness to that of the groups in pinned connection. These results detail the reasons why the Day 4 pile groups experienced higher accelerations, bending moments, and horizontal deflections than the pile groups from Day 5 as stated in section 4.1. Final conclusions on this research are detailed in the following section.

Table 8:Summary of Damping Estimation Results

Day	System and Condition	Damping Ratio		Shear Modulus/ System Stiffness
1	Soil Only	6.9%		130000 psf (6.2 MPa)
2	Soil With Single Piles No Weights	8.1%		80000 psf (3.8 MPa)
3	Soil With Single Piles Weighted	8.1%		90000 psf (4.3 Mpa)
4	Soil With Group Piles Weighted : Fixed	3.5"	9.3%	38.4 kip/in
		5.5"	9.4%	49.6 kip/in
5	Soil With Group Piles Weighted : Pinned	3.5"	10.6%	32.6 kip/in
		5.5"	10.9%	49.1 kip/in

Soil Bed Analysis

Skid Box Analysis

5. Conclusions

This paper presents the results of a full-scale shake table study of helical piles installed in a dense sand medium. Then seismic behavior of helical piles loaded individually and grouped in 2x2 configurations was evaluated. Additionally, effects of pinned and fixed connections were investigated in grouped helical piles. The following discoveries were made:

- Filter design is a very important step when integrating numerical data and incorrect cutoff frequencies and/or methods can cause exponential errors in the analysis and results
- Grouped helical piles exhibited significantly reduced bending moment, horizontal accelerations, and lateral displacements as opposed to individual piles when supporting nearly twice the per pile axial load.
- Accurate soil-pile system damping estimations can only be determined through measurements taken at the top of the soil-pile system.
- The installation of individual helical piles into a dense sand medium enhanced the damping and decreased the shear modulus of the soil system due to soil disturbance during the installation process.
- General trends from past research studies of increasing damping ratio and decreasing soil shear modulus with increasing number of cycles and increasing strain amplitude were observed in this study
- When comparing the Skid box analysis to the soil bed analysis for small displacements and strains, it is observed that the effective damping ratio of the grouped pile-soil system is increased by as little as 1.2% and as

much as 2.8% when compared to results obtained from the soil and soil-pile systems of Days 2 and 3, respectively.

- The damping ratio of the system increased by 2.4% to 4% when comparing the initial soil system (without piles) to the grouped pile-soil system for small strain and small displacement analysis.
- The 5.5” diameter pile group displayed greater stiffness parameters when compared to the 3.5” pile group, but both exhibited nearly identical damping ratios, indicating that all elements installed into the soil deposit acted as one system.
- When designing a helical pile foundation system under seismic conditions, the connection type should be strongly considered. While a fixed connection will provide greater stiffness and therefore, lower deflection for a given load, a pinned connection will increase the damping of the system and decrease horizontal accelerations and bending moments transmitted between the foundation and superstructure.
- A static LPILE analysis can approximate the lateral deflection of a pile group subjected to seismic loading for small displacements using a single pile equivalent of which the equivalent moment of inertia is equal to the summation of the pile group’s moment of inertia. Additionally, the equivalent wall thickness should equal the average wall thickness of the piles in the group. This will allow the equivalent pile diameter to be determined.

- Helical piles performed satisfactorily under seismic conditions throughout all testing in the dense sand medium, revealed no signs of degradation after exhumation; even after bending moment calculations indicated some piles achieved their ultimate plastic bending moment, and therefore warrant consideration for research in seismically active areas.

6. Recommendations for Future Works

In terms of the experimental considerations for future projects, the following recommendations for future research include:

- Measurement and/or calibration of instrumentation before and during the installation process
    - One of the goals of this study was to determine the axial load distribution along the helical pile shaft to analyze the contribution of the helical plates. However, failing to record strain gage measurements prior to and during pile installation left permanent crowd (installation) forces in the piles which could not be determined and made it impossible to determine effected the axial load distribution.
- Further steps to increase protection of strain gages in dense, angular sand by additional fiber glass and resin wrapping or metal tab protection.
    - 27 strain gages, mainly those close to the pile tips, were unable to record data due to damage they sustained during the installation process in the dense sand.
- Inclusion of pile caps which fit the pile heads tightly
    - Pile caps used for Day 3 testing were slightly oversized and caused excessive vibrations in the accelerometer recordings leaving the data unusable. The testing should have been stopped and shims added to stop the rocking in order to have accurate accelerometer measurements.

- Accelerometers should always be mounted at the center of the inertial mass and a redundant measurement, such as a string potentiometer should be used to validate displacement. In addition, accelerometers should be mounted at the piles heads to be able to determine relative displacement of the structure instead of simply total overall displacement.
- Different soil deposits, such as clay, should be used to further investigate helical pile performance
- Further investigation into group connection types (fixed and pinned) to reinforce results discovered. This study utilized two steel bolts to simulate fixed (2 bolts) and pinned (1 bolt) conditions due to time constraints. To achieve a more fully fixed connection, concrete pads should be used. This would require significantly more time on the table.
- Implementation of small strain base motions with constant frequency for more accurate damping calculations. The White Noise input was random and finding a sinusoidal wave within that random input was challenging and time consuming. Using a constant frequency input would make the damping calculation much easier.
- Investigation into dynamic rocking behavior of helical piles should be performed as this is assumed to be a great benefit of helical plates. Two by two group piles with different number of helix plates should be tested side by side, along with a non-helical pile foundation, with additional instrumentation to determine the effect of the helix on a foundation's rocking characteristics.

- Additional studies on small diameter helical pile groups should be performed keeping all piles the same with consistent geometries as opposed to those which comprised the Skid 1 pile group in this study. This would reduce variables and allow for a simpler comparison.
- Seismic study of helical piles and helical pile groups in which the helical plates are installed in effective embedment depths to enhance their lateral performance. There have been some studies that showed if a helical plate left within 15d of the surface, that it improves the lateral capacity of the helical pile. However, it also increases the stiffness. Using a shallow helix in a group setting may or may not improve the overall behavior of the group depending on how the stiffness, but extra disturbance from the additional helix, affects the damping behavior.

7. References

Abdelghany, Y. (2008). *MONOTONIC AND CYCLIC BEHAVIOUR OF HELICAL SCREW PILES UNDER AXIAL AND LATERAL LOADING.* London, Ontario, Canada: The University of Western Ontario. Retrieved January 26, 2016

Abdoun, T., & Dobry, R. (2002). Evaluation of Pile Foundation Response to Lateral Spreading. *Soil Dynamics and Earthquake Engineering, 22*, 1051-1058. doi:0267-7261/02/$

American Society of Civil Engineers. (2016). *Minimum Design Loads and Associated Criteria for Buildings and Other Structures.*

American Society of Testing and Material International. (2008). *ASTM D4643-08 Standard Test Method for Determination of Water (Moisture) Content of Soil by Microwave Oven Heating.* Retrieved May 6, 2016, from ASTM Digital Library.

American Society of Testing and Material International. (2011). *ASTM D3080/3080M-11 Standard Test Method for Direct Shear Test of Soils under Consolidated Drained Conditions.* Retrieved May 6, 2016, from ASTM Digital Library.

American Society of Testing and Materials International. (2004). *ASTM D6913−04 Standard Test Methods for Particle-Size Distribution (Gradation) of Soils Using Sieve Analysis.* Retrieved May 6, 2016, from ASTM Digital Library.

American Society of Testing and Materials International. (2011). *ASTM D1586-11 Standard Test Method for Standard Penetration Test (SPT) and Split-Barrel Sampling of Soils.* Retrieved May 6, 2016, from ASTM Digital Library.

American Society of Testing and Materials International. (2016). *ASTM D4253-16 Standard Test Methods for Maximum Index Density and Unit Weight of Soils Using a Vibratory Table.* Retrieved May 6, 2016, from ASTM Digital Library.

American Society of Testing and Materials International. (2016). *ASTM D4254-16 Standard Test Methods for Minimum Index Density And Unit Weight of Soils and Calculation of Relative Density.* Retrieved June 2016, from ASTM Digital Library.

Ashford, S. A., Juirnarongrit, T., Sugano, T., & Hamada, M. (2006). Soil-Pile Response to Blast-Induced Lateral Spreading. I: Field Test. *Journal of Geotechnical and Geoenvironmental Engineering, 132*(2), 152-162. Retrieved September 2016

Boulanger, R. W., & Idriss, I. M. (2008). *Soil Liquefaction during Earthquakes.* Earthquake Engineering Research Institute (EERI). Retrieved September 2016

Brennan, A. J., Thusyanthan, I., & Madabhushi, G. (2005). Evaluation of Shear Modulus and Damping in Dynamic Centrifuge Tests. *J. Geotech. Geoenviron. Eng., 131*(12), 1-10.

Cerato, A. (2016a). All Shook Up! Preliminary Results of Seismic Tests on Single and Grouped Helical Piles in Sand. *Keynote Presentation. DFI Helical Piles and Tiebacks Seminar*. Ontario, CA. August 2016.

Cerato, A. (2016b). Helical Pile Design. *Invited Lecture. 51st Annual Shallow Exploration Drillers Clinic (SEDC).* Catoosa, Oklahoma. April 2016.

Cerato, A. (2016c). Large Shake Table Test on Helical Piles: Test Program and Preliminary Results. *Plenary Presentation. DFI SuperPILE 2016.* Chicago, IL. June 2016.

Cerato, A. (2017). Helical Piles Splendidly Handle Significant Shaking in Sands.... Seriously. KEYNOTE Presentation. *DFI Helical Piles and Tieback Committee (HPTC) Specialty Conference.* Montreal, Canada, September 18-19, 2017.

Cerato, A., & Victor, R. (2008). Effects of Helical Anchor Geometry on Long-Term Performance for Small Wind Tower Foundations Subject to Dynamic Loads. *The Journal of the Deep FOundations Institute (DFI), Vol. 2*, 30-41.

Cerato, A., & Victor, R. (2009). Effects of Long-Term Dynamic Loading and Fluctuating Water Table on Helical Anchor Performance for Small Wind Tower Foundations. *ASCE Journal of Performance of Constructed Facilities, Vol. 23, No. 4*, 251-261.

Chang, C. Y., Power, M. S., Tang, Y. K., & Mok, C. M. (1989). Evidence of Nonlinear Soil Response During a Moderate Earthquake. *Proc., 12th Int. Conf. on Soil Mechanics and Foundation Engineering*, (pp. 1927-1930). Balkema, Rotterdam, The Netherlands.

Cubrinovski, M., Kokusho, T., & Ishinhara, K. (2006, February 20). Interpretation from large-scale shake table tests on piles undergoing lateral spreading in liquefies soils. *Soil Dynamics and Earthquake Engineering*(26), 275-286. Retrieved September 2016

Deep Foundations Institute (DFI). (2013). *Introduction to Helical Piles and Helical Anchors.* Retrieved March 5, 2016

El Naggar, M. H., & Abdelghany, Y. (2007). *SEISMIC HELICAL SCREW FOUNDATIONS SYSTEMS (SHSFS).* London, Ontario, Canada: The University of Western Ontario. Retrieved January 26, 2016

El Sharnouby, M. M., & El Naggar, M. H. (2012). Axial monotonic and cyclic performance of fibre-reinforced polymer (FRP) – steel fibre–reinforcedhelical pulldown micropiles (FRP-RHPM). *Can. Geotechnical J., 49*, 1378-1392. Retrieved January 26, 2016

El Sharnouby, M. M., & El Naggar, M. H. (2013). Lateral Static and Cyclic Behaviour of the Composite Steel-Bire Reinforced helical Pulldown Micropiles-Innovative

Foundation Solutions for Seismic Applications. *Proceedings of the 21st Symposium of the Vancouver Geotechnical Society.*

Ellis, E. A., Soga, K., Bransby, M. F., & Sata, M. (1998). Effect of Pore Fluid Viscosity on the Cyclic Behavior of Sands. In T. Kimura, O. Kusakabe, & J. Takemura (Ed.), *Proc., Centrifuge 98*, (pp. 217-222). Balkema, Rotterdam, The Netherlands.

ElSawy, M. (2017). *Seismic Performance of Steel Helical Piles.* A Thesis Submitted in Partial Fulfillment of the requirements for the degree in Master of Engineering Science, Western University, Ontario, Canada.

ElSawy, M., El Naggar, M., Cerato, A., & Elgamal, A. (2018a). Data Reduction and Dynamic p-y curves of Helical Piles from Large Scale Shaketable Tests. *Submission to Journal of Geotechnical and GeoEnvironmental Engineering*.

Elsawy, M., El Naggar, M., Cerato, A., & Elgamal, A. (2018b). Seismic Performance of Helical Piles in Dry Sand from Large Scale Shake Table Tests. *Submission to Geotechnique*.

Elsawy, M., Heidari, M., El Naggar, M., Cerato, A., & Elgamal, A. (2017). Interpretation of Seismic Response Data from Full Scale Helical Pile Tests. *DFI 42nd Annual Conference on Deep Foundations.* New Orleans, LA. October 24-27, 2017.

Gerber, T. M. (2003). *P-Y Curves for Liquefied Sand Subject to Cyclic Loading Based on Testing of Full-Scale Deep Foundations.* Brigham Young University, Department of Civil and Environmental Engineering. Ann Arbor, MI: ProQuest Information and Learning Company. Retrieved September 2016

Haeri, S. M., Kavand, A., Rahmani, I., & Torabi, H. (2012). Response of a Group of Piles to Liquefaction-Induced Lateral Spreading by Large Scale Shake Table Testing. *Soil Dynamics and Earthquake Engineering, 38*, 25-45. doi:10.1016/j.soildyn.2012.02.002

Hardin, B. O., & Drnecich, V. P. (1972). Shear Modulus and Damping in Soils. *J. Soil Mech. Found. Div., 98*(7), 667-692.

Hirade, T., Mizuno, H., Iiba, M., Sugimoto, M., & Mori, T. (2000). *Oscillator Tests of Pile Foundations in Dissipation Process of Excess Pore Water Pressure after Liquefaction.* 12WCEE. Retrieved September 2016

Hoyt, R., & Clemence, S. (1989). Uplift Capacity of Helical Anchors in Soil. *12th International Conference on Soil Mechanics and Foundation Engineering.* Rio de Janeiro, Brazil: A.B. Chance Company.

ICC-ES. (2013). *Acceptance Criteria for Helical Pile Systems and Devices (AC358).* ICC-ES.

Idriss, I. M., Singh, R. D., & Dobry, R. (1978). Nonlinear Behavior of Soft Clays During Cyclic Loading. *J. Geotech. Eng. Div., 104*(12), 1427-1447.

International Building Code. (2012). Country Club, ILL: ICC.

International Building Code. (2015). Country Club, ILL: ICC.

Kokusho, T. (1980). Cyclic Triaxial Test of Dynamic Soil Properites for Wide Strain Range. *Soils Found., 20*(2), 45-60.

Kokusho, T., Yoshida, Y., & Esashi, Y. (1982). Dynamic Properties of Soft Clay for Wide Strain Range. *Soils Found., 22*(4), 1-18.

Lundgreen, C. (2010). *Damping Ratios for Laterally Loaded Pile Groups in Fine Grained Soils and Improved Soils.* Master's Thesis, Brigham Young University, Department of Civil and Environmental Engineering.

Mashiri, M. S., Vinod, J. S., & Neaz Sheikh, M. (2015). Liquefaction Potential and Dynamic Properties of Sand-Tyre Chip (STCh) Mixtures. *Geotechnical Testing Journal*. doi:10.1520/GTJ20150031

Ministry of Business, Innovation & Employment Hikina Whakatutuki. (2012a). *Supplementary Guidance; Part A: Technical Guidance.* Canterbury, New Zealand: Ministry of Business, Innovation & Employment Hikina Whakatutuki. Retrieved September 2016

Ministry of Business, Innovation & Employment Hikina Whakatutuki. (2012b). *Supplementary Guidance; Part B: Technical Information.* Canterbury, New Zealand: Ministry of Business, Innovation & Employment Hikina Whakatutuki. Retrieved September 2016

Ministry of Business, Innovation & Employment Hikina Whakatutuki. (2013). *Supplementary Guidance to 'Guidance on Repairing and Rebuilding houses affected by the Canterbury Earthquakes', December 2012.* Canterbury, New Zealand: Ministry of Business, Innovation & Employment Hikina Whakatutuki. Retrieved September 2016

Ministry of Business, Innovation & Employment Hikina Whakatutuki. (2015). *Supplementary Guidance; Part C: Assessing, Repairing and Rebuilding Foundations in TC3.* Canterbury, New Zealand: Ministry of Business, Innovation & Employment Hikina Whakatutuki. Retrieved September 2016

Mizuno, H., Sugimoto, M., Mori, T., Iiba, M., & Hirade, T. (2000). *Dynamic Behavior of Pile Foundation in Liquefaction Process - Shaking Table Tests Utilizing Big Shear Box.* 12WCEE. Retrieved September 2016

Motamed, R., Towhata, I., Honda, T., Tabata, K., & Abe, A. (2013). Pile Group Response to Liquefaction-Induced Lateral Spreading: E-Defense Large Shake Table Test.

Soil Dynamics and Earthquake Engineering, 51, 35-46. doi:10.1016/j.soildyn.2013.04.007

Naeini, A. J., Choobbasti, A. J., & Saadati, M. (2013). Seismic Behaviour of Pile in Three-Layered Soil (case study: Babol City Center Project). *Arab Journal of Geoscience, 6*, 4487-4497. doi:10.1007/s12517-012-0671-x

Perko, H. A. (2007, Decemeber). Creating Acceptance for Helical Foundations. *Code Updates: Code Developments and Announcement Section, Structure Magazine*, 49-50. Retrieved November 2016

Perko, H. A. (2009). *Helical Piles: A Practical Guide to Design and Installation.* Hoboken, NJ: J. Wiley.

Pitilakis, K., Kirtas, E., Sextos, A., Bolton, M., Madabhushi, S., & Brennan, A. (2004). Validation by Centrifuge Testing of Numerical Simulations for Soil-Foundation-Structure Systems. *Proc. 13th World Conf. on Earthquake Engineering*, *Paper no. 2772.* Vancouver, B.C., Canada.

Prasad, Y. V., & Rao, S. N. (1994). Pullout behaviour of model pile and helical pile anchors subjected to lateral cyclic loading. *Can. Geotechnical J., 31*, 110-119. Retrieved January 26, 2016

Prasad, Y. V., & Rao, S. N. (1996, November). Lateral Capacity of Helical Piles in Clays. *Journal of Geotechnical Engineering, 122*(11), 938-941. Retrieved November 2016

Robertson, P. K., & Wride, C. E. (1997). Cyclic Liquefaction and its Evaluation Based on the SPT and CPT. *Proceedings of the National Center for Earthquake Engineering Research. Report No 970022, 1997.* NCEER.

Rollins, K. M., Ashford, S. A., & Baez, J. I. (2000). *Comparison of Deep Foundation Performance in Improved and Non-improved Ground using Blast-Induced Liquefaction.* American Society of Civil Engineers. Retrieved September 2016

Rollins, K. M., Ashford, S. A., & Lane, J. D. (March 26, 2001). Full-Scale Lateral Load Testing of Deep Foundations Using Blast-Induced Liquefaction. *International Conferences on Recent Advances in Geotechnical Earthquake Engineering and Soil Dynamics.* Scholars' Mine. Retrieved September 2016

Rollins, K. M., Evans, M. D., Diehl, N. B., & Daily, W. D. (1998). Shear Modulus and Damping Relationships for Gravels. *J. Geotech. Geoenviron. Eng., 124*(5), 396-405.

Rollins, K. M., Gerber, T. M., & Kwon, K. H. (2009). Increased Lateral Abutment Resistance from Gravel Backfills of Limited Width. *Journal of Geotechnical and Geoenvironmental Engineering, ASCE 136, no. 1*, 230-238.

Rollins, K. M., Gerber, T. M., Lane, J. D., & Ashford, S. A. (2005). Lateral Resistance of a Full-Scale Pile Group in Liqefied Sand. *Journal of Geotechnical and Geoenvironmental Engineering, 131*(1), 115-125. Retrieved September 2016

Rollins, K. M., Hales, L. J., Ashford, S. A., & Camp III, W. M. (2006). *P-Y Curves for Large diameter Shafts in Liquefied Sand from Blast Liquefaction Tests.* American Society of Civil Engineers. Retrieved September 2016

Rollins, K. M., Hussein, M., Tobita, T., & Iai, S. (2010). Soil-Pile Separation Effect on the Performance of Pile Group Under Static and Dynamic Lateral Loads. *Canadian Geotechnical Journal, NRC Research Press, Vol. 47, No. 11*, 1234-1246.

Seed, H. B., Tokimastu, K., Harder, L. F., & Chung, R. F. (1985). Influence of SPT Procedures in Soil Liquefaction Resistance Evaluations. *Journal of Geotechnical Engineering, Vol. 111, No. 12, December 1985*.

Seed, H. B., Wong, R. T., Idriss, I. M., & Tokimatsu, K. (1986). Moduli and Damping Factors for Dynamic Analyses of Cohesionless Soils. *J. Geotech. Eng.*, *112*(11), 1016-1032.

Skempton, A. W. (1986). Standard Penetration Test Procedures and the Effects in Sands of Overburden Pressure, Relative Density, Particle Size, Ageing and Over Consolidation. *Geotechnique, 36:3, September, 1986*.

Slifka, L. D. (2004). *An Accelerometer Based Approach to Measuring Displacement of a Vehicle Body.* A Thesis Submitted to the Horace Rackham School of Graduate Studies of the University of Michigan In partial fulfillment of the requirements for the degree of Master of Science in Engineering, Department of Electrical and Computer Engineering, Dearborn, Michigan.

Tang, L., Ling, X., Zhang, X., Su, L., Liu, C., & Li, H. (2015). Response of a RC Pile Behind Quay Wall to Liquefaction-Induced Lateral Spreading: A Shake-Table Investigation. *Soil Dynamics and Earthquake Engineering, 76*, 69-79. doi:10.1016/j.soildyn.2014.12.0150267-7261/

Teymur, B., & Madabhusi, S. P. (2002). Shear Stress-Strain Analysis of Sand in ESB Model Container by Harmonis Wavelet Techniques. In R. Phillips, P. J. Guo, & R. Popescu (Ed.), *Proc., Int. Conf. on Physical Modeling in Geotechnics*, (pp. 201-206). Balkema, Rotterdam, The Netherlands.

Vargas, T. (2017). *Understanding the Seismic Response of Single Helical Piles in Dry Sands Using a Large-Scale Shake Table Test.* A Thesis Submitted in Partial Fulfillment of the Requirements for the Degree in Master of Science in Civil Engineering and Environmental Science, University of Oklahoma, Norman, Oklahoma.

Vucetic, M., & Dobry, R. (1991). Effect of Soil Plasticity on Cyclic Response. *J. Geotech. Eng., 117*(1), 89-107.

Weaver, T., Ashford, S., & Rollins, K. (2005). Lateral Resistance of a 0.6 m Drilled Shaft in Liquefied Sand. *Journal of Geotechnical and Geoenvironmental Engineering, 131*(1), 94-102. Retrieved September 2016

Wilson, J. M. (1988). *A Theoretical and Experimental Investigation into the Dynamic Behavior of Soils.* PhD Thesis, University of Cambridge, Cambridge, U.K.

Woods, J. (2016, July). Personal Communication with Pile Tech in Canterbury, New Zealand. (A. Cerato, S. Allred, & T. Vargas, Interviewers)

Youd, T. L., & Noble, S. K. (1997). Liquefaction Criteria Based on Statistical and Probabilistic Analyses. *Proceedings of the NCEER Workshop on Evaluation of Liquefaction Resistance of Soils, Technical Report NCEER-97-022,* pp. 201-205.

Zeghal, M., Elgamal, A. W., Tang, H. T., & Stepp, J. C. (1995). Lotung Downhole Array. II: Evaluation of Soil Nonlinear Properties. *J. Geotech. Eng., 121*(4), 363-378.

Zeghal, M., Elgamal, A. W., Zeng, X., & Arulmoli, K. (1999). Mechanism of Liquefaction Response in Sand-Silt Dynamic Centrifuge Tests. *Soil Dyn. Earthquake Eng., 18*(1), 71-85.

8. Appendix A: Literature Review Summary Tables

Table 9: Summary Table of Liquefaction Literature Review

Author(s)	Year	Title	Reference	Reference No.
Scott A. Ashford Kyle M. Rollins Juan I. Baez	2000	Comparison of deep Foundation Performance in Improved and Non-improved Ground Using Blast-Induced Liquefaction	Rollins et al. (2000)	1
Hatsukazu Mizuno Michio Sugimoto Toshihiro Mori Masanori Iiba Tsutomu Hirade	2000	Dynamic Behavior of Pile Foundation in Liquefaction Process-Shaking Table Tests Utilizing Big Shear Box	Mizuno et al. (2000)	2
Hatsukazu Mizuno Michio Sugimoto Toshihiro Mori Masanori Iiba Tsutomu Hirade	2000	Oscillator Tests of Pile Foundation in Dissipation Process of Excess Pore Water Pressure After Liquefaction	Hirade et al. (2000)	3
Tarek Abdoun Ricardo Dobry	2002	Evaluation of Pile Foundation Response to Lateral Spreading	Abdoun and Dobry (2002)	4
Travis M Gerber	2003	P-Y Curves for Liquefied Sand Subject to Cyclic Loading Based on Testing of Full-Scale Deep Foundations	Gerber (2003)	5
Kyle M. Rollins Lukas J. Hales Scott A. Ashford William M. Camp III	2006	P-Y Curves for Large Diameter Shafts in Liquefied Sand from Blast Liquefaction Tests	Rollins et al. (2006)	6
M. Cubrinovski T. Kokusho K. Ishihara	2006	Interpretation From Large-Scale Shake Table Tests on Piles Undergoing Lateral Spreading in Liquefied Soils	Cubrinovski et al. (2006)	7
Scott A. Ashford Teerawut Juirnarongrit Takahiro Sugano Masanori Hamada	2006	Soil-Pile Response to Blast-Induced Lateral Spreading. I: Field Test	Ashford et al. (2006)	8
Mahmoud N. Hussien Tetsuo Tobita Susumu Iai Kyle M. Rollins	2010	Soil-Pile Separation Effect on the Performance of a Pile Group Under Static and Dynamic Lateral Loads	Rollins et al. (2010)	9
S Mohsen Haeri Ali Kavand Iraj Rahmani Hooman Torabi	2012	Response of a Group of Piles to Liquefaction-Induced Lateral Spreading by Large Scale Shake Table Testing	Haeri et al. (2012)	10
Ramin Motamed Ikuo Towhata Tsuyoshi Honda Kentaro Tabata Akio Abe	2013	Pile Group Response to Liquefaction-Induced Lateral Spreading: E-Defense Large Shake Table Test	Motamed et al. (2013)	11
Adel Javdani Naeini A. J. Choobbasti M. Saadati	2013	Seismic Behaviour of Piles in Three-Layered Soil (case study: Babol City Center Project	Naeini et al. (2013)	12
M. S. Mashiri J. S. Vinod M. Neaz Sheikh	2015	Liquefaction Potential and Dynamic Properties of Sand-Tyre (STCh) Mixtures	Mashiri et al. (2015)	13
Liang Tang Xianzhang Ling Xiaoyu Zhang Lei Su Chunhui liu Hui Li	2015	Response of a RC Pile Behind Quay Wall to Liquefaction-Induced Lateral Spreading: A Shake-Table Investigation	Tang et al. (2015)	14

Ref. No.	Foundation Type	Soil Information	Layered System Type	Ground Water Level
1	One single concrete cast-in-steel-section (CISS) piles 0.6 m outsided diameter 2x2 grouped steel pipe piles 324 mm outside diameter	0-1.5 m - Excavated 1.5-6 m Loose Sand with Silt (Liquefiable) 6-10 m Soft Fat Clay 10-13 m Loose silty sand 13-18 m Soft Fat Clay	Two-Layered system	1.5m (bottom of excavation depth)
2	2 pile group both Steel Hollow Square Section (HSS) with: 40 cm width 10 cm thickness 5.82 m length	0-5.82 m Kasumigaura Sand with : D_{50} = 0.311 mm Uniformity Coefficient = 3.01	Two-Layered System	Cases 1 through 3: GWL is at groud surface Case 4: GWL is at ground surface and wick drains installed Case 5: GWL is 1.4 m below ground surface
3	2 pile group both Steel Hollow Square Section (HSS) with: 40 cm width 10 cm thickness 5.82 m length	0-5.82 m Kasumigaura Sand with : D_{50} = 0.311 mm Uniformity Coefficient = 3.01	Two-Layered System	Cases 1 through 3: GWL is at groud surface Case 4: GWL is at ground surface and wick drains installed Case 5: GWL is 1.4 m below ground surface
4	Model pile simulated prototype pile with: 0.6 m O.D. 8 m length EI = 8000 kN*m^2 Tested as single pile and 2x2 pile group	**Test 1** (Prototype Depths) 0-6 m Fine Nevada Sand (Liquefiable) with: D_r = 40% 6-8 m Slightly Cemented Sand **Test 2** (Prototype Depths) 0-2 m Slightly Cemented Sant 2-8 m Fine Nevada Sand (Liquefiable) with: D_r = 40% 8-10 m Slightly Cemented Sand	**Test 1:** Two-Layered System **Test 2:** Three-Layered System	Test 1 & 2: GWL at ground surface
5	3x3 Grouped steel pipe piles with: O.D. = 324 mm wall thickness = 10 mm 310 MPa minimum yield strength (404.6 MPa average) 12.8 m length 12.8 m embedment depth One single steel pipe pile with similar dimensions installed 12.5 m below surface	**Single Pile Location** 0-1.5 m Fine Sand with Shells 1.5-5.5 m Interbedded Fine Sand and Silty Sand 5.5-7.5 m Fine Silty Sand 7.5-9.2 m Gray Silty Clay 9.2-10 m Sand **3x3 Pile Group Location** 0-1.5 m Fine Sand with Shells 1.5-5.5 m Interbedded Fine Sand and Silty Sand 7.5-9.2 m Gray Silty Clay 9.2-10 m Sand	Two-Layered System	**Single Pile Location** GWL is about 0.5m below the ground surface **3x3 Pile Group Location** GWL is about 0.1m below the ground surface
6	Reinforced Concrete CISS drilled shaft 2.59 m O.D. 47 m embedment depth Avg 30 day compressive strength of 37.2 MPa (5.4 ksi) Reinforced with #18 bars (36) Confining #6 bar spirals with 89 mm pitch	0-1.5 m Loose Poorly Graded Sand to Silty Sand, fine, Avg N=5 1.5-3 m Soft Sand Fat Clay, w=106, LL=104, PI=69 3-6 m Loose Poorly Graded Sand, fine, Avg N=6 6-10.5 m Silty and Clayey Sand, Avg N=7, w=30 10.5-14 m Loose to Medium Dense Poorly Graded Sand, Avg N=12 15-20 m Cooper Marl Fat Clay, Avg N=15, 40<w<50, 50<LL<150, 20<PI<80	Three-Layered System	GWL typically located between the ground surface and a depth below of 1.5 m

Ref. No.	Foundation Type	Soil Information	Layered System Type	Ground Water Level
7	Single Solid Steel Pipe Pile with: 31.8 cm O.D. 4.9 m long ~4.8 m embedment depth Fixed at base Free pile head Single Pre-stressed high-strength concrete pile (PHC-pile) with: 30 cm O.D. 4.9 m long, ~4.5 m embedment depth Fixed at base Free at pile head	0-1 m Kasumigaura Sand (Dry Crust Layer) 1-4.8m Kasumigaura Sand (Saturated, Liquefiable) D_{50} = 0.265 mm U_c = 2.36 F_c = 3% D_r = 50%	Three-Layered System	GWL located 1 m below ground surface
8	Steel Pipe Piles O.D. = 318 mm 10.5 mm Wall thickness 11.5 m Nominal Length 400 MPa Yield Strength Installed 3-3.5 m into bedrock Tested as: Single Pile 4-pile group (3.5 pile diameters, center-to-center spacing) 9-pile group (3.5 pile diameters, center-to-center spacing)	0-4 m Very Loose to Loose Poorly-Graded Silty Sand (SM) N ~8 on average 40% < D_r <60% φ_{AVG} = 29° 4-7.5 m Very Soft Lean to Fat Clay (CL-CH) Avg Undrained Shear Strength = 15 kPa 7.5-8.5 m Medium Dense Sand 8.5 - BTD Very Dense Gravel Bedrock	Two-layered System	GWL located 1 m below ground surface
9	Single steel pipe pile and 3x5 pile group all with same dimensions 324 mm O.D. 9.5 mm wall thickness 11.6 m embedment depth Free rotation at pile heads.	0-3 m Soft Clay 3-5 m Sand 5-7 m Soft Clay 7-18 m Sand	N/A	GWL located at ground surface
10	7 Total Hollow Aluminum Alloy Piles with: 1.25 m height 5.0 cm O.D. 4.74 cm I.D. EI = 4.387 kN*m^2 1 pile used as reference 1 pile used as a visual One group of 2 piles in parallel with direction of shaking One group of 3 piles perpendicular to direction of shaking	0-1 m Firoozkuh Silica Sand no. 161 (liquefiable) D_r = 15% D_{50} = 0.24 mm Coefficient of Uniformity = 1.49 4° slope in longitudinal direction 1-1.25 m Firoozkuh Silica Sand no. 161 (compacted, non-liquefiable) Dr = 80% D50 = 0.24 mm Coefficient of Uniformity = 1.49 4° slope in longitudinal direction	Two-Layered System	GWL is located at about the ground surface

Ref. No.	Foundation Type	Soil Information	Layered System Type	Ground Water Level
11	Steel Pipe Piles $A = 9.45 \times 10^{-4}$ m^2 $E = 2.06 \times 10^{11}$ N/m^2 O.D. = 152.4 mm Wall Thickness = 2.0 mm $I = 2.672 \times 10^{-6}$ m^4 Hollow Cylindrical Steel Columns $A = 4.767 \times 10^{-3}$ m^2 $E = 2.06 \times 10^{11}$ N/m^2 O.D. = 267.4 mm Wall Thickness = 5.8 mm $I = 4.080 \times 10^{-5}$ m^4	0-3.75 m Liquefiable Sand $D_r = 60\%$ 3.75-4.5 m Non-Liquefiable Sand Base $D_r = 90\%$ *Note: Piles were embedded into cement-mixed sand for this depth Albany Silica Properties: Poorly-Graded $D_{50} = 0.2$ mm Coefficient of Uniformity = 1.64 Fines Content = 0.18%	Two-Layered System	GWL is located 50 cm below ground surface
12	Solid Concrete Pile with: 0.8 m O.D. Yield Moment = 560 kN*m 14 m embedment depth 0.7 m pile length above ground surface E = 30000 MPa	0-8 m Lean to Fat Clay $4<N<25$ $35<E$ $(kg/cm^2)<157$ $0.3<C_u$ $(kg/cm^2)<1.01$ $\varphi = 8^o$ 8-12 m Silty Clayey Sand $9<N<44$ $82<E$ $(kg/cm^2)<229$ $\varphi = 30^o$ 12-16 m Lean to Fat Clay $6<N<27$ $45<E$ $(kg/cm^2)<173$ $0.5<C_u$ $(kg/cm^2)<1.3$ $\varphi = 10^o$	Three-Layered System	GWL is located at the ground surface
13	N/A	Specimens are of Poorly Graded Sand with: $D_{50} = 0.35$ mm Coefficient of Uniformity = 1.58	N/A	N/A
14	Reinforced Concrete Pile Fixed at base of box Fabricated with fine aggreagate concrete Galvanized with fine iron wires 60 kg weight mounted on pile head for inertial effects K_r (bending stiffness) = 63500 N*m/rad 1.91 m height 0.1 m diameter Yield Moment = 500 N*m Plastic Moment = 1380 N*m Initial EI = 1.03×10^5 $N*m^2$	0-0.3 m Non-liquefiable Clay crust Consolidated normally as reconstituted silty clay with: LL = 29.8 PL = 18.2 density of 1650 kg/m^3 0.3-1.5 m Liquefiable Sand $45\% < D_r < 50\%$ Saturated density = 1950 kg/m^3 $D_{50} = 0.51$ mm Coefficient of Uniformity = 2.98 Fines Content = 2%	Three-Layered System	GWL is located 0.3 m below ground surface

Ref. No.	Liquefaction Mitigation Measure	Testing Type	Objective
1	Installation of an array of stone columns throughout project site to stiffen liquefiable soil	Pre-treatment and Post-treatment: Pre-blast lateral static control tests and Post-blast lateral displacement controlled cyclic tests	To analyze deep foundation behavior of single and grouped piles in liquefiable soil before and after mitigation measurements
2	Case 4 added wick drains to determine their mitigation effect	Shake Table Test: 6 m height, 11.6 m length, 3 m width in liquefiable sand	To analyze processes occurring DURING liquefaction including pile behavior, effect of wick drains, effect of liquefiable soil which is not completely saturated
3	Case 4 added wick drains to determine their mitigation effect	Oscillator tests performed after shaking during pore water dissipation process. Oscillator - Eccentric moment set to constant 100 kg*cm. Sweep up and sweep down method application	To analyze soil and pile behavior and dynamic properties AFTER liquefaction process during pore water pressure dissipation
4	Replacing surface soil around pile and pile cap of 3 layered soil system with frangible material that will yielld under constant lateral soil forces	100g-ton RPI centrifuge tests in 2 layered (top liquefiable) and 3 layered (sandwich liquefiable) soil systems. Input motion of 40 sinusoidal cycles and peak base accleration of 0.3g . Box was inclined downslope to induce lateral spreading	To study the pile behavior in two types of liquefiable strata and the effect of replacing the surface crust around the pile with soft clay as a mitigation measure
5	N/A	Pre-blast and Post-blast testing consisted of several lateral cyclic displacement controlled tests on the grouped and single pile	To develop substantial P-Y curves for liquefiable sand and a correlating empirical formula to derive P-Y curves at different locations for different sizes of piles
6	N/A	Pre-blast and Post-blast testing consisted of several lateral cyclic load controlled tests on the single pile	To develop substantial P-Y curve for the local liquefiable soil for large diameter shafts to be used in construction project. To check derived P-Y curves of local liquefiable soil with empirical formula proposed by Gerber (2003)
7	N/A	2 Phases: Phase 1 - table shaken with sine wave excitation with peak base acceleration = 0.217g at 2 Hz frequency, for 30 seconds. Phase 2 - rigid loading frame attached to outer side of laminar box and initiated lateral ground movement at a rate of 4.1 cm/sec. Model was subject to low-amplitude (0.027g), high-frequency (10 Hz) base shaking	To analyze and determine the effects on two single piles of different material under liquefaction induced lateral spreading pressures. And determine the stiffness degradation factor of the liquefied soil
8	N/A	Full-Scale Blast Induced Lateral Spreading Test conducted on: Single Pile (free-head condition) 4-pile group (fixed-head condition) 9-pile group (fixed-head condition)	Evaluate loading conditions on the piles due to kinematic loading from laterally spreading soils Assess ther performance of two different quay walls which were subjected to lateral spreading Conduct damage and performance assessments of the piles
9	Correction to FEM analysis programs. Considering soil-pile separation	Static load controlled lateral tests, Dynamic load controlled lateral tests using statnamic device with 311 kN capacity. FEM analysis conducted for both static and dynamic tests but under 2 conditions for comparison with measured field results: with soil-pile separation and without soil-pile separation	To affirm FEM analysis models of laterally loaded grouped and single piles incorrectly estimate bending moment and head deflections from considering no soil-pile separation
10	N/A	Shake Table Test of multiple different groud motions. Sinusoidal base accelerations with 3.0 Hz frequency and 0.2g amplitude. Duration of 12 sec	To study the response of a group of piles subjected to liquefaction-induced lateral spreading using a large scale 1-g shake table test

Ref. No.	Liquefaction Mitigation Measure	Testing Type	Objective
11	N/A	Two Shake Table Tests on two different quay walls (sheet-pile and gravity type both in landslide) with two dimensional (horizontal and vertical) input motion Simulated 80% of 1995 Kobe (Takatori) Earthquake Max horizontal acceleration = 5.96 m/s^2 Max Vertical Acceleration = 1.71 m/s^2	To study the group effects on piles subject to liquefaction induced lateral spreading behind a waterfront structure
12	N/A	Analyzed three different recorded ground motions in Flac2D finite difference program of a single pile in a sandwiched liquefied zone	To learn the pile and soil behavior under different magnitudes of ground peak acceleration and predominant frequencies
13	Inclusion of tyre chips in poorly graded sands to reduce liquefaction potential and effects	strain controlled consolidated undrained cyclic Triaxial tests conducted at constant frequency of 1 Hz and single amplitude shear strains of: 0.15, 0.23, 0.38, and 0.50% on specimens of 100 mm diameter by 200 mm height	To determine the mitigation effects of mixing tyre chips in poorly graded sands, and to determine the optimal content of tyre chips to add for most effective mitigation
14	N/A	Shake table test with base motion in longitudinal direction Predominant Frequency = 2 Hz Amplitude = 0.2g Laminar Container Dimensions 1.7 m Height 2.2 m Width 3.5 m Length	To analyze the response of reinforced concrete pile beahvior behind a steel sheet-pile quay wall subjected to liquefaction-induced laterall spreading

Ref. No.	Results
1	Treatment increased secant stiffness of Pre-blast tests on grouped piles by 24% and on single pile by 44%. Increased Post-blast secant stiffness on grouped piles by 288% and on single pile by 367%
2	Early stages of liquefaction - pile behavior is mostly influenced by inertial forces. With progress of liquefaction - behavior is much affected by soil motion. At complete liquefaction - pile behaves with soil in same direction. Effect of wick drains is very small during ground motion, but 4 times increase in dissipation rate after excitation. Low ground water table greatly reduces the piles internal bending moment
3	The stiffness of the soil and the coefficient of the horizontal subgrade reaction are recovered with dissipation progress of excess pore water pressures. At higher excess pore water ratios, the resonant frequencies of the foundation are low and damping ratios are large. At lower excess pore water ratios, the resonant frequencies are high and their damping ratios become small.
4	Max bending moments occurred at the interfaces between liquefied soil and non-liquefied strata in all tests. Max moment decreases in pile groups due to frame effect. 3 layered soil system caused bending moments to nearly double in magnitude and cause pile and pile cap failure compared to the 2 layer soil system.Introduction of soft clay around the pile and pile cap of the 3 layered system revealed dramatic reduction bending moments of the pile in the surface crust (from 300 kN*m to 10 kN*m) and reduced max pile head displacement by a factor of ~2.
5	Derived p-y curves for liquefiable sand revealed concave-up shape (increasing soil resistance with increasing pile deflection). Resulted from dilation of the surrounding sand during shearing which reduces the excess pore pressure ratio. Proposed empirical formula for p-y curve of liquefiable sand: p=A(B*y)^c : where A = 3.00*10^-7*(z+1)^6.05, B = 28.01*(z+1)^0.11, C = 2.85*(z+1)^-0.41, p = soil resistance (kN/m), y = deflection (cm), z = depth (m). Pile size correction factor = (0.438 + 1.736*d) * (d/0.324) : where d = the diameter or width of the pile or shaft (m): Limitations include depth of liquefiable zone is less than or equal to 6 meters, relative density is about 50%, max soil resistance = 15 kN/m
6	Results of derived p-y curves show concave up shape (increasing soil resistance with increasing lateral deflection), noted as more linear than the TILT project (Gerber 2003). Derived p-y curves found to match well using the Gerber empirical formula with the pile diameter correction factor. p-y used in LPILE analysis to check accuracy and resulted in good agreement

Ref. No.	Results
7	PHC pile - followed ground movement, bending moment at base sharply increased from start of lateral spreading, reached yield moment at ground displacement of 9 cm and failed at 17 cm. Steel pile - did not follow ground movement, revealed large lateral resistance, pile displacement gradually increased during the first 6 seconds then remained constant at 5 cm during the remainder, reached ~60% of yield moment. Lateral Stiffness degradation factors for the liquefied strata were found to be within the range of 1/30 - 1/80 on average and showed a gradual decrease with increasing lateral ground displacement.
8	Ground surface experieced much more displacement down-slope of the piles as compared to up-slope (~1 m and ~30 cm Respectively) The free-head (single pile) experienced much more pile head displacement than the grouped (fixed) pile heads due to the effect of pile head restraint in the groups contributing to resist the moment induced by the lateral soil pressure Max moment in all piles occurred at ~9m depth (bottom of the soft clay) Max moment magnitude in the grouped piles was significantly less than the single pile experienced Rotational restraint at the pile cap led to a stiffer response under loading applied by the mobile layer In the liquefied sand layer (depth 1 m - 4 m) the moment distribution the piles was linear, indicating zero soil reaction The larger the degree of fixity at the pile tip, thi higher the developed moment in the pile
9	FEM analysis without soil-pile separation - for the single pile under static loading underestimates deflection and max bending moment up to 50% and 22% respectively. Overestimates the lateral load capacity by up to 43%. - For grouped piles under static loading - results in excessive increases in the overall soil resistance during pile deformation, underestimates the deflection of the trailing pile which increases as loading progresses, overestimates the ultimate lateral load-carrying capacity of the trailing pile by up to 73%. - For grouped piles under dynamic loading, underestimates the max deflection by up to 23.3%, underestimates bending moment values.
10	Pile heads reached max displacement a few seconds after lateral spreading (max 36.1 mm, max ground displacement = 82.8 mm) then bounced back to a small residual displacement (6.2 mm) during the remainder of shaking. Bending moments in piles had similar trend reaching a maximum (~0.2 kN*m) after lateral spreading then decreased dramatically during the remainder of shaking. Max lateral soil pressure (~12 kPa) occured at ~1 m depth on P4 (an outside pile of the 3 pile group perpendicular to direction of shaking)
11	Lateral ground deformations up to 2.2 m occurred Piles horizontally displaced between 1.0 and 1.4 m at the pile heads Footing of the superstructure tilted seaward Lateral displacement of the soil decreased as the distance from the quay wall increased toward the land Max movements occurred at the ground surface Large bending moments occurred in the rear row piles at a depth of 2 m Large bending moments occurred at the pile heads from the connections to the pile cap Thre rear row pile received larger lateral forces and sustained more significant damage compared to the front row piles The tilted mass supporting structure may have applied excessive axial forces i the rear row piles The pile group structurally collapsed during shaking The rear piles sustained much greater rotations when compared to the front piles

Ref. No.	Results
12	Max bending moment increases when the peak acceleration increases and/or when the predominant frequency decreases. Max lateral displacement of the pile head increases when the peak acceleration increases and/or the predominant frequency decreases. Settlement of the pile increases as the predominant frequency decreases.
13	Liquefaction potential decreases at any single amplitude shear strain with the addition of TCh ≥ 20% (gravimetric content). Max number of cycles required for liquefaction occurred at a proportion of TCh between 30 and 33%. STCh mixtures showed minimizing the shear modulus degradation at multiple cycles. Damping ratios increase with the increase of TCh proportions up to 30%.
14	Bending moments gradually increased in depth and the max value ocurred near the base due to the free pile head condition Moments were analyzed by separating the Recorded Moment into Cyclic Moments and Monotonic Moments (due to lateral spreading) The Max Moment in the pile occured during the transition from Stage 1 into Stage 2 Larger lateral soil deformation with relatively low superstructure acceleration produced greater monotonic moments <u>Results divided into 4 stages</u>: **Stage 1 - Prior to liquefaction (0-2.6 sec)** No permanent deformation occurred Monotonic Moments were approximately negligible **Stage 2 - Liquefaction-Induced Lateral Spreading (2.6-15.6 sec)** Superstructure reached max displacement of ~0.06 m, and soil deformation reached ~0.14 m Monotonic Moments gradually increased as the ground deformation accumulated and rapidly attained a max after the onset of lateral spreading **Stage 3 - Slow Flow (15.6-23.2 sec)** Ground deformation increased slowly, While the max pile displacement was reached and then rebound due to slow soil flow Monotonic Moments decreased as the liquefied soil continued to flow slowly around the pile **Stage 4 - No Lateral Spreading (23.2-30 sec)** Soil flow nearly stopped and the displacement exhibited primarily cyclic behavior until the shaking ended Monotonic Moment continued to decrease as the lateral spreading had stopped Recorded Moment was mainly controlled by inertial forces At end of shaking ground displacement reached ~0.18 m while the soil displacement reached 0.2 m at a depth of 0.4 m

Ref. No.	Relevant Figures and/or Tables
1	Figure 1: Soil Profile and SPT N Values (pg. 29) Figure 3: Pre- and Post-treatment CPT Results (pg. 31) Figures 4 & 5: Pre-treatment Load Displacement Curves for 4 pile group and single 0.6 m CISS, respectively (pg.32) Figures 8 & 9: Post-treatment Load Displacement Curves for 4 pile group and single 0.6 m CISS, respectively (pg. 34)
2	Table 1: Soil Properties (pg. 2) Table 2: Test Series and Objectives (pg. 3) Figure 3: Test Plan and Setup (pg. 4) Table 3: Ground Condition Changes for each Case (pg. 4) Figure 7: Max PWP, Pile Base Acceleration, and Bending Moment Result Curves for Cases 1-3 (pg. 6) Figure 9: Comparison of Cases 3, 4, & 5 Test Results (pg. 7)
3	Figure 7: Pore Water Pressure Dissipation Proccess After Earthquake Excitation (pg. 5) Figure 8: Dissipation of Pore Water Pressure at Different Stages (pg. 5) Figure 9: Resonant Curves of Footing Displacement (pg. 6) Figure 10: Relationship between resonance frequency and average excess pore water pressure ratio (pg. 6) Figure 11: Distribution of Bending Moment at Several Stages (pg. 6) Figure 12: Distribution of Earth Pressure at Several Stages (pg. 7)
4	Figure 5: Lateral Spreading Pile Centrifuge Model in two-layer soil profile (Test 1) (pg. 1054) Figure 6: Prototype lateral displacement of pile head and ground surface, and pile bending moment at a depth of 5.75 m (pg. 1054) Figure 8: Lateral Speading Pile Centrifuge Model in three-layer soil profile (Test 2) (pg. 1055) Figure 9: Max bending moments for piles with and without inertial mass for Test 2 (pg. 1056) Figure 10: Lateral Speading Pile Centrifuge Model Profile for retrofitting (Test 2) (pg. 1056) Figure 11: Bending Moment Comparison of Pile with and without retrofitting (Test 2) (pg. 1057)
5	Figures 3-5 through 3-7: Idealized Soil Profiles for Single Pile Location with various Properties and In-Situ Test Results (pg. 49-51) Figures 3-8 through 3-15: Boring Logs and CPT Results for location of Single Pile (pg. 52-59) Figures 3-18 through 3-19: Idealized Soil Profiles for 3x3 Pile Group Location with vairous Properties and In-Situ Test Results (pg. 64 & 65) Figures 3-20 through 3-28: Boring Logs and CPT Results for location of 3x3 Pile Group (pg. 66-74) Figures 4-2 & 4-3: Configuration of the Test Setup for Single Pile and 3x3 Pile Group (pg. 80 & 81) Figures 4-7 through 4-9: Load-Displacement Curves of the Single Pile, Pre- and Post-Blast (pg. 91-93) Figures 4-19 through 4-21: Load-Displacement Curves of the 3x3 Pile Group, Pre- and Post-Blast (pg. 105-107) Figures 4-30 through 4-35: Pre-and Post-Blast Load-Displacement Curves of Piles in the 3x3 Pile Group to Analyze Group Effects on each row (pg. 116-121) Figures 5-2 through 5-15: Pre- and Post-Blast Maximum Bending Moment Profiles for piles in the 3x3 Pile Group (pg. 131-144) Figures 5-16 & 5-17: Comparisons of Pre- and Post-Blast Bending Moment Profiles of Piles in each row of the 3x3 Pile Group (pg. 145 & 148)

Ref. No.	Relevant Figures and/or Tables
6	Figure 1: Idealized soil profile for the test site (pg. 13) Figure 2: Interpreted soil profile and results of CPT sounding at test site (pg. 14) Figure 3: Progile and cross-section through test shaft MP-3 at Mt. Pleasant test site (pg. 16) Figure 4: Layout of test pile MP-1 along with blast hole locations and piezometers (pg. 17) Figure 5: Excess pore pressure ratio (R_u) vs. depth for the vertical arrays at 1.83, 7.32, and 10.36 m from the center of test pile MP-1 (pg. 21) Figure 6: Pile head vs. deflection curves for test pile MP-1 prior to blasting and for two load tests following blasting (pg. 21) Figure 7: Comparison of back-calculated and computed p-y curves for the liquefied sand at Charleston, South Carolina test site (pg 22)
7	Figure 2: Physical model and loading phases (dynamic and lateral spreading) of large-scale shake table test (pg. 277) Figure 3: Moment-Curvature relationships of test piles (pg. 277) Figure 4: Recorded excess pore pressures at five depths in the sand deposit during shaking and lateral spreading (pg. 278) Figure 5: Measured displacements and bending moments of piles during lateral ground movement of both Steel Pipe pile and PHC Pile (pg. 279) Figure 6: Experimental p-δ curves at three depths in the non-liquefied sand near the ground surface (pg. 280) Figure 7: Measured pressure-displacement relations in the surface layer in terms of resultant pressure per unit width of the pile (pg. 280) Figure 9: Ratio of measured ultimate lateral pressure and Rankine passive pressure obtained in experimental studies on single piles in sand (pg.281) Figure 10: Relative displacement required to fully mobilize the passive pressure as a function of relative density of sand: summary of data from expermental studies (pg. 282) Figure 11: Analytical model used for back-calculated β (stiffness degradation factor) (pg. 282) Figure 12: Pile response (pile displacements and bending moments) computed in analyses using different values of β (pg. 283) Figure 13: Back-calculated degradation of stiffness in the liquefied layer as a function of lateral ground displacement (pg. 283) Figure 14: Numerical models used in parametric analyses (pg. 284) Figure 15: Comparison of effects from the liquefied layer and non-liquefied surface layer on the response of piles with different relative stiffness (pg. 284)
8	Figure 1: Site layout for the first lateral spreading test Figure 2: Typical soil profile, in situ test results and correlated engineering properties of the soil Figure 3: Grain size distribution of the soil at test site Figure 5: Moment-Curvature relationship of test piles and cross-sectional area diagram Figure 8: excess pore pressure versus time nearby nine-pile group at various depths for the first test Figure 9: Example of GPS data from the first test at a surface location 9 m up-slope from the nine-pile group Figure 11: Surface displacement vectors from GPS and survey data Table 1: Summary of Horizontal down-slope surface movement increments Figure 12: Pile Responses (displacement, rotation, moment, and soil reaction) versus depth for the single pile, four-pile group, and nine-pile group Figure 13: Moment distribution of each (instrumented) pile from the first test for the four-pile group and the nine-pile group

Ref. No.	Relevant Figures and/or Tables
9	Figure 1: Idealized soil profile at the Salt Lake City International Air-port (pg. 1235) Figure 3: General layout and meshing of the FE model (pg. 1237) Figure 4: Shear strength parameters for the soil profile used in this study compared to shear strengths obtained from laboratory and field tests (pg. 1237) Table 1: Idealized soil layers and model parameters for soil elements (pg. 1238) Table 2: Model parameters for the pile element (pg. 1238) Figure 5: Separation-contact model for a joint element at the pile-soil interace (pg. 1238) Table 3: Model parameters for the join element (pg. 1238) Figure 8: Load-relative displacement relationship of pile-soil system in a simplified model of one pile in a group (pg. 1239) Figure 9: Undrained cyclic shear test simulation of a single soil element (pg. 1239) Figure 10: Single pile response (load-deflection, load-max moment, moment-depth) Curves under static load (pg. 1240) Figure 12: Statically loaded pile group: computed and measured average load per pile versus deflection for piles 1 and 5 (pg. 1240) Figure 13: Statically loaded pile group: variation of earth pressure and pore pressure with deflection curves computed with and without separation (pg. 1241) Figure 14: Statically loaded pile group: ratio of the computed and measured loads of each pile relative to the load of the single pile (pg. 1241) Figure 15: statically loaded pile group: computed (with and without separation) and measured bending moment vs depth for the trailing pile (pg. 1242) Figure 16: Time sequence of total load applied to the pile group in numerical analysis (pg 1242) Table 4: Shear strains, degradation parameters, and degradation indices corresponding to target deflections in soft clay soil layer (pg. 1243) Figure 17: Dynamically loaded pile group: computed and measured load-deflection curves of group pile with target deflections (pg. 1243) Figure 18: Dynamically loaded pile group: time histories of earth pressure for two points in front of and behind the trailing pile without separation (pg. 1243) Figure 19: Dynamically loaded pile group: computed (with and without separation) and measured bending moment vs depth for the trailing pile (pg. 1244)
10	Figure 1: Plan view and cross section of the physical model and the location of installed instruments (pg. 26) Table 1: Scaling factors for 1-g shaking table test (pg. 27) Table 2: Properties of Firoozkuh silica sand no. 161 (pg. 27) Table 3: Mechanical and geometrical properties of model piles (pg. 28) Figure 3: Acceleration Time Histories of soil in free field (pg. 28) Figure 4: Sample excess pore water pressure time histories in free field and close to the pile (pg. 29) Figure 5: Time histories of ground surface displacement and lateral displacement of the pile heads (pg. 30) Figure 6: Recorded bending moment time histories in different model piles at the base of liquefied layer (pg. 31) Figure 7: Longitudinal profile of bending moments in the model piles (pg. 32) Figure 8: Time history of bending moment (recorded and decomposed into cyclic and monotonic components) in pile 1 at the base of liquefied layer (pg. 33) Figure 9: Distribution of monotonic componenet of lateral soil pressures along the piles obtained in this study and those recommended by JRA code (pg. 34) Figure 10: Time histories of monotonic componenet of total lateral forces in different piles of the model (pg. 35) Figure 11: Comparison between back-calculated monotonic componenet of max total lateral forces from this study and JRA recommended value for single pile (pg. 35) Figure 12: Reduction in bending moments and shear forces in different piles comparing to pile 3 (pg. 35) Figure 14: Sketch of the soil deformed shape during lateral spreading and the related contour map (pg. 36) figure 15: Back-calculated p-y curves for model piles (pg. 37) Figure 16: Pore pressure time histories in free field and near pile 3 (pg. 38) Figure 17: Net pore water pressure exerted on pile 3 (pg. 39) Figure 23: Proposed p-multipliers from multiple references (pg. 41) Figure 24: Comparison of experimental and API recommended p-y curves (pg. 42) Figure 25: Comparison between measured and computed bending moments along the model piles (pg. 43) Table 4: Relative displacements between soil and pile at ground surface based on measured and calculated results at t = 3.0 s (pg. 43) Figure 26: Variation of p-multiplier with relative displacement between soil and pile (pg.43)

Ref. No.	Relevant Figures and/or Tables
11	Figure 2: Schematic illustrations of second large-scale test in E-Defense Figure 3: Grain size distribution of Albany Silica Sand (pg.37) Table 1: Basic geotechnical properties of albany silical sand (pg. 37) Table 2: Material properties of piles and columns (pg. 37) Figure 4: Acceleration time histories and 5% damped response spectra of measured motion on table (pg. 38) Figure 6: Location of sensors (pg. 39) Figure 7: Recorded excess pore water pressures at two locations; middle of pile group and landside (pg. 39) Figure 8: Residual displacements of soil and piles measured manually (pg. 40) Figure 10: Position of inclinometers (pg. 40) Figures 11, 12, & 13: Recorded Lateral soil displacement time histories and profiles for behind the quay wall, inside the pile group, and on landside of pile group (pg. 41 & 42) Figure 14: Time histories of recorded bending strain in two different piles at three depths (pg. 42) Figure 15: Profiles of recorded bending strain in two different piles (pg. 42) Figure 19: Time histories of recorded earth pressures in Pile B2 (pg. 44) Figure 20: Time histories of soil and piles displacements (pg. 44) FIgure 21: Distribution of max monotonic lateral pressure in depth prior to structural failure of piles and comparison with recommended values (pg. 45) Figure 22: Comparison between observed soil displacements at E-Defense test and predicted values using simplified methods (pg. 45) Figure 23: Comparison between distribtution of measured lateral soil displacmeents on ground surface and predicted values using simplified methods (pg. 45) Figure 24: Comparison of measured and predicted profiles of soil displacement (pg. 45)
12	Figure 1: Detail of Borehole (pg. 4488) Table 1: Geotechnical properties of the site (pg. 4489) Figure 2: Schematic diagram of finite difference model (pg. 4489) Table 2: Pile Properties for numerical analysis (pg. 4490) Figure 3: Time histories of Manjil, Bam and Kobe strong ground motions with 0.5g peak acceleration values (pg. 4490) Table 3: Simulated eathquakes and their properties (pg. 4491) Figure 4: Pore water pressure ratio time histories of the three earthquakes with peak ground accelerations of 0.5g (pg. 4491) Figure 5: Development of excess pore pressure ratio for three different eathquake predominant frequency values (pg. 4492) Figure 6: Bending moment of the pile in each earthquake considering the effect of max acceleration (pg. 4492) Figure 7: variation of max bending moment of the pile head with different peak acceleration values (pg. 4493) Figure 8: Lateral displacement of the pile in each earthquake considering the effect of max acceleration (pg. 4493) Figure 9: Time history of lateral displacement of the pile for the bam and kobe earthquakes with different predominant frequencies (pg. 4494) Figure 10: Variation of max lateral displacement of the pile head with different peak acceleration values (pg. 4494) Figure 11: Settlement of the pile due to surcharge increment in Bam, Kobe, and Manjil earthquakes with peak ground acceleration = 0.5g (pg. 4495) Figure 12: Variation of max moment to yield moment with different predominant frequencies (pg. 4495) Figure 13: Variation of pile bending moment along pile depth (pg. 4496) Figure 14: Variation of pile displacement along pile depth (pg. 4496)

Ref. No.	Relevant Figures and/or Tables
13	Figure 1: Sieve analysis of sand Table 1: Initial properties of STCh mixture specimens Figure 3: Cyclic behavior (hysteresis loops, stress paths, and pore pressure ratio) of STCh mixtures at single amplitude shear strain = 0.15% Figure 4: Variation of single amplitude shear strain with number of cycles to liquefaction for STCh mixtures Figure 5: Number of cycles to liquefaction versus gravimetric proportions of TCh Figure 6: Number of cycles to liquefaction versus STCh mixture void ratio Figure 7: STCh mixtures max shear stress at single amplitude shear strains of: 0.23%, 0.38%, and 0.50% Figure 8: Average shear stress factor for STCh mixtures Figure 9: Shear modulus versus number of cycles to liquefaction for different gravimetric porportions of STCh mixtures Figure 10: damping ratio versus number of cycles to liquefaction for different gravimetric proportions of STCh mixtures Figure 11: Variation of travel time with the gravimetric proportion of TCh Table 2: Dimensionless elastic stiffness parameter A for STCh mixtures Figure 12: Max shear modulus versus effective confining pressure for different STCh mixtures Figure 13: Normalized shear modulus curve for san-scrap tyre mixtures Figure 14: Damping ratio curve for sand-scrap tyre mixtures
14	Table1: Geotechnical Propeties of Harbin Sand (pg. 70) Figure 2: Experimental setup and instrumentation (pg. 70) Figure 3: Nonlinear moment-curvature relationship of the pile (pg. 71) Table 2: Material Properties of the RC pile (pg. 71) Table 3: material properties of sheet pile (pg. 71) Figure 4: Free-Field accelerations (pg. 71) Figure 5: Free-Field Excess Pore Pressure time histories at different depths (pg. 72) Figure 6: Accelerations of superstructure and ground surface (pg. 72) Figure 7: Soil lateral displacement time history at multiple depths (pg. 72) Figure 8: Lateral displacments of the ground surface and superstructure (pg. 72) Figure 9: Representative moment time histories for the pile (pg. 73) Figure 10: Decomposition of recorded bending moment into monotonic and cyclic components (pg. 73) Figure 11: Recorded and Decomposed Soil Pressure time histories for multiple depths (pg. 74) Figure 12: Analytical model for analysis of nonlinear pile response subjected to lateral spreading soils (pg. 75) Figure 13: Example of superposition principle for the total pile displacement (pg. 76) Figure 14: Comparison of the experimental and computed pile response (moment and displacement profiles) (pg. 77) Figure 15: Influence of the axial force on the pile response (moment and displacement profiles) (pg. 77) Figure 16: Influence of pile diameter on the pile response (moment and displacement profiles (pg. 78)

Ref. No.	Relevant Photos
9	Figure 2: Photo of the full-scale lateral load test layout (pg. 1235) Figure 11: Photo of gap formation behind a pile when pile is deflected laterally to the right (pg. 1240)
10	Figure 2: Photos (side and top views) of the physical model of the SUT shake table (pg. 27) Figure 13: Photos of the surface of the model before and during shaking (pg. 36) Figure 18: Photo from the side of the model showing the upslope part (pg. 39) Figure 19: Photo and illustration of Heave and subsidence around the half single pile during the lateral spreading (pg. 39) Figure 21: Development of sand boils in different places at surface of the model (pg. 40)
11	Figure 1: Shake Table Experiment Setup (pg. 36) Figure 9: Extensive damage in model (pg. 40) Figure 16: Photo of damage to piles (pg. 43) Figure 17: close-up photo of damage to piles (pg. 43) Figure 18: Photo of damage to pile heads (pg. 43)
13	Figure 1: Photo of tyre chips with ruler
14	Figure 1: Shake Table Experiment (pg. 70)

9. Appendix B: Damping Curves

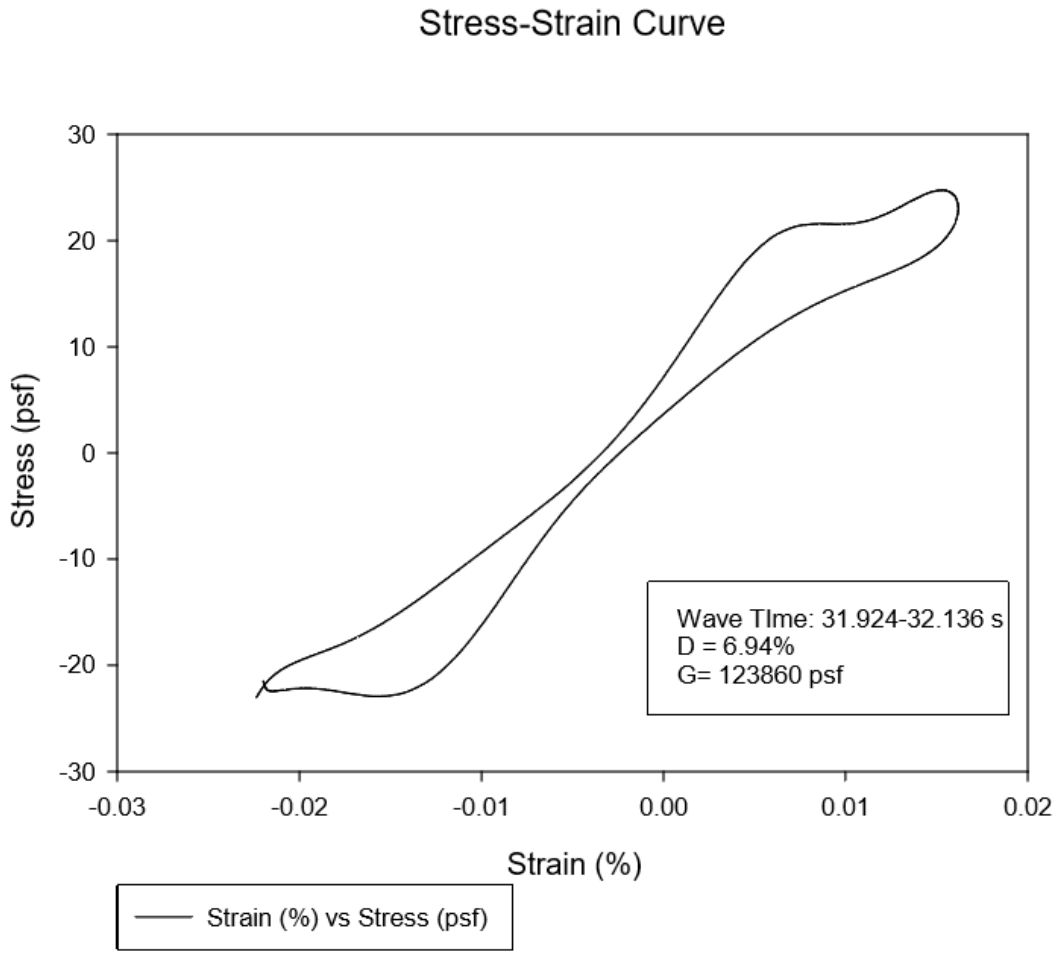

Figure 54: Day 1 Curve 1

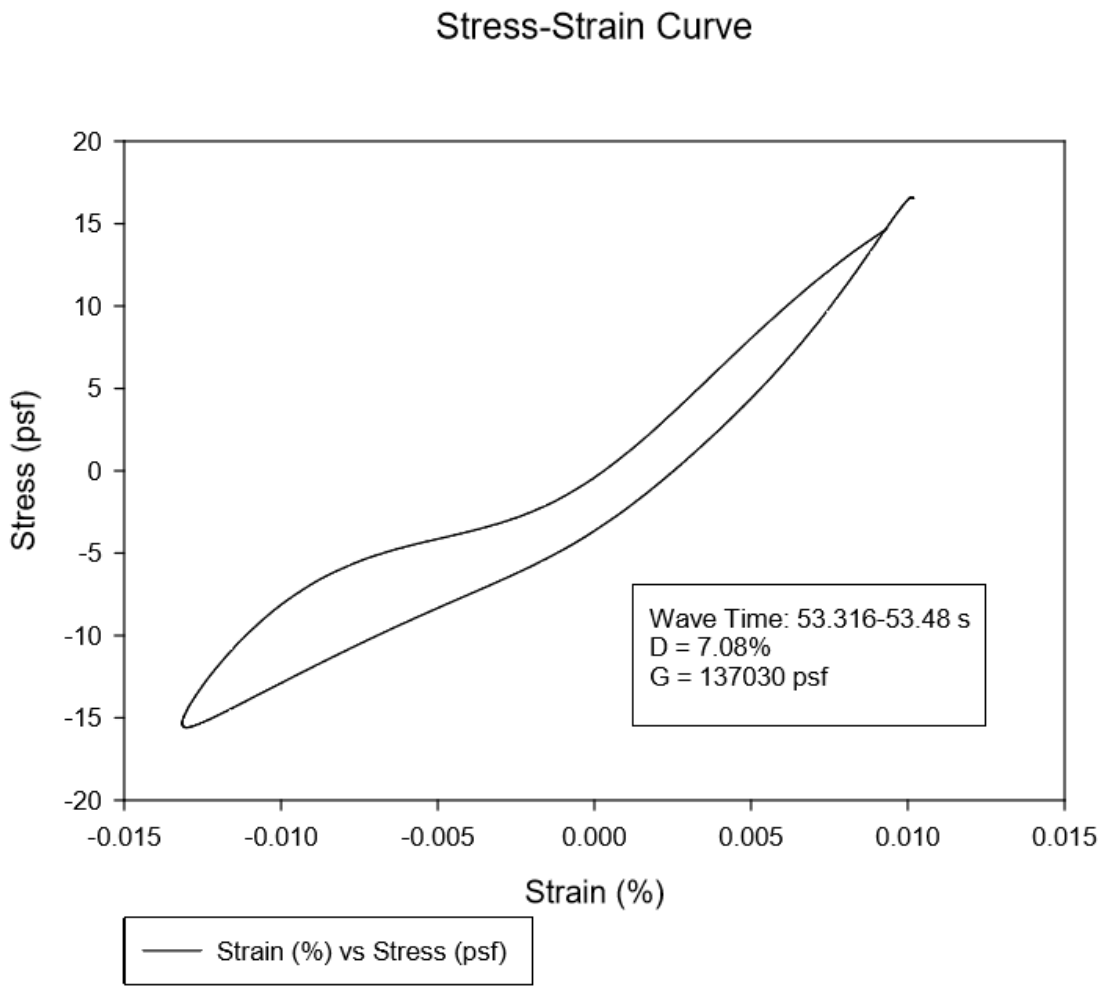

Figure 55: Day 1 Curve 2

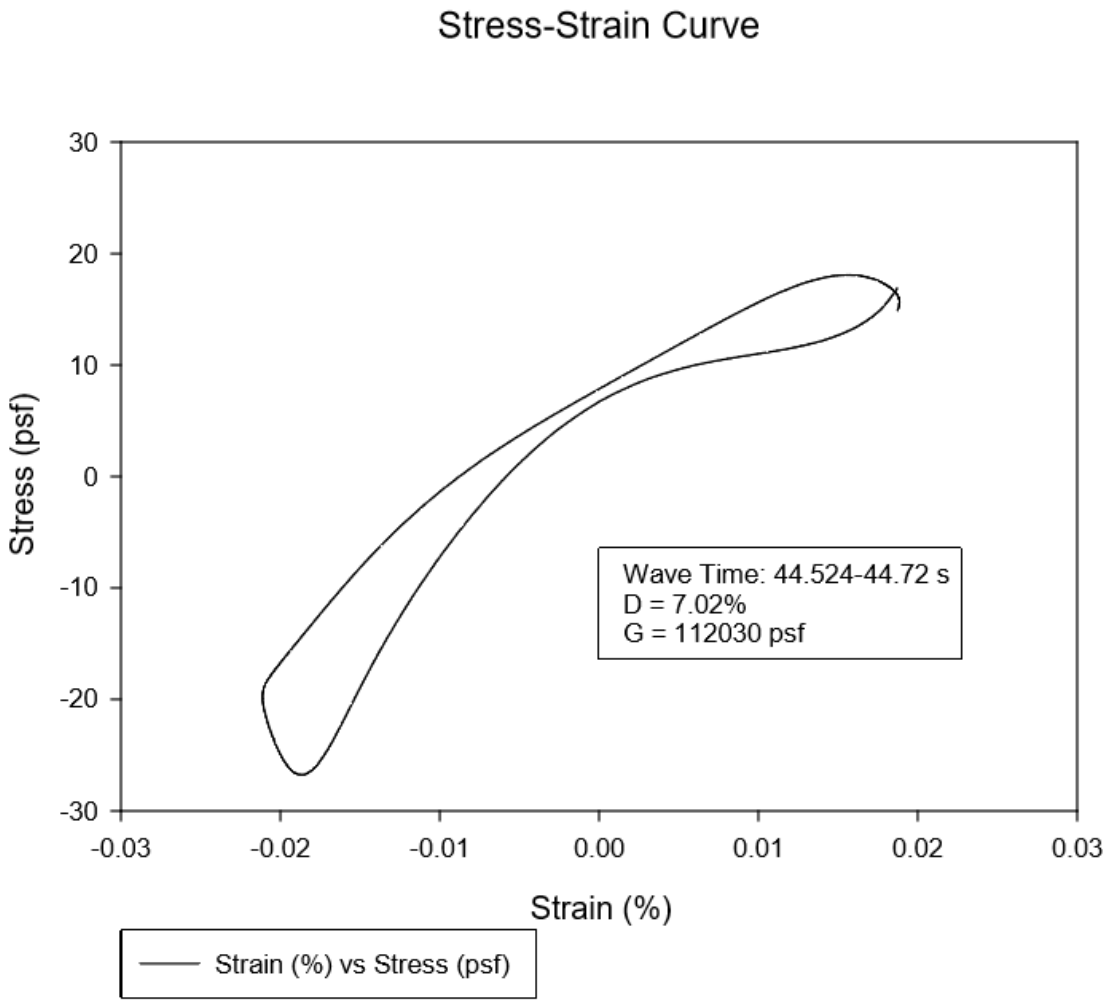

Figure 56: Day 1 Curve 3

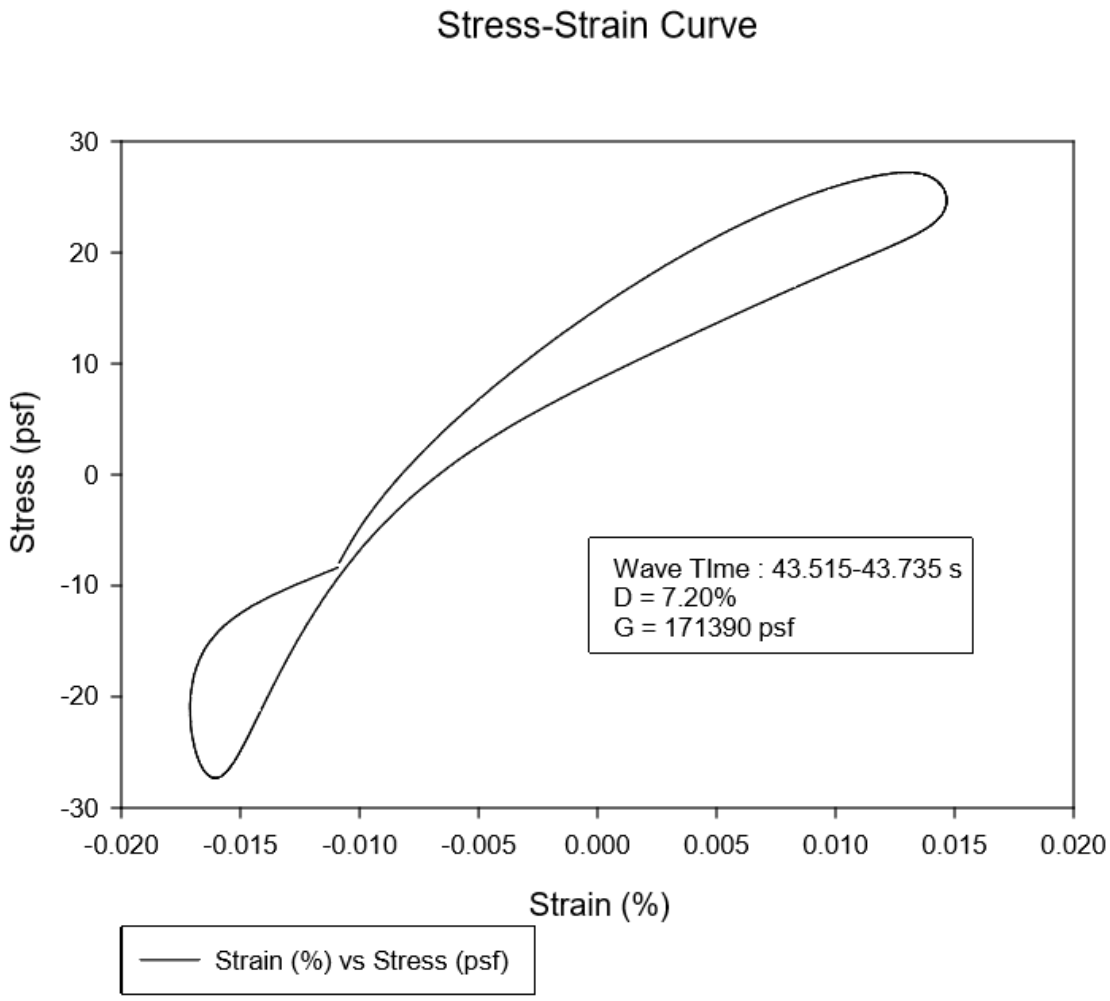

Figure 57: Day 1 Curve 4

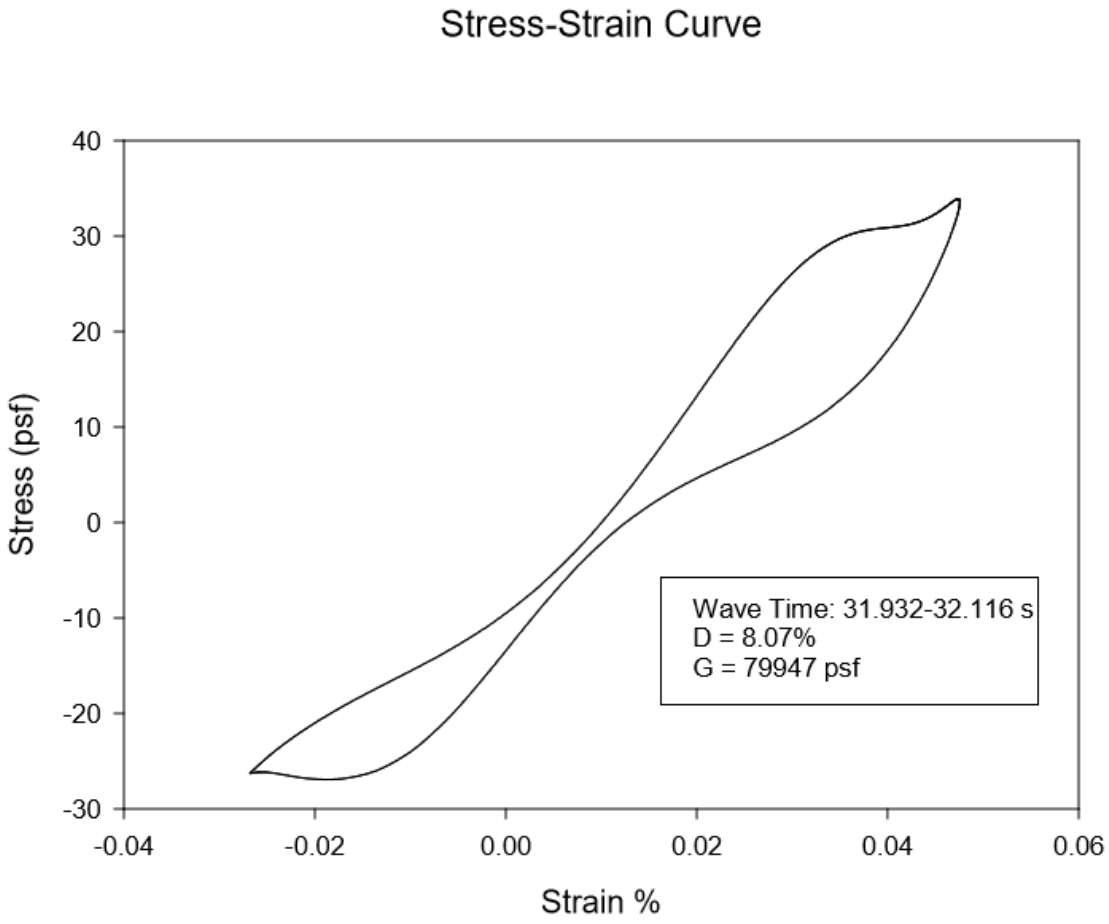

Figure 58: Day 2 Curve 1

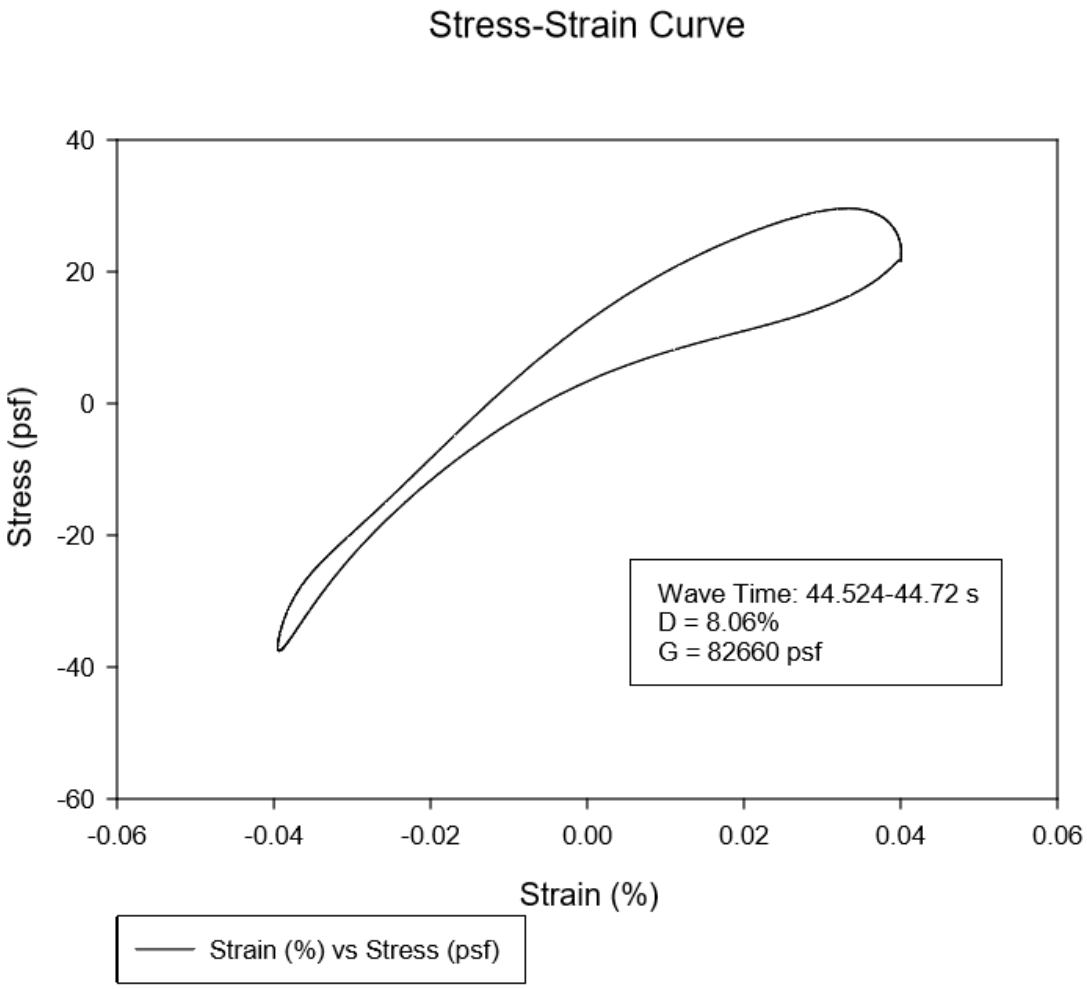

Figure 59: Day 2 Curve 2

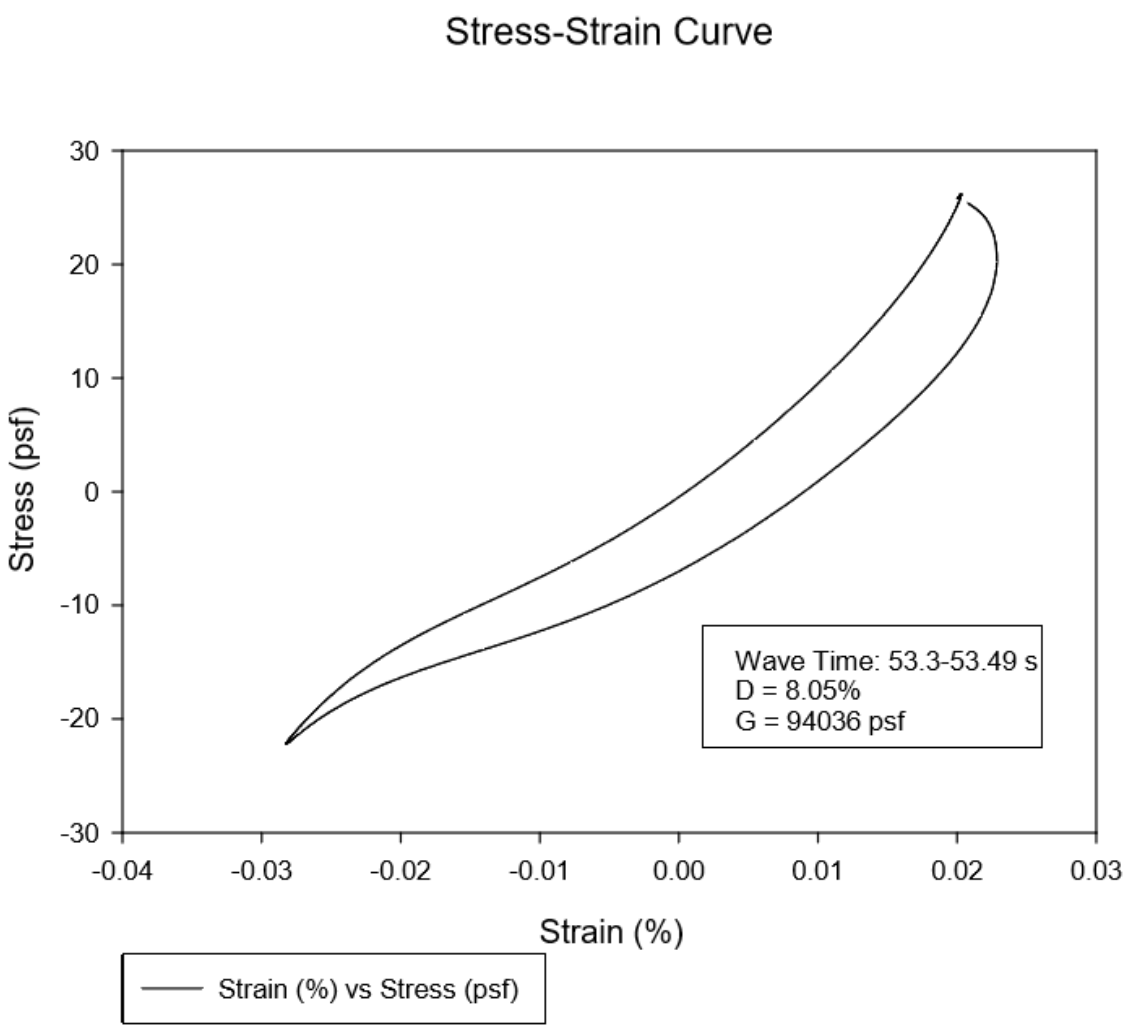

Figure 60: Day 2 Curve 3

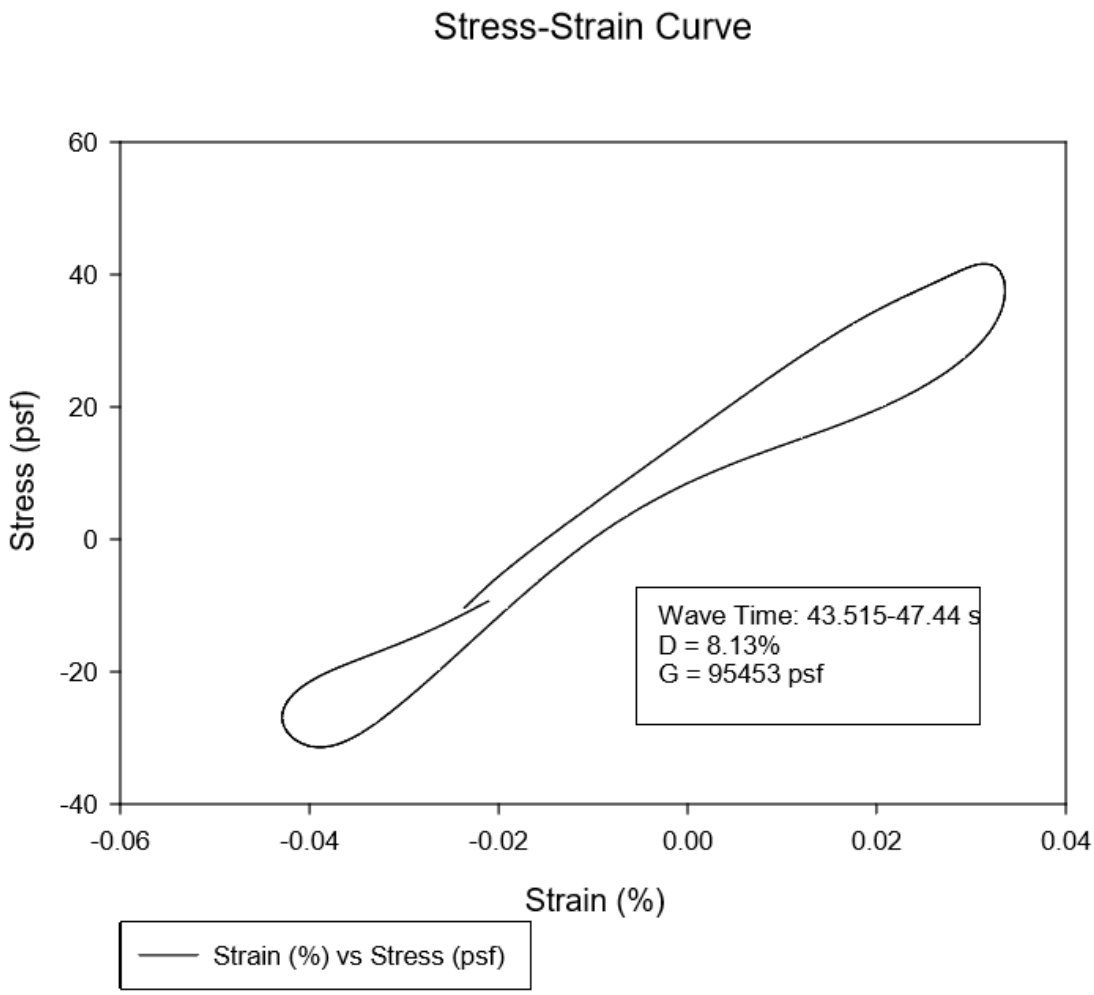

Figure 61: Day 2 Curve 4

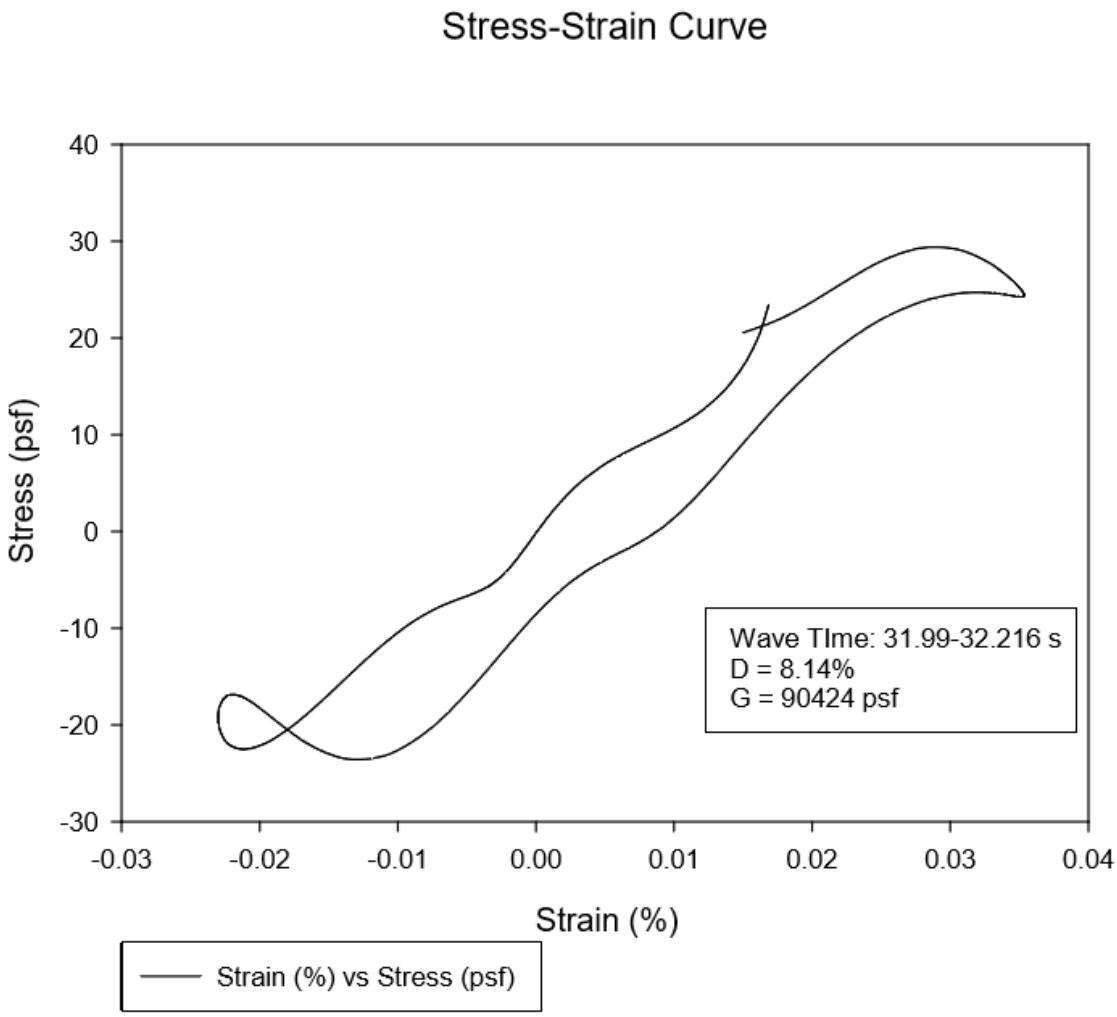

Figure 62: Day 3 Curve 1

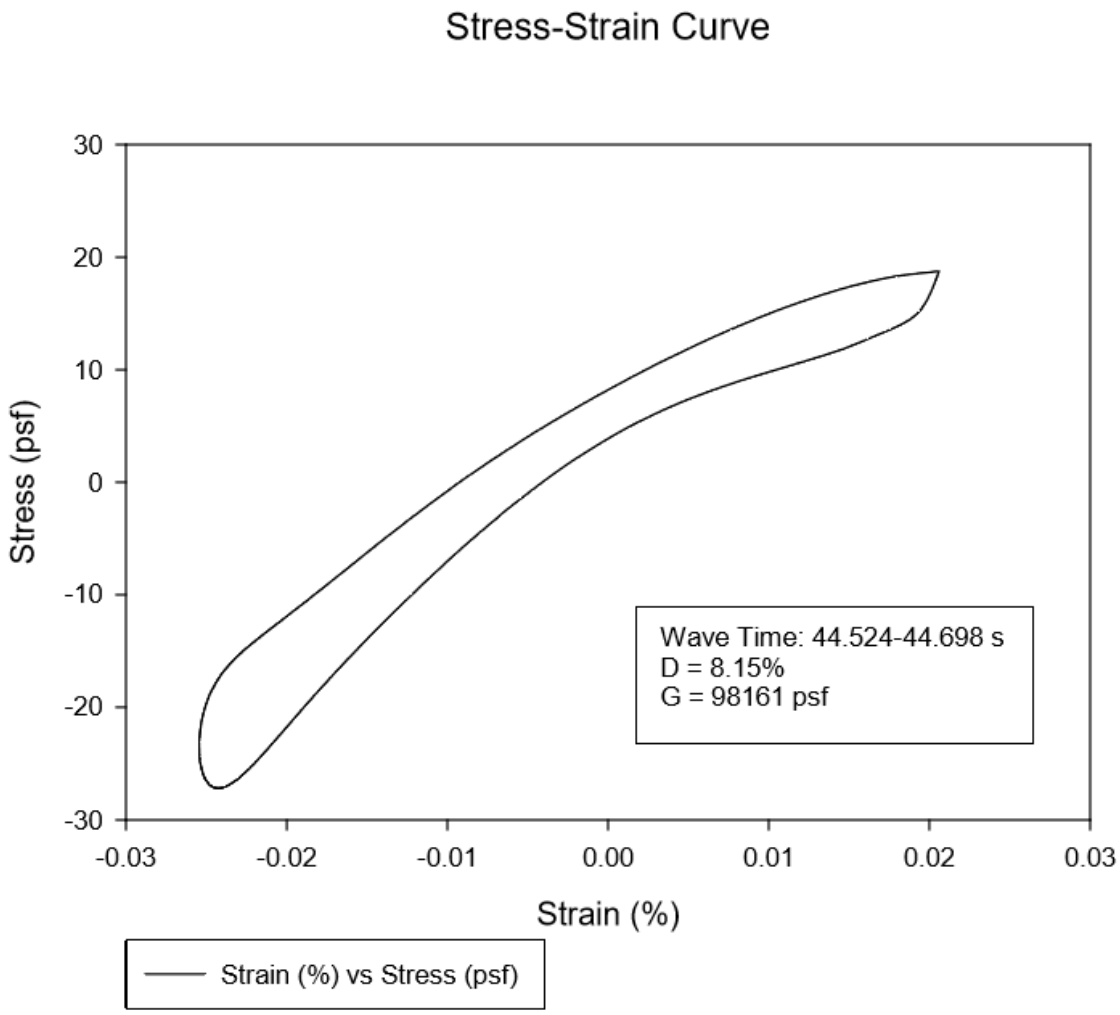

Figure 63: Day 3 Curve 2

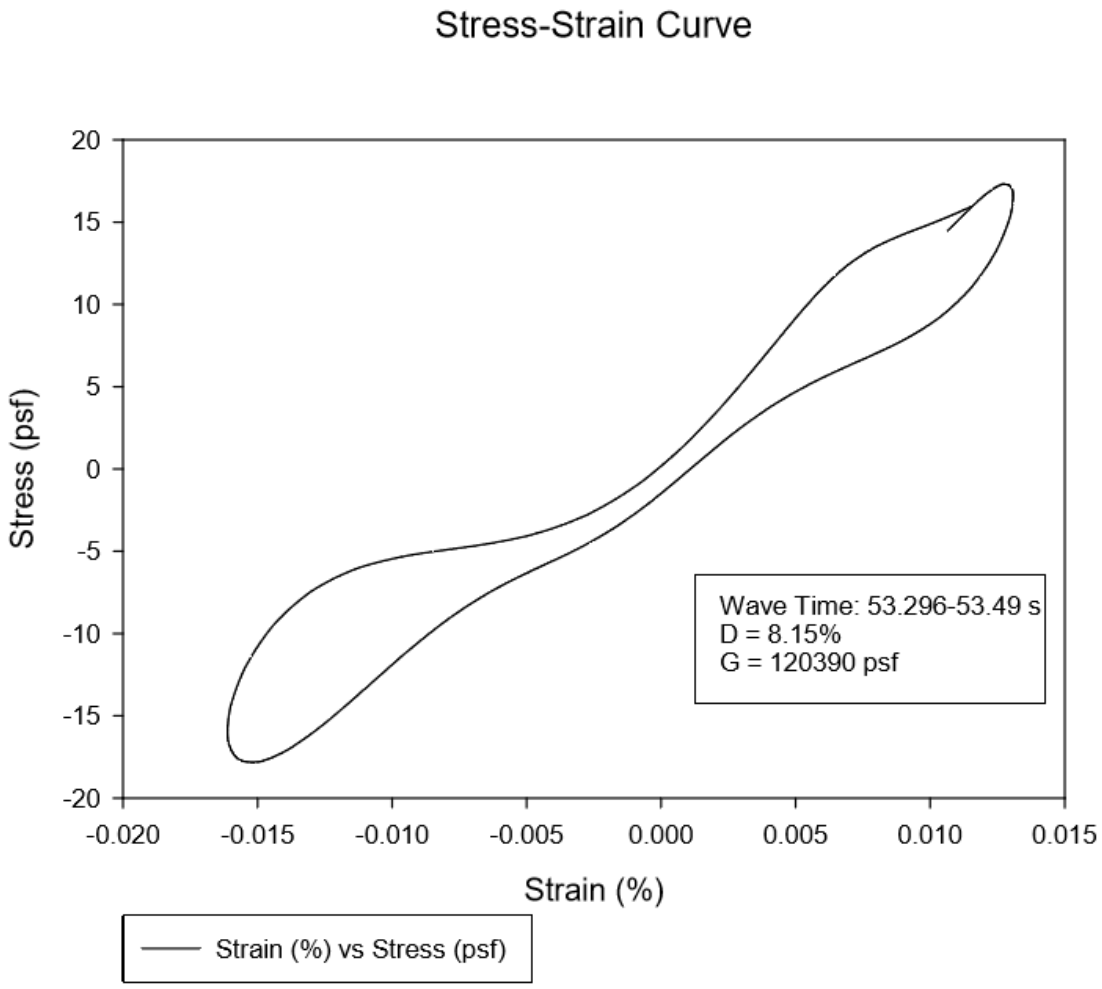

Figure 64: Day 3 Curve 3

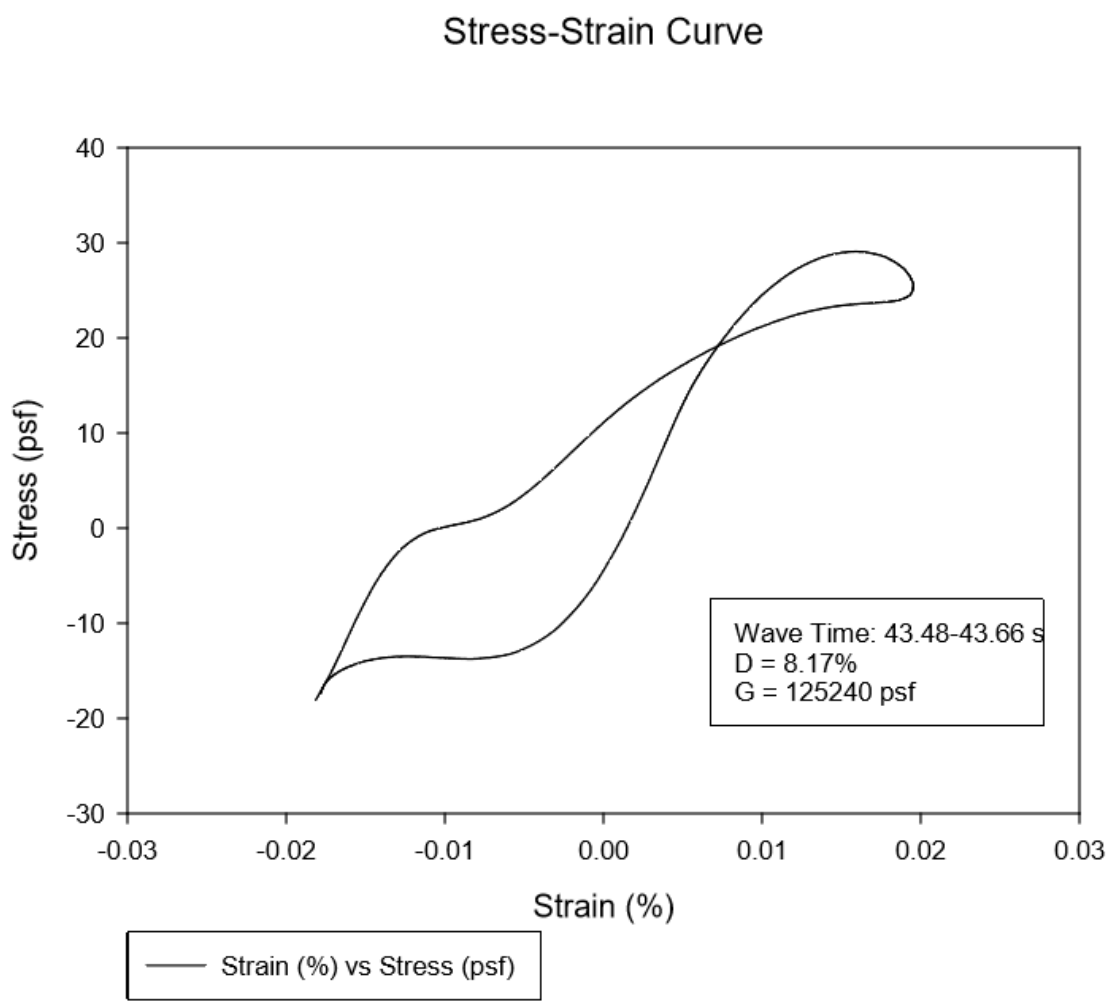

Figure 65: Day 3 Curve 4

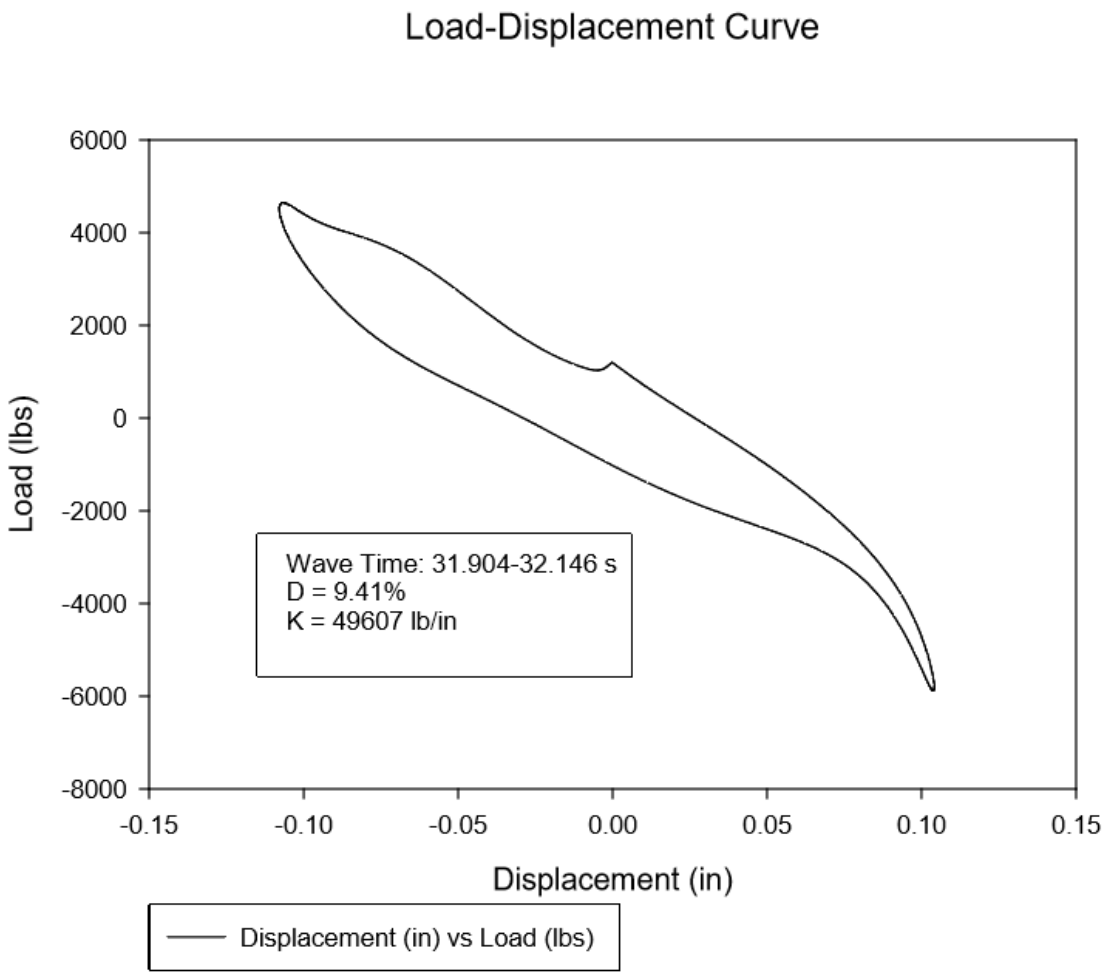

Figure 66: Day 4 Curve 1

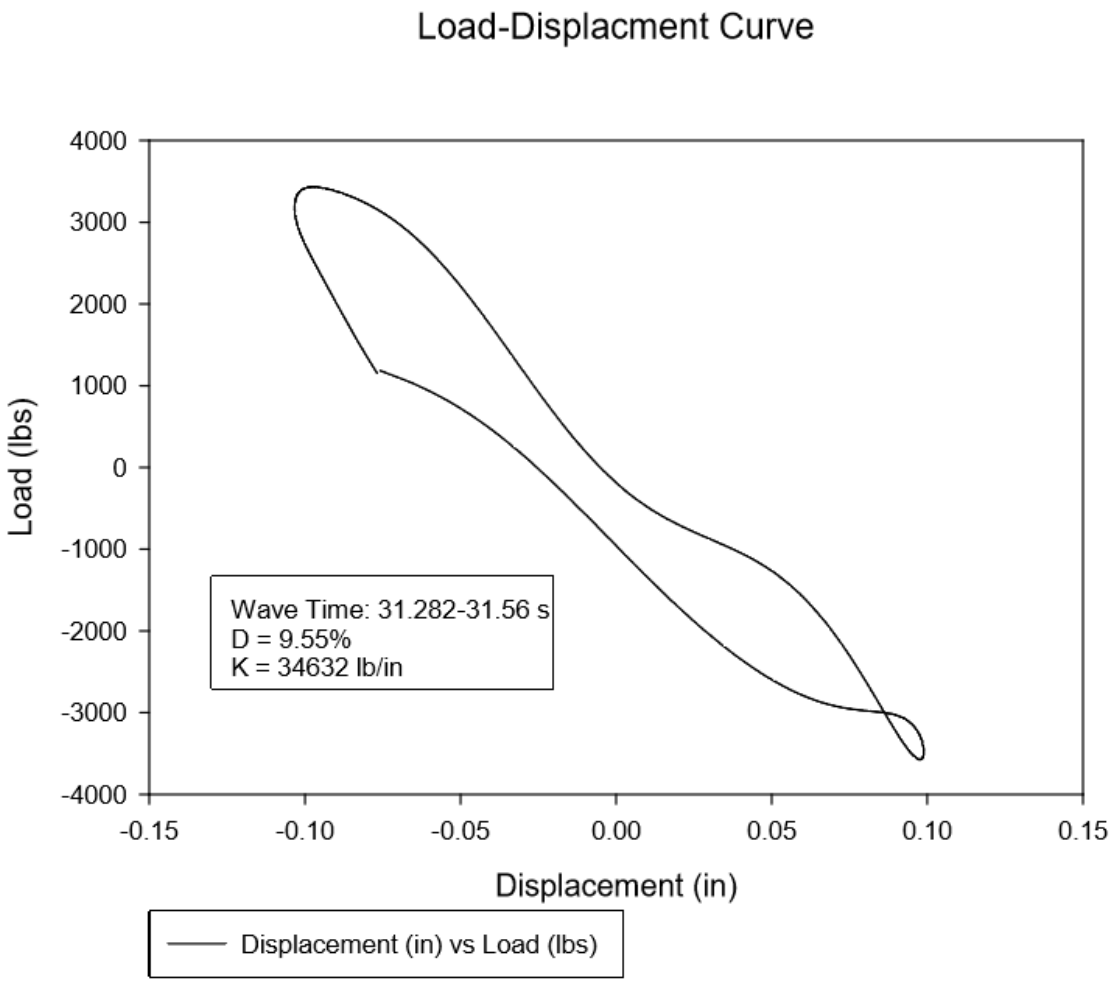

Figure 67: Day 4 Curve 2

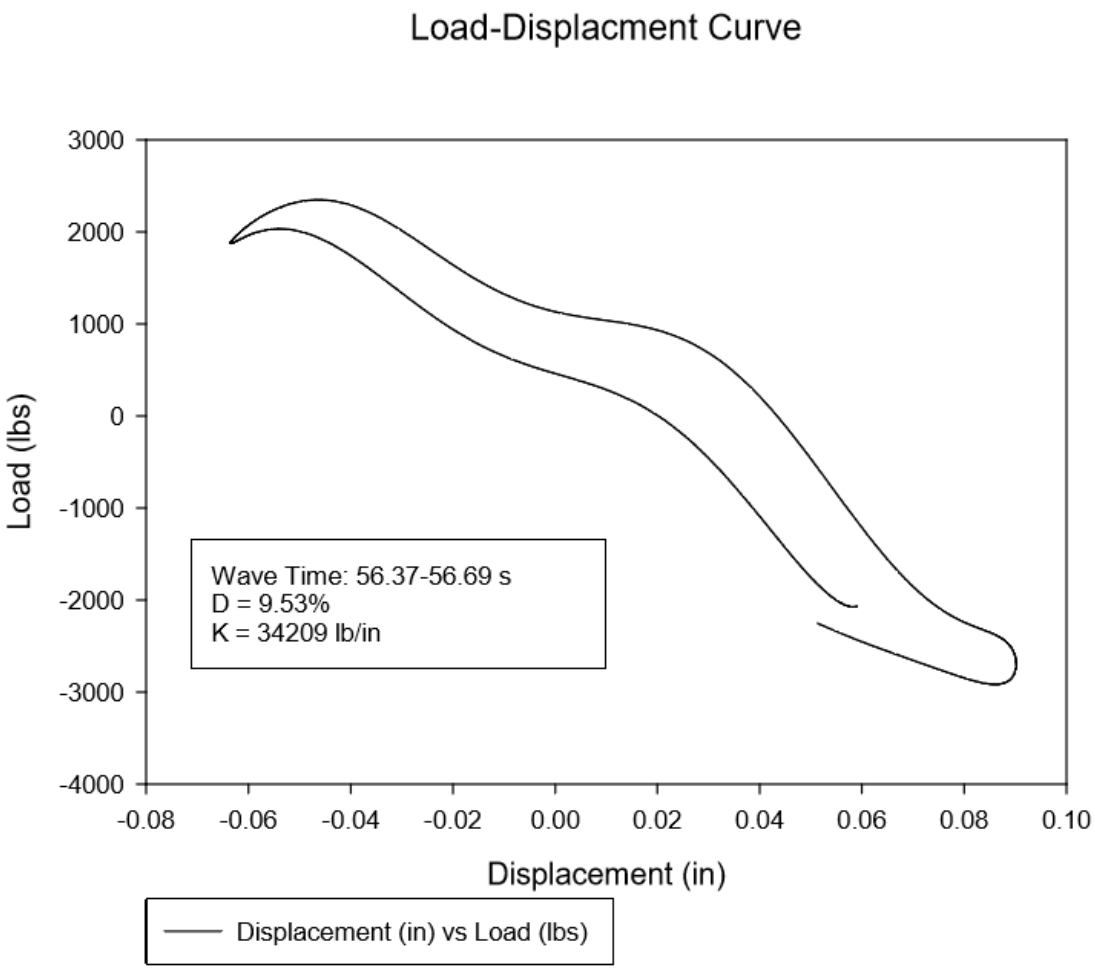

Figure 68: Day 4 Curve 3

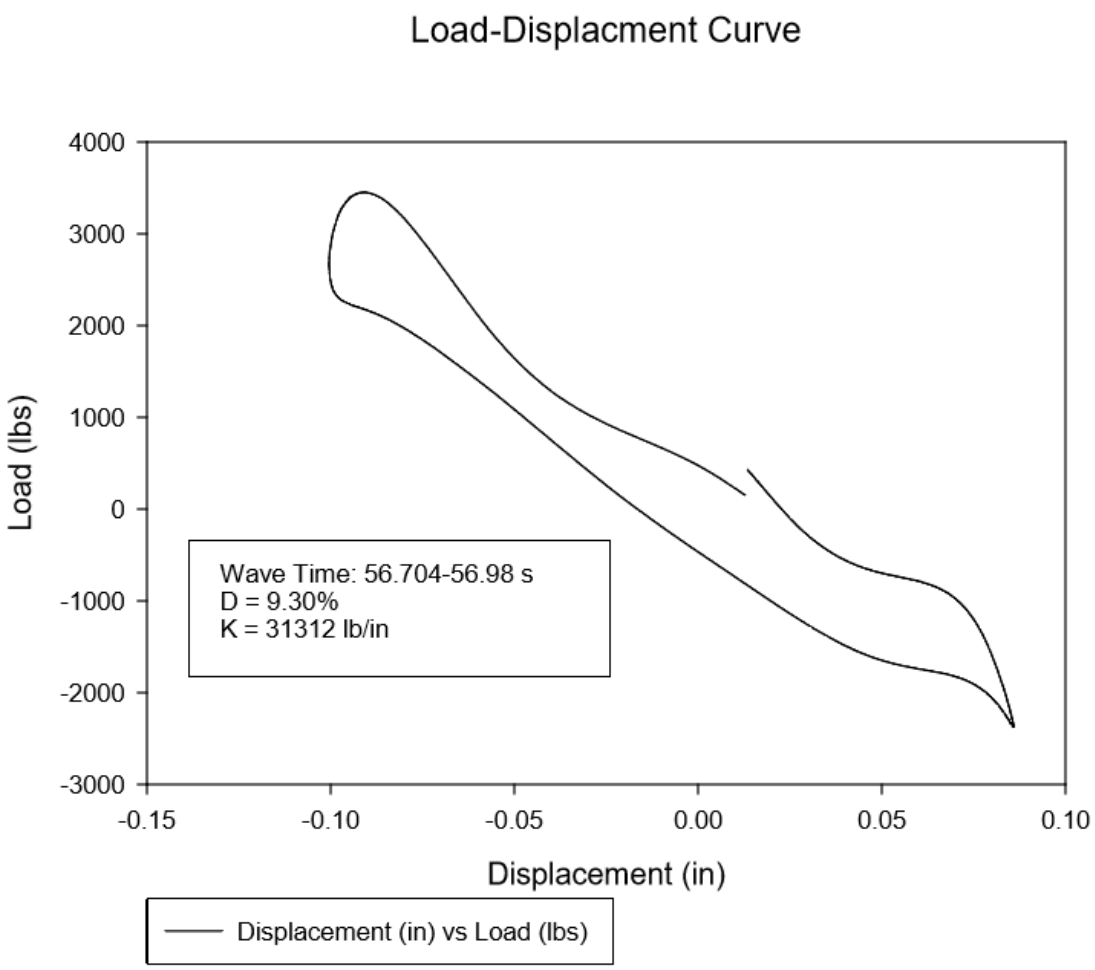

Figure 69: Day 4 Curve 4

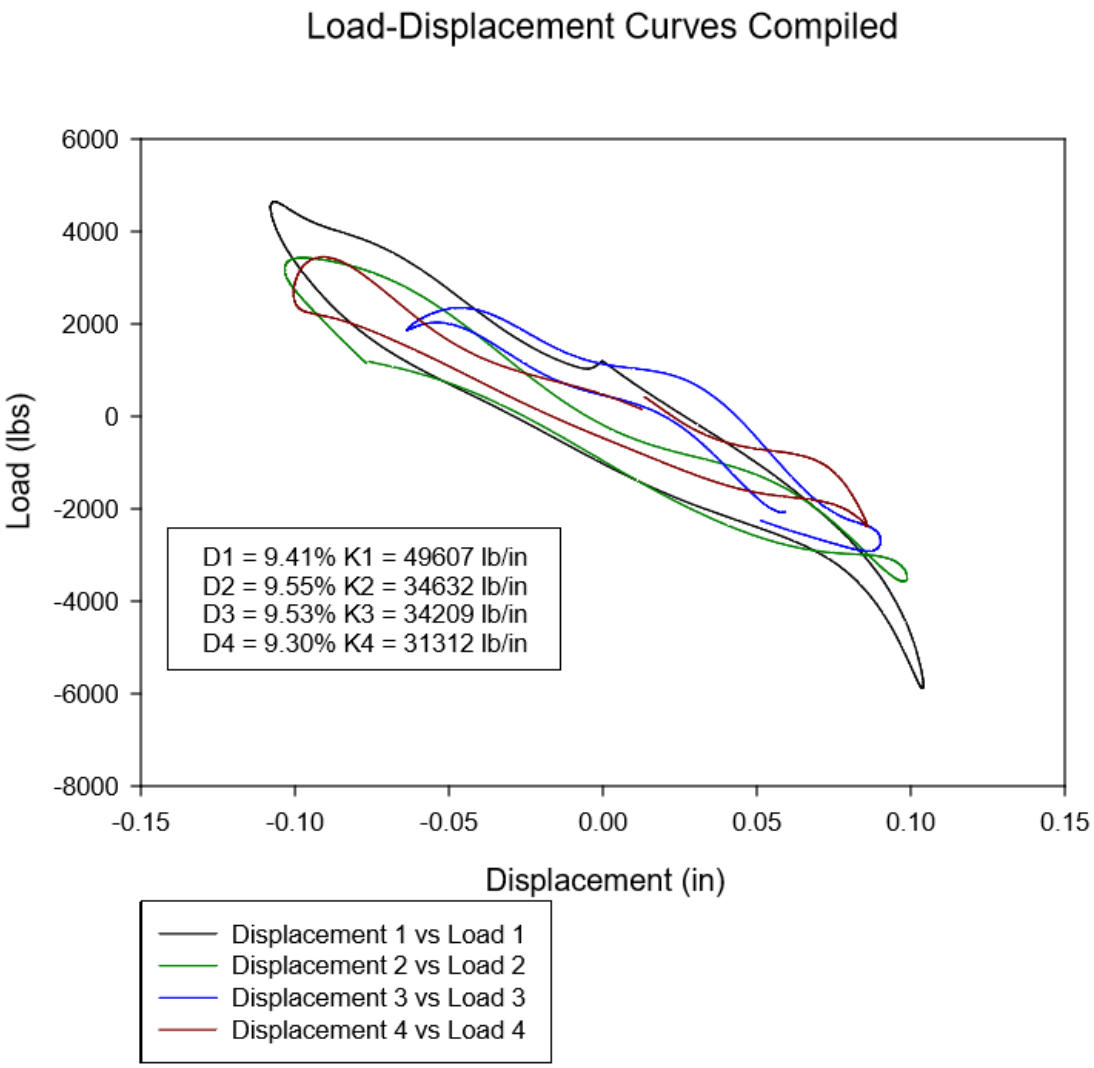

Figure 70: Day 4 Compiled Curves

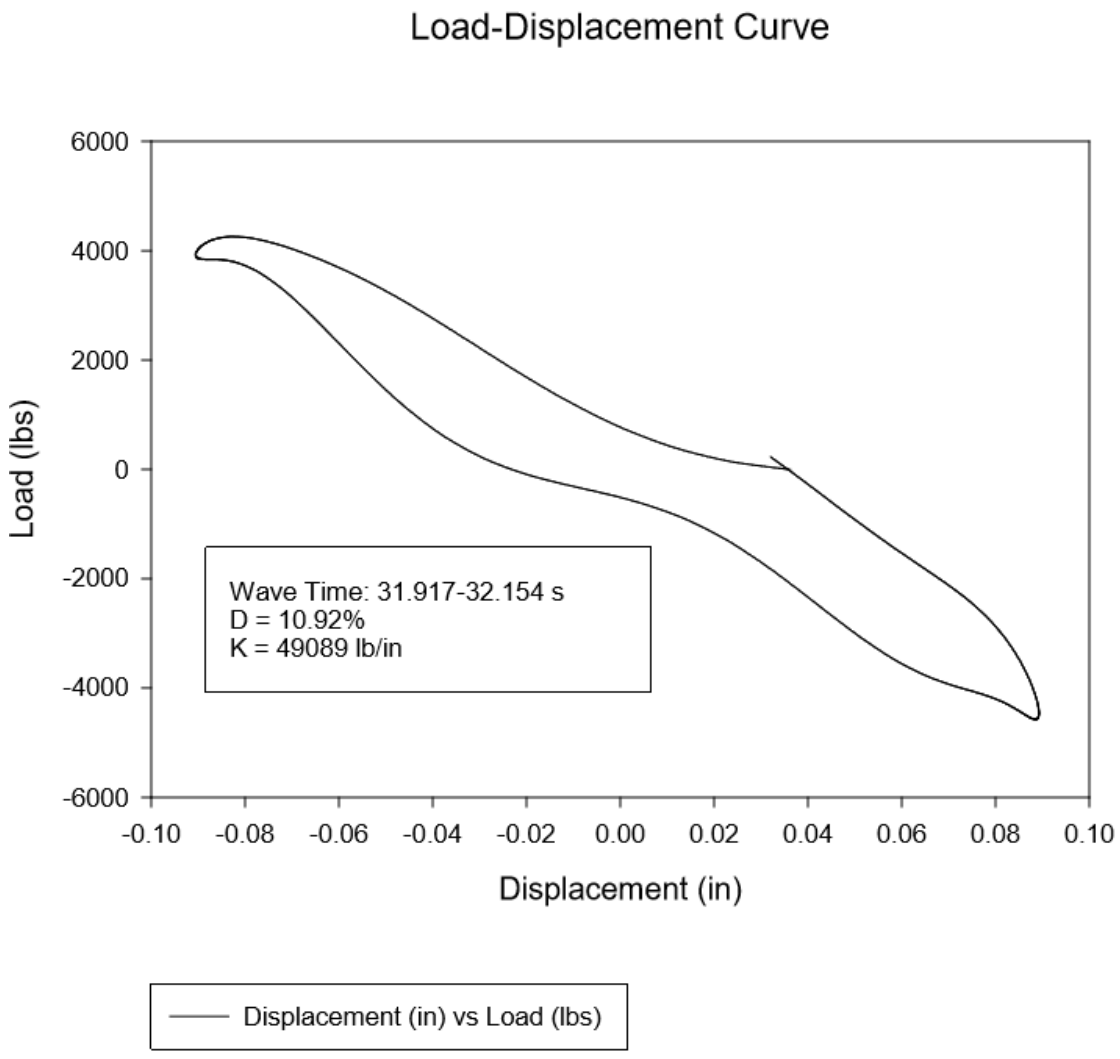

Figure 71: Day 5 Curve 1

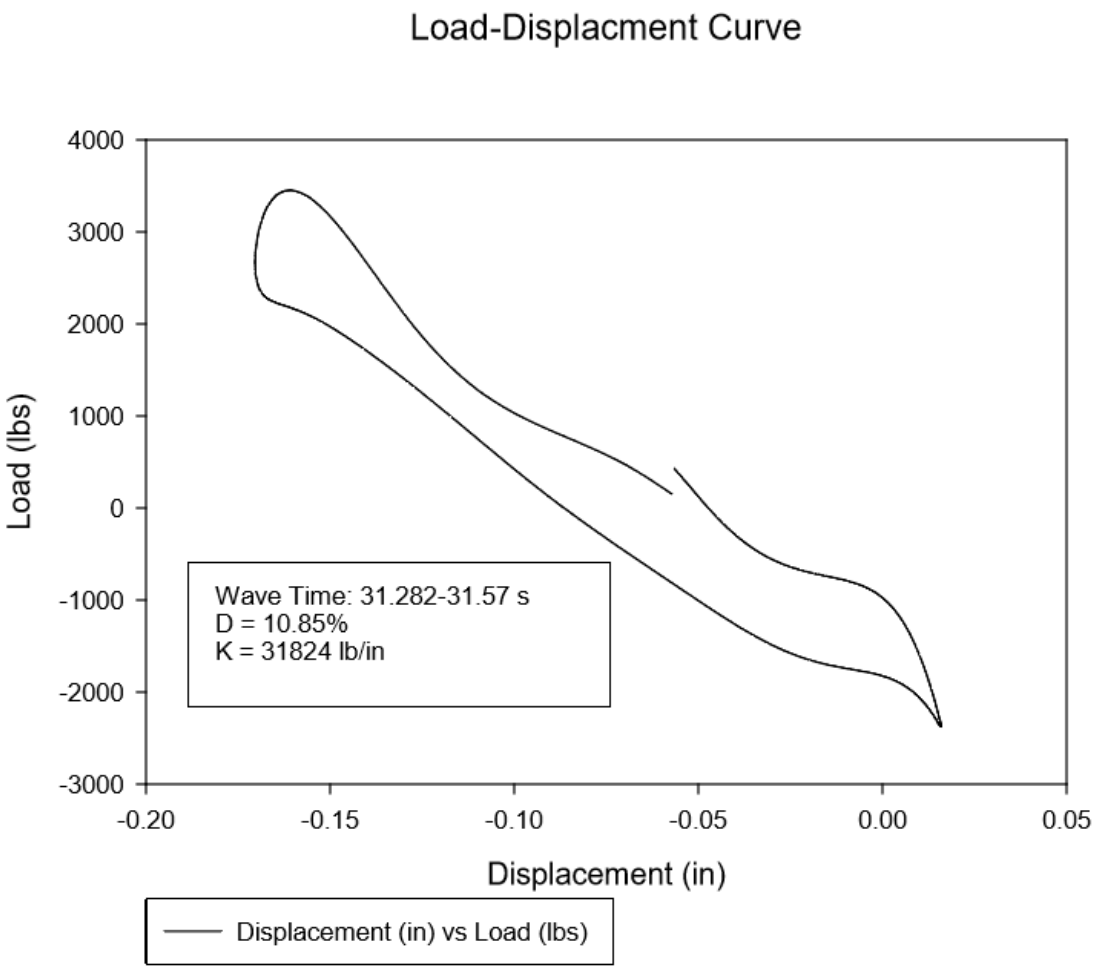

Figure 72: Day 5 Curve 2

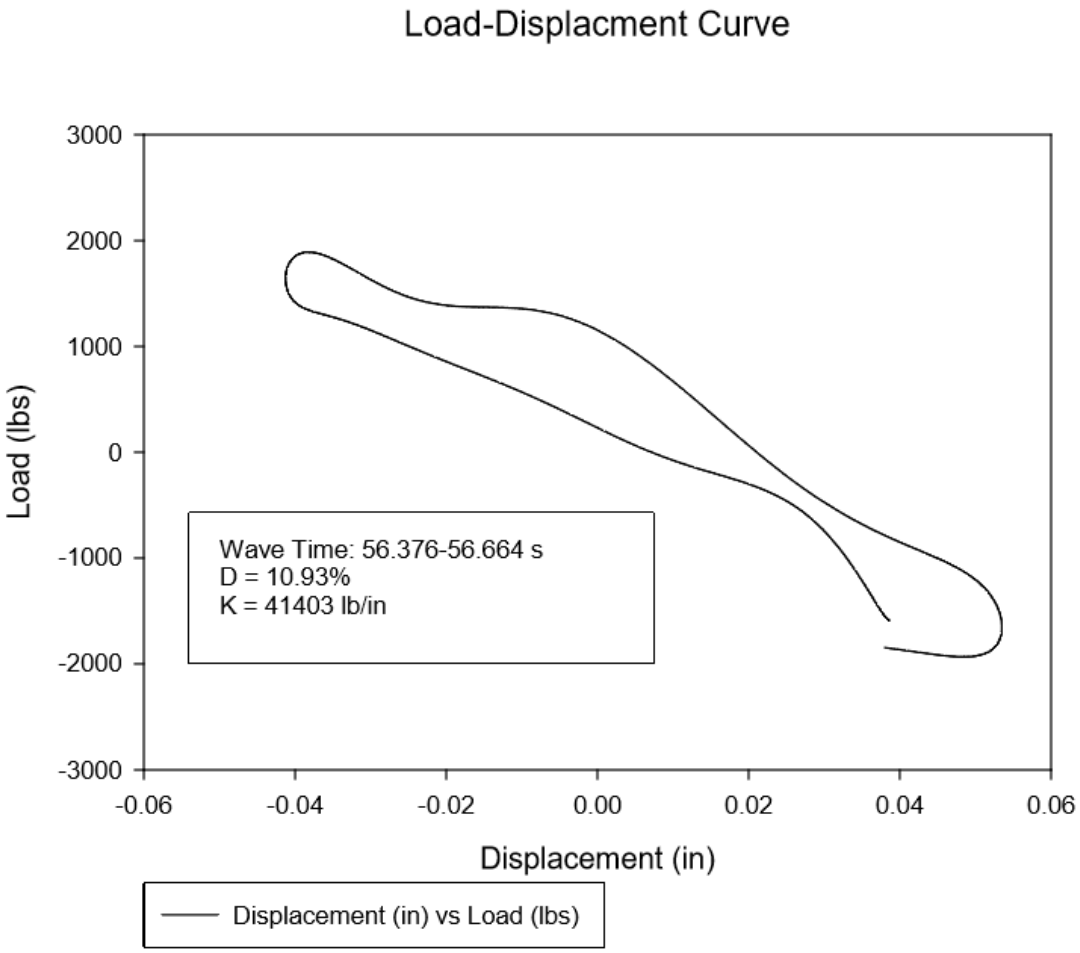

Figure 73: Day 5 Curve 3

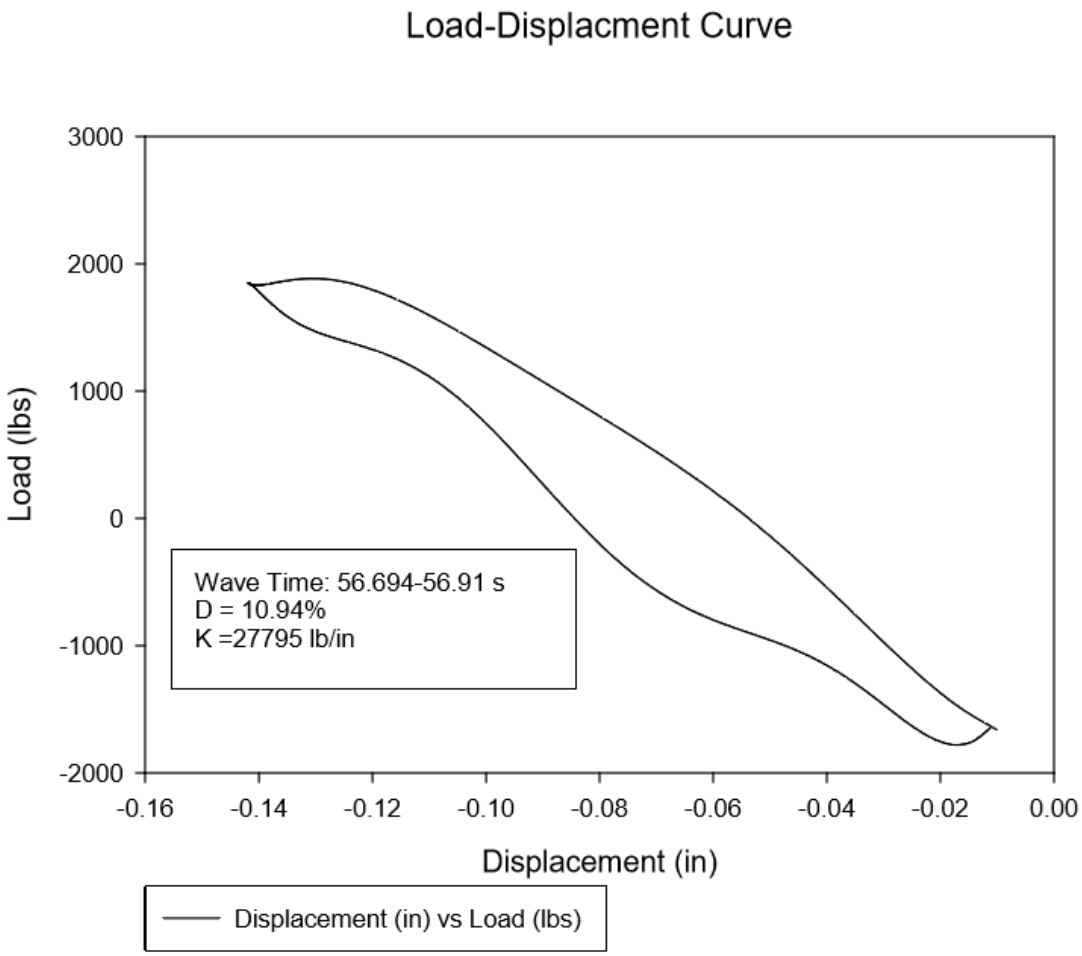

Figure 74: Day 5 Curve 4

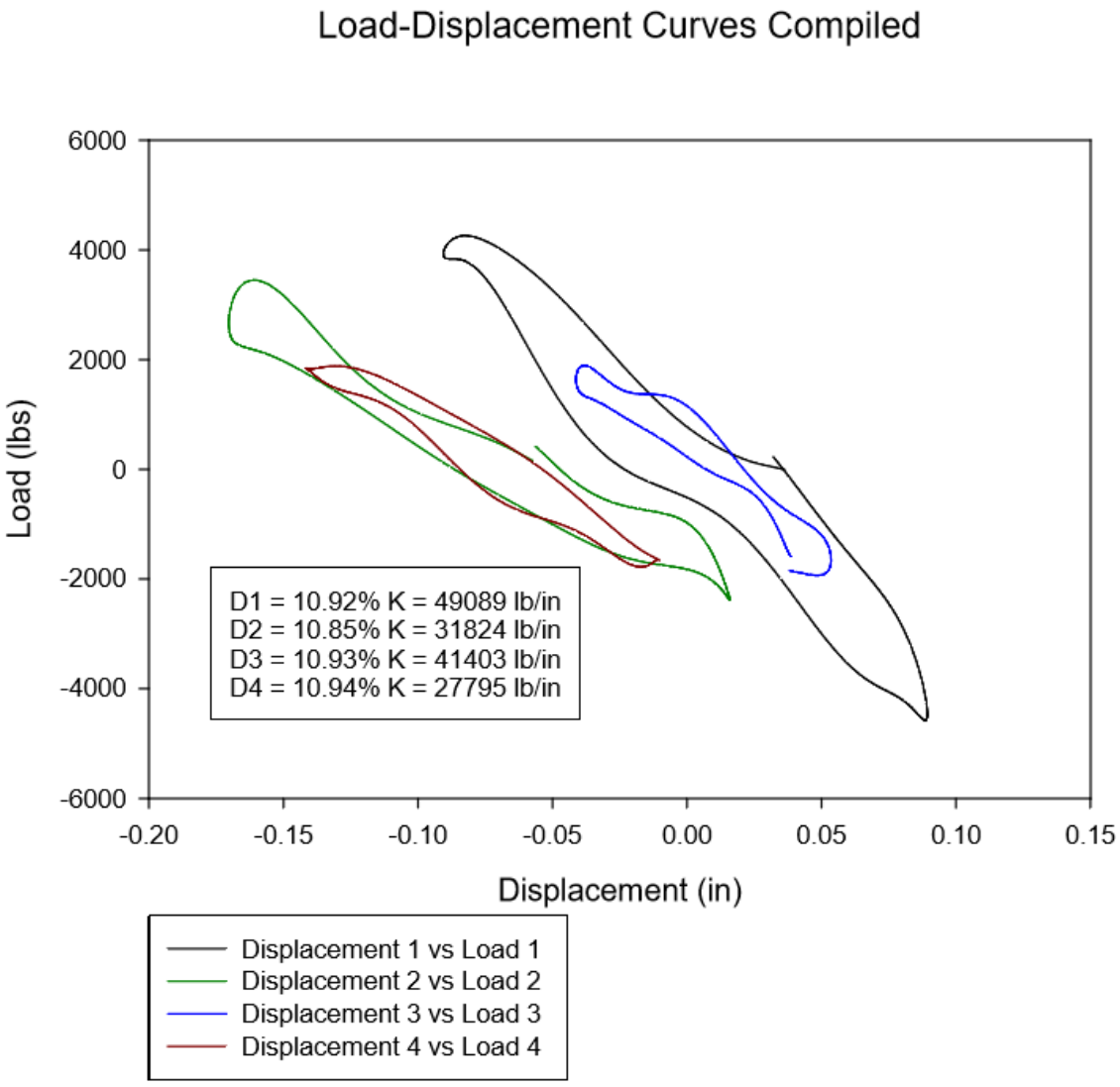

Figure 75: Day 5 Compiled Curves

10. Appendix C: Acceleration Recordings

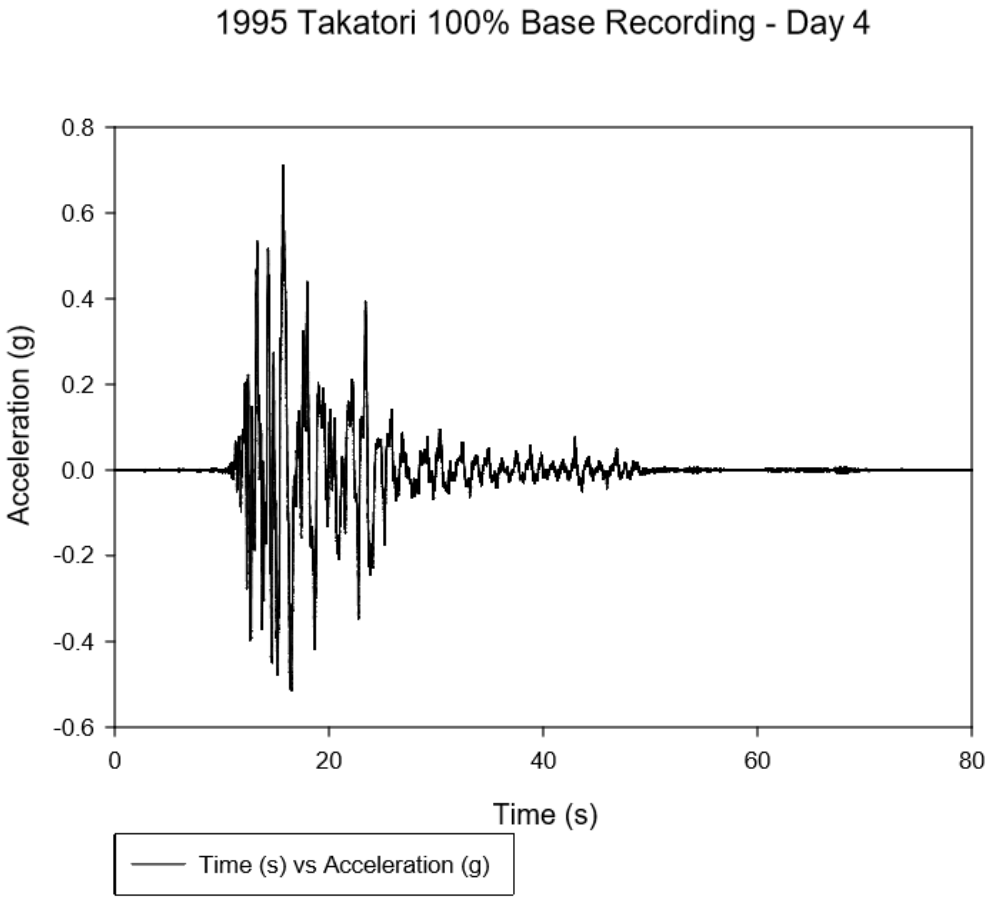

Figure 76: 1995 Takatori 100% Base Recording - Day 4

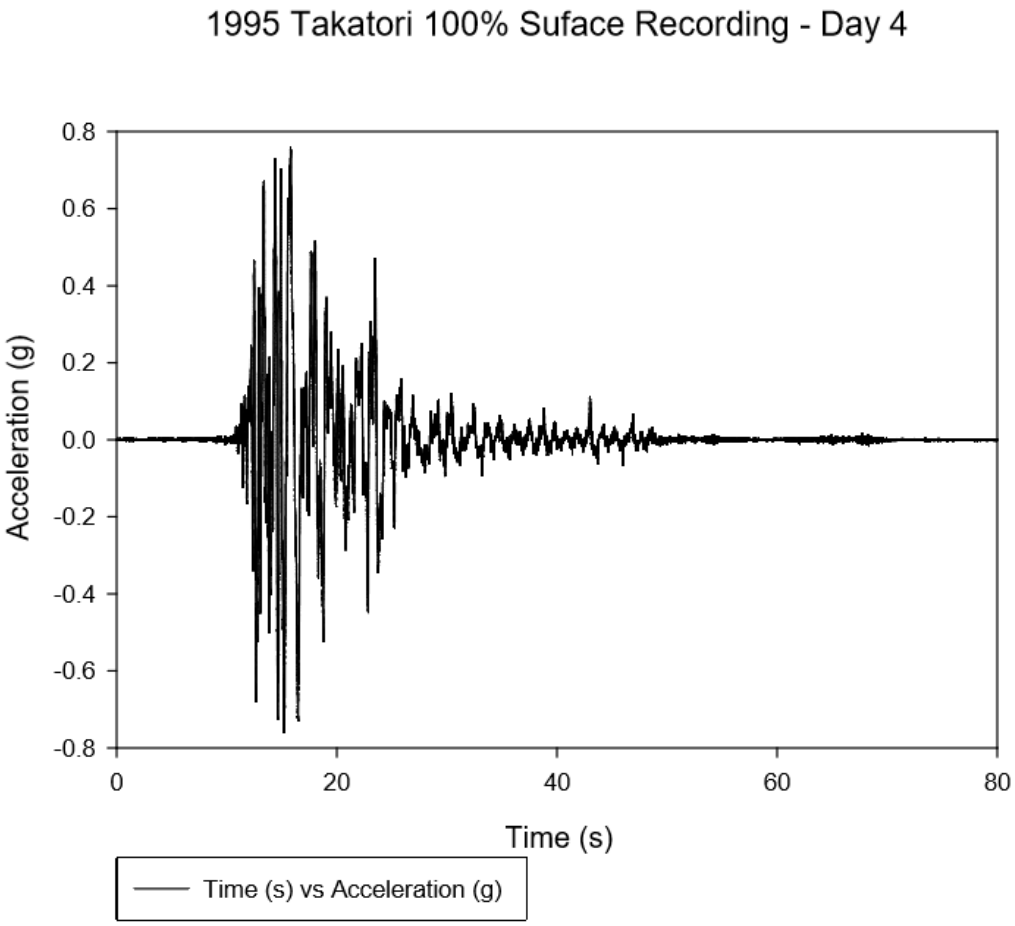

Figure 77: 1995 Takatori 100% Surface Recording - Day 4

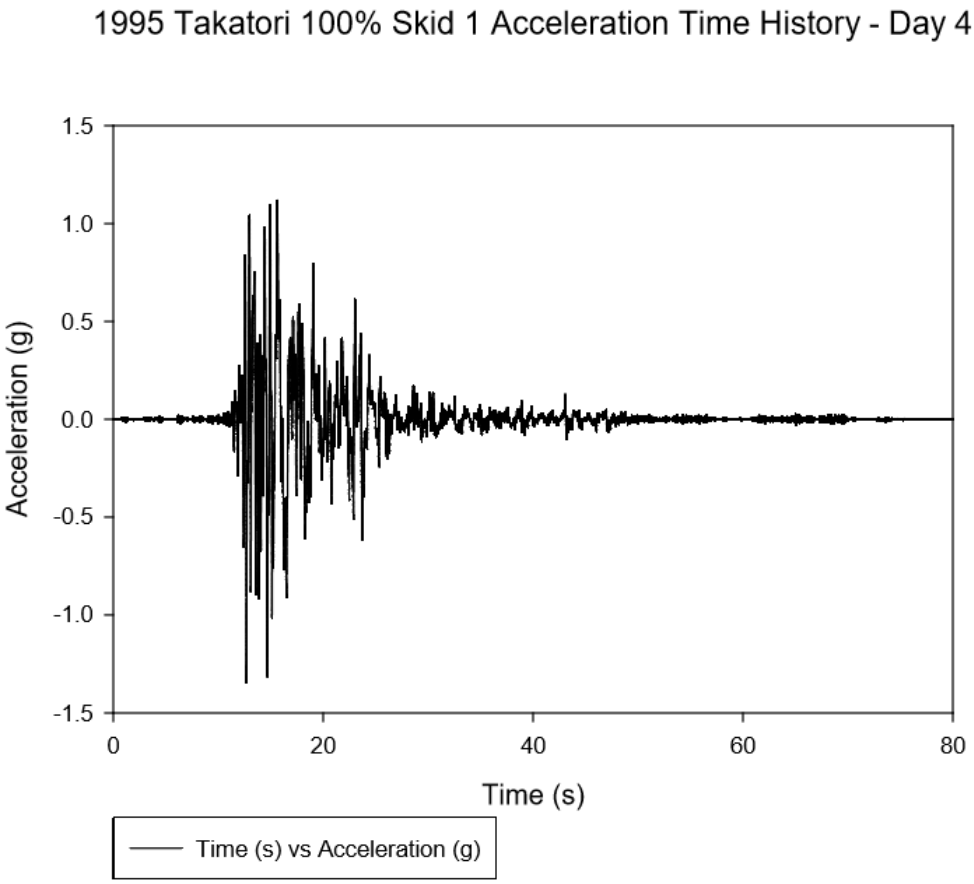

Figure 78: 1995 Takatori 100% Skid 1 Recording - Day 4

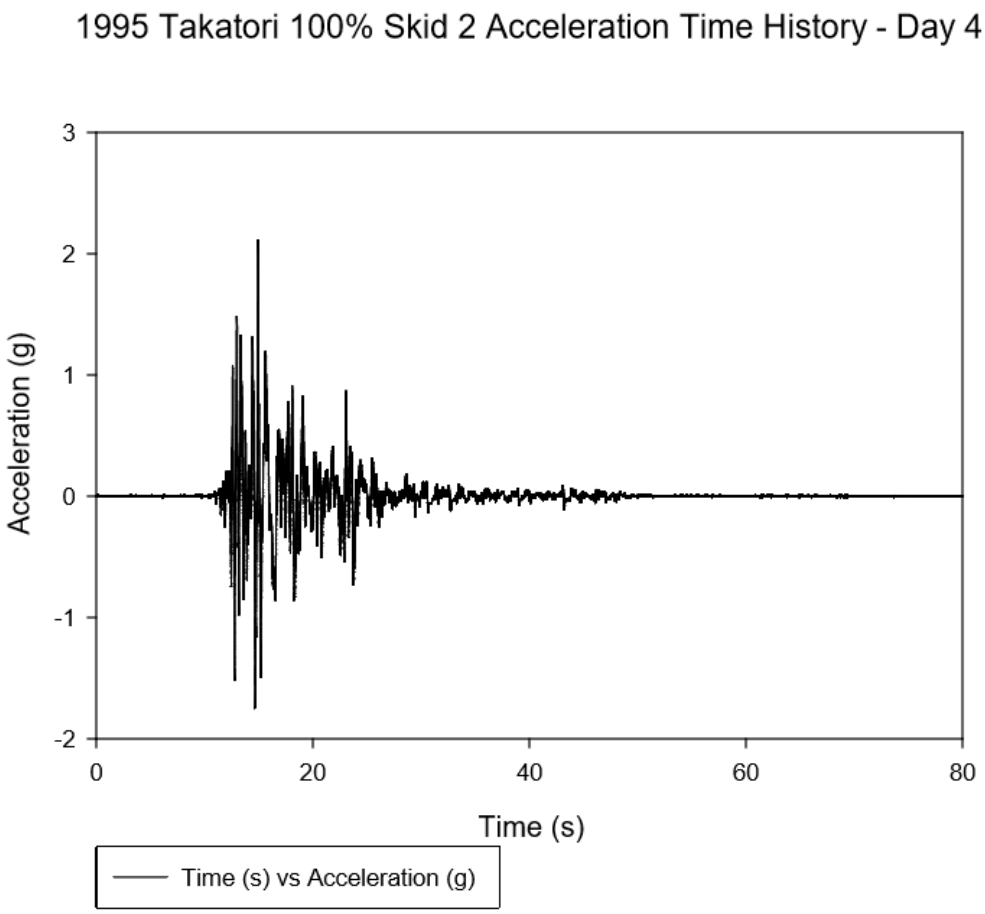

Figure 79: 1995 Takatori 100% Skid 2 Recording - Day 4

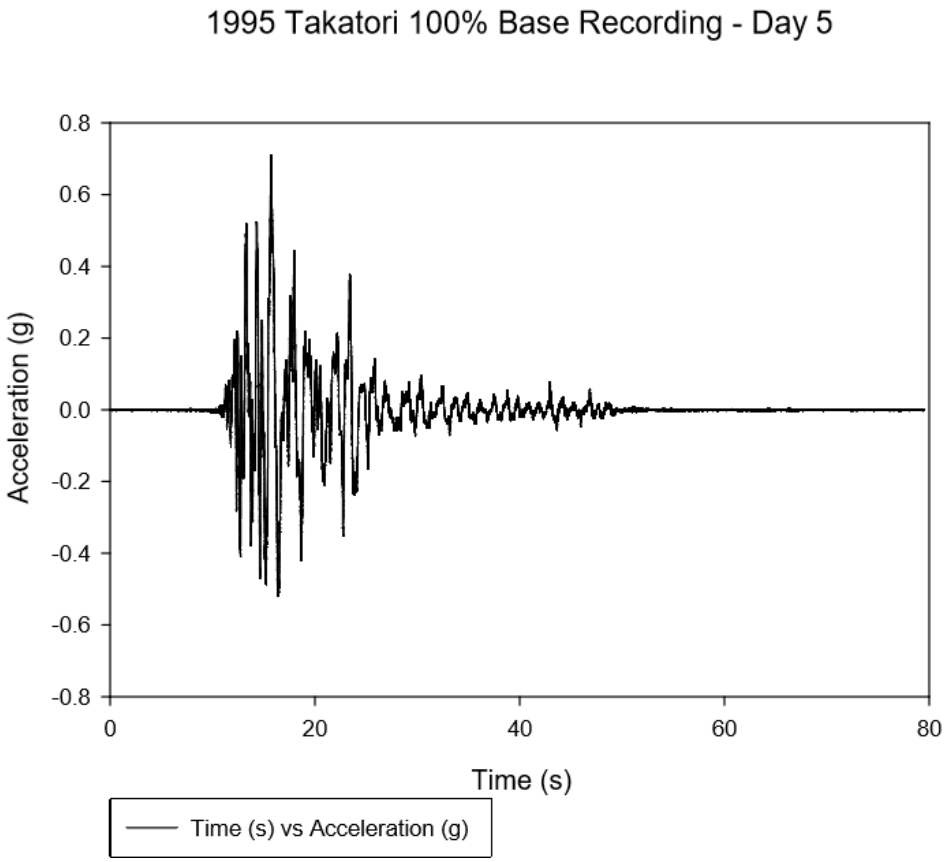

Figure 80: 1995 Takatori 100% Base Recording - Day 5

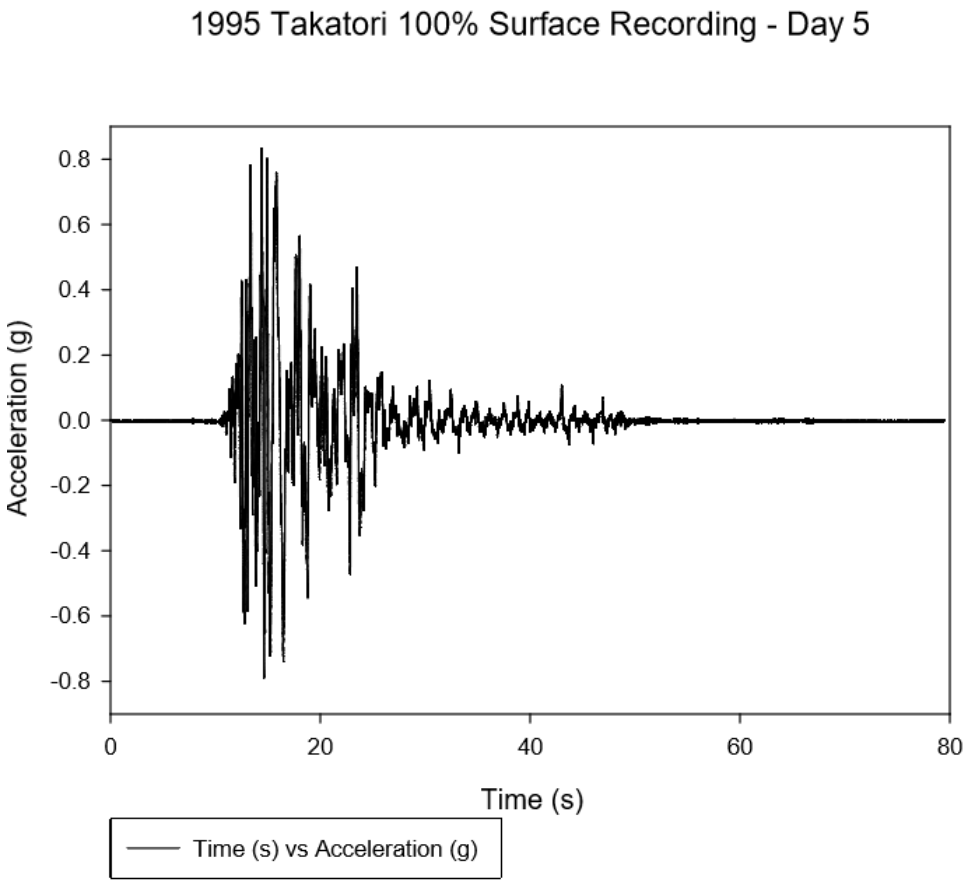

Figure 81: 1995 Takatori 100% Surface Recording - Day 5

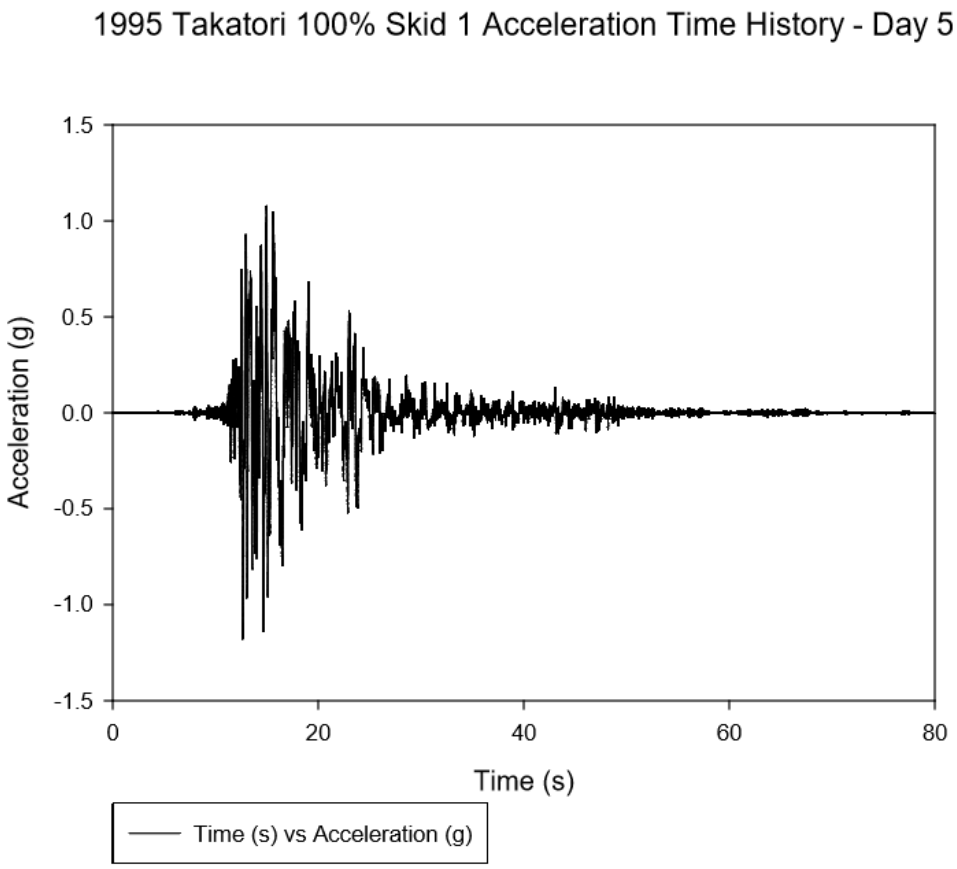

Figure 82: 1995 Takatori 100% Skid 1 Recording - Day 5

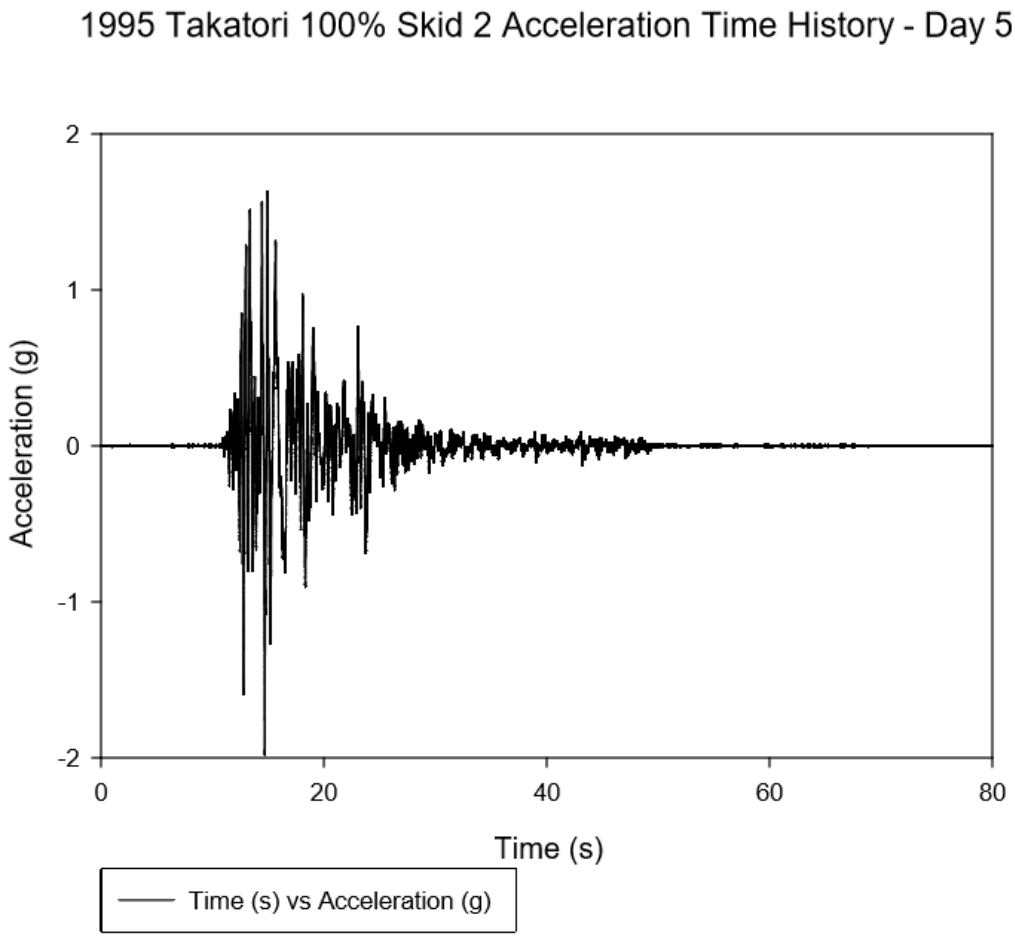

Figure 83: 1995 Takatori 100% Skid 2 **Recording - Day 5**